GRI-87/0211

ANALYSIS OF NATURAL FRACTURES AND BOREHOLE ELLIPTICITY, TRAVIS PEAK FORMATION, EAST TEXAS

TOPICAL REPORT
(July 1986 - May 1987)

TIGHT GAS SANDS

Gas Research Institute
8600 West Bryn Mawr Avenue
Chicago, Illinois 60631

ANALYSIS OF NATURAL FRACTURES AND BOREHOLE ELLIPTICITY, TRAVIS PEAK FORMATION EAST TEXAS

TOPICAL REPORT
(July 1986 - May 1987)

Prepared by

Stephen E. Laubach, Robert W. Baumgardner, Jr.,
and Karen J. Meador

Bureau of Economic Geology
W.L. Fisher, Director
The University of Texas at Austin
Austin, Texas 78713

For

GAS RESEARCH INSTITUTE
Contract No. 5082-211-0708
Richard J. Scheper, GRI Project Manager

July 1987

DISCLAIMER

LEGAL NOTICE. This report was prepared by the Bureau of Economioc Geology as an account of work sponsored by the Gas Research Institute (GRI). Neither GRI, members of GRI, nor any person acting on behalf of either:

a. Makes any warranty or representation, expressed or implied, with respect to the accuracy, completeness, or usefulness of the information contained in this report, or that the use of any apparatus, method, or process disclosed in this report may not infringe privately owned rights; or

b. Assumes any liability with respect to the use of, or for damages resulting from the use of, any information, apparatus, method, or process disclosed in this report.

50272-101

REPORT DOCUMENTATION PAGE	1. REPORT NO. GRI-87/0211	2.	3. Recipient's Accession No.

4. Title and Subtitle
Analysis of natural fractures and borehole ellipticity, Travis Peak Formation

5. Report Date
September 1987

6.

7. Author(s) Stephen E. Laubach, Robert W. Baumgardner, Jr., and Karen J. Meador

8. Performing Organization Rept. No.

9. Performing Organization Name and Address
Bureau of Economic Geology
The University of Texas at Austin
University Station, Box X
Austin, TX 78713

10. Project/Task/Work Unit No.

11. Contract(C) or Grant(G) No.
(C) 5082-211-0708
(G) (Gas Research Institute)

12. Sponsoring Organization Name and Address
Gas Research Institute
8600 West Bryn Mawr Ave.
Chicago, Illinois 60631

Project Manager:
Richard J. Scheper

13. Type of Report & Period Covered
Topical
July 1986 - May 1987

14.

15. Supplementary Notes

16. Abstract (Limit: 200 words) This report summarizes petrographic studies of natural and coring-induced fractures in 7 cores from the Travis Peak Formation, a low-permeability gas sandstone in East Texas, and also presents an analysis of fracturing and wellbore elongation based on Borehole Televiewer, Formation Microscanner, and Ellipticity logs from 12 Travis Peak wells. Natural, vertical extension fractures in sandstone are open or only partly mineral filled in the cored depth range (approximately -5,000 to -10,000 ft), and they are therefore potential gas reservoirs as well as a potentially important influence on commercial hydraulic fracture treatment. Crack-seal structure in fracture-filling quartz shows that fracturing and quartz cementation were contemporary; this result, together with evidence of timing of fracturing and the large water volumes that are inferred to have passed through the Travis Peak, suggests that natural hydraulic fracturing influenced fracture development. Healed transgranular microfractures that occur in sandstone can be used to ascertain natural fracture trends in core that lacks macrofractures, and coring-induced petal-centerline fractures can be used to infer stress orientations. Fractures trend ENE to E. In the upper Travis Peak, borehole ellipticity trends ENE, parallel to fracture trends, and in the lower Travis Peak ellipticity trends NNW, parallel to the direction of least horizontal stress.

17. Document Analysis a. Descriptors

East Texas, borehole ellipticity, coring-induced fractures, geophysical log analysis, Hosston Formation, hydraulic fracture treatment, microfractures, natural fractures, stress, tight gas sandstones

b. Identifiers/Open-Ended Terms

petrography of natural and coring-induced fractures in the Travis Peak Formation, East Texas fracture trends, stress history and fracture of tight gas reservoirs, influences on hydraulic fracture treatment

c. COSATI Field/Group

18. Availability Statement	19. Security Class (This Report)	21. No. of Pages
Release unlimited	Unclassified	140
	20. Security Class (This Page) Unclassified	22. Price

RESEARCH SUMMARY

Title	Analysis of natural fractures and borehole ellipticity, Travis Peak Formation, East Texas
Contractor	Bureau of Economic Geology, The University of Texas at Austin, GRI Contract No. 5082-211-0708, entitled "Geologic Analysis of Primary and Secondary Tight Gas Sand Objectives."
Co-Principal Investigators	R. J. Finley and S. P. Dutton
Report Period	July 1986 - May 1987
Objectives	To identify the mode, distribution, and orientation of natural fractures in the Travis Peak Formation with particular emphasis on Waskom field, Harrison County, Texas, location of the GRI Staged Field Experiment No. 1; to develop new methods for characterization of natural fractures in core; to integrate fracture and diagenetic history as a first step in developing a stress history for the Travis Peak; to document the pattern of borehole ellipticity and to compare it to the natural fracture pattern and to indicators of in situ stress.
Technical Perspective	Previous work on the Travis Peak has established the regional structural and diagenetic framework of the formation across East Texas and North Louisiana. Several cores are available from cooperative wells, and extensive core, Borehole Televiewer, Formation Microscanner, and Borehole Ellipticity logs are available from the Staged Field Experiment well. With these cores and logs, characterization of the natural fracture array within its structural and diagenetic context began. This report summarizes the results of petrographic studies of fractures in Travis Peak core, including mineralogy and microstructure indicative of the timing, conditions, and mode of fracturing, and suggests some constraints that these results place on stress history and some implications for hydraulic fracture treatment.
Results	Natural, vertical extension fractures in Travis Peak sandstone in Waskom field trend east-northeast and have characteristics that suggest intermittent natural hydraulic fracture. Many fractures in sandstone are open in the subsurface and could contain hydrocarbons. Preliminary evidence suggests that fracture

abundance increases within gentle east-trending monoclines. Fractures propagated during burial and precipitation of porosity-occluding quartz cement. Fractures are interpreted to have propagated at depths of 3,000 to 5,000 ft on the basis of a correlation of vein-mineral precipitation sequence with the diagenetic mineral precipitation sequence, together with previously determined estimates of the burial depth of the diagenetic minerals. Healed microfractures (post-depositional planes of minute fluid inclusions) can be used to define natural macrofracture trends. Coring-induced petal-centerline fractures can be used to predict the propogation direction of hydraulically-induced fractures. Natural fractures are not always parallel to coring-induced fractures, and therefore natural fractures could intersect hydraulically-induced fractures at low angles, with potential effects on gas production and hydraulic fracture treatment. In the upper Travis Peak, borehole ellipticity trends east-northeast, parallel to fracture trends, and in the lower Travis Peak ellipticity trends north-northwest, parallel to the direction of least horizontal stress; evidently, different mechanisms govern borehole ellipticity in different parts of the formation. This result shows that a knowledge of the mechanism producing borehole ellipticity is required before confident predictions of hydraulic fracture propagation direction can be made from ellipticity analysis.

Technical Approach

Fractures were examined in core from seven wells and were oriented by standard and digital multishot and paleomagnetic techniques (compiled by CER Corporation) and by Borehole Televiewer and Formation Microscanner logs. Petrographic studies based on core from 11 wells used 110 oriented thin sections and several unoriented thin sections used in previous diagenetic studies. Petrographic and scanning electron microscopes were used for fracture characterization and mineral identification. Borehole ellipticity logs provided by ResTech, Inc., were used to define borehole ellipticity patterns.

CONTENTS

Figures

TABLES

INTRODUCTION

The Travis Peak Formation, an areally extensive tight gas sandstone in East Texas and North Louisiana, serves as a laboratory for technology development in tight gas production. Incorporated into the geologic component of the Gas Research Institute's (GRI) program are regional and local studies of Travis Peak depositional systems, diagenetic history, and hydrocarbon maturation based on extensive collection of core and regional studies of structural geology, modern and paleostresses and potential structural influences on hydraulic fracture propagation. This report describes two aspects of the ongoing structural geologic research.

Characterization of natural and coring-induced fractures in Travis Peak core from the Staged Field Experiment No. 1 well and adjacent cooperative wells provides basic information on natural fractures. Results of the fracture study (reported in Part One) include evidence of natural fracture trend, mode of formation, size, porosity, and distribution, as well as insight into the stress history of the basin, and new techniques for determining natural fracture trends in core. Natural fractures could influence gas production and hydraulic fracture treatment in the Travis Peak.

Borehole Ellipticity logs, in conjunction with Borehole Televiewer and Formation Microscanner logs, can be used to evaluate fracture patterns and orientation of stresses and to predict the direction of hydraulic fracture propagation. Preliminary results (reported in Part Two) show that borehole ellipticity trends northeastward in the upper Travis Peak and northwestward in the lower Travis Peak. Comparison of ellipticity to stress and fracture trends indicates that fractures control ellipticity in the upper Travis Peak and stress-induced spalling controls ellipticity in the lower Travis Peak.

PART ONE:

FRACTURE ANALYSIS OF THE TRAVIS PEAK FORMATION, EAST TEXAS

ABSTRACT

The Lower Cretaceous Travis Peak Formation in East Texas is a tabular sandstone and shale unit approximately 2,000 ft thick. Depth to the top of the formation ranges between 5,900 and 9,500 ft. Fractures in the Travis Peak were sampled from 985 ft of core from seven wells in East Texas. Natural fractures strike east-northeast to northeast and provide potential natural conduits and reservoirs for gas. Fractures in sandstone exhibit features due to intermittent fracturing and sealing ("crack-seal"), indicating that the fractures are the result of episodes of fluid pressure in excess of hydrostatic. Correlation of the vein-mineral precipitation sequence with the diagenetic history suggests that fractures propagated at depths of between 3,000 and 5,000 ft during the migration of quartz-precipitating fluids; previous $\delta^{18}O$ studies of quartz cement suggest that the fluids may have been deeply circulating meteoric water. Fracture permeability provides a mechanism for the passage of large fluid volumes recorded by the precipitation of extensive quartz cement. Fractures stopped propagating before maximum burial depth was achieved: during approximately 5,000 ft of subsequent burial, fractures either remained partly open or were sealed by post-kinematic ankerite and clay minerals.

Natural fractures could influence the success of hydraulic fracture treatment by promoting leakoff, fracture branching, and fluctuations in pumping pressure and by influencing the induced fracture orientation. The preferred orientation of healed microfractures, which are documented in non-orogenic sedimentary rocks for the first

time in this study, may prove to be a useful tool for testing relations among natural fracture trends, current stresses, and direction of fracture propagation. East-northeast-trending coring-induced petal-centerline fractures are approximately parallel to the direction of maximum horizontal strain recovery (ϵ_{Hmax}) measured with anelastic strain recovery experiments and to fractures created in hydraulic stress tests, suggesting that these coring-induced fractures reflect contemporary stresses. They can therefore be used to predict the propagation direction of hydraulically-induced fractures. Although the range of natural fracture trends overlaps the trend of hydraulically-induced fractures, petal-centerline fractures and natural fractures are not always parallel, indicating that hydraulically-induced fractures may not propagate parallel to natural fractures.

INTRODUCTION

Fractures are common in sedimentary rocks, but their origin is often conjectural because different loading paths can lead to fracture propagation (Engelder, 1985). For example, extension fractures can be (1) unloading fractures formed near the earth's surface in response to thermal-elastic contraction of rock accompanying uplift and erosion, (2) tectonic fractures formed by regional extension, (3) hydraulic fractures formed at depth in response to fluid overpressure, or (4) the result of some combination of these influences. One way to determine which of these loading paths is important in the evolution of sedimentary basins is to determine the timing and fracture mechanism for fractures in rocks with different loading histories.

The objective of this study is to provide basic information on fractures in rocks that have experienced a relatively simple burial history. Such a history limits the

possible loading paths that produce fracture propagation. An extensive regional coring program of the Lower Cretaceous Travis Peak Formation in the East Texas Basin permitted characterization of fracture shape, attitude, microstructure, and fracture-fill mineralogy for subsurface fractures. These observations were used to address basic questions concerning the relation of fracture propagation to fluid migration, diagenesis and evolving rock mechanical properties, and burial depth. Results have implications for quantitative stress history models of basin evolution (Voight and St. Pierre, 1974; Narr and Currie, 1982; Warpinski, 1986).

Fracture studies are important because (1) they provide information on the origin of fracture arrays; (2) fractures are potentially valuable as indicators of at least part of their host rock's strain history; (3) minerals filling fractures can provide constraints on the diagenetic conditions during and after fracturing; and (4) fluid inclusions within mineralized fractures provide a direct sample of fracture-filling fluids. Fractures are also economically important as channelways and reservoirs for hydrocarbons, and they may influence the success of operations such as hydraulic fracture treatments designed to enhance hydrocarbon recovery.

Mapping subsurface fracture trends is difficult, even with an extensive coring program, because widely spaced macrofractures may not be sampled. Petrographic study of Travis Peak sandstone led to the discovery of healed microfractures with preferred orientation. These microfractures can be used to infer natural macrofracture trends in core that lacks macroscopic fractures and may be useful in mapping subsurface fracture trends. The healed microfractures appear under the petrographic microscope as planes 0.5 to 2 mm long, composed of minute (<10 μm) fluid inclusions.

Fractures are also commonly produced by the coring process. Previous studies have suggested that the strike of one type of coring-induced fracture, the petal-

centerline fracture, could be a useful indicator of maximum principal horizontal stress trajectory. Alternatively, petal-centerline fractures could follow natural fracture trends. Evidence from the Travis Peak supports the interpretation that petal-centerline fractures indicate stress trajectories, not natural fracture trends. This result has implications for hydraulic fracture treatment of the Travis Peak.

GEOLOGIC SETTING

The study area is located in the northern Gulf of Mexico basin, which developed by rifting initiated in the Late Triassic to Middle Jurassic as Pangea began to fragment. By 150 mya seafloor spreading was underway in the Gulf (Buffler and others, 1980; Pindell, 1984). Stretching involved in the rifting process produced thinning and heating of the lithosphere, which subsequently cooled and gradually subsided (McKenzie, 1978; Nunn and others, 1984). The thick sequence of predominantly shallow water Mesozoic and Cenozoic sedimentary rocks in the Gulf basin, including the Lower Cretaceous Travis Peak Formation, was deposited during the thermal subsidence phase of basin evolution.

The Travis Peak Formation, which contains abundant low-permeability sandstone, extends across East Texas, North Louisiana, and southern Mississippi (Saucier and Finley, 1984; Dutton, 1987). The Travis Peak rests on limestone of the Cotton Valley Formation and is overlain by limestone of the Sligo Formation (Saucier and others, 1985; Fracasso, 1987). In East Texas, the Travis Peak is approximately 2,000 ft thick, and depth to the top of the formation ranges from 5,900 to 9,500 ft. The formation consists of interbedded fine-grained quartzarenite, subarkose, and mudstone (Dutton, 1986, 1987; Fracasso, 1987). Abundant quartz cement has reduced permeability in

much of the formation to less than 0.1 md (Dutton, 1987).

The northern Gulf of Mexico basin is a structural province characterized by gentle bedding dips, subdued structure, and low tectonic stress. Structural features within the study area include the north-trending Sabine Uplift (Murray, 1961; Granata, 1963; Halbouty and Halbouty, 1982; Jackson, 1986), the East Texas Basin, the northeast- and east-trending Mexia-Talco fault zone, the east-trending Elkhart-Mount Enterprise fault zone, the east-trending Angelina-Caldwell flexure (fig. 1) and various structures caused by diapiric movement of salt. Recent movement on the Elkhart-Mount Enterprise fault zone (Collins and others, 1980) and hydraulic fracture stress tests in the Travis Peak (Holditch and others, 1987a, 1987b) suggest that the modern least horizontal stress in this area trends north-northwest.

The largest structure in the study area is the Sabine Uplift, a basement-cored, low amplitude anticline centered near the Texas-Louisiana state line. The uplift developed initially in the early Late Cretaceous and was reactivated in the early Tertiary (Granata, 1963; Halbouty and Halbouty, 1982; Jackson, 1986). Each movement episode produced less than 1,600 ft of uplift at the crest of the arch (Jackson, 1986). Episodes of arch uplift were contemporary with episodes of compressive deformation in the backarc region of the southern North American Cordillera, to changes in relative plate motions between North America and Pacific Basin plates, and to changes in seafloor spreading patterns in the Atlantic. Movement on the arch may be the result of Cretaceous episodes of mild northeast-directed compression of the Gulf of Mexico basin resulting from these plate interactions (Jackson, 1986; Jackson and Laubach, 1987). The present elliptical shape of the Sabine Uplift evident on regional structural maps is probably the result of Tertiary structural overprint by the east-trending Angelina-Caldwell flexure (Jackson, 1986).

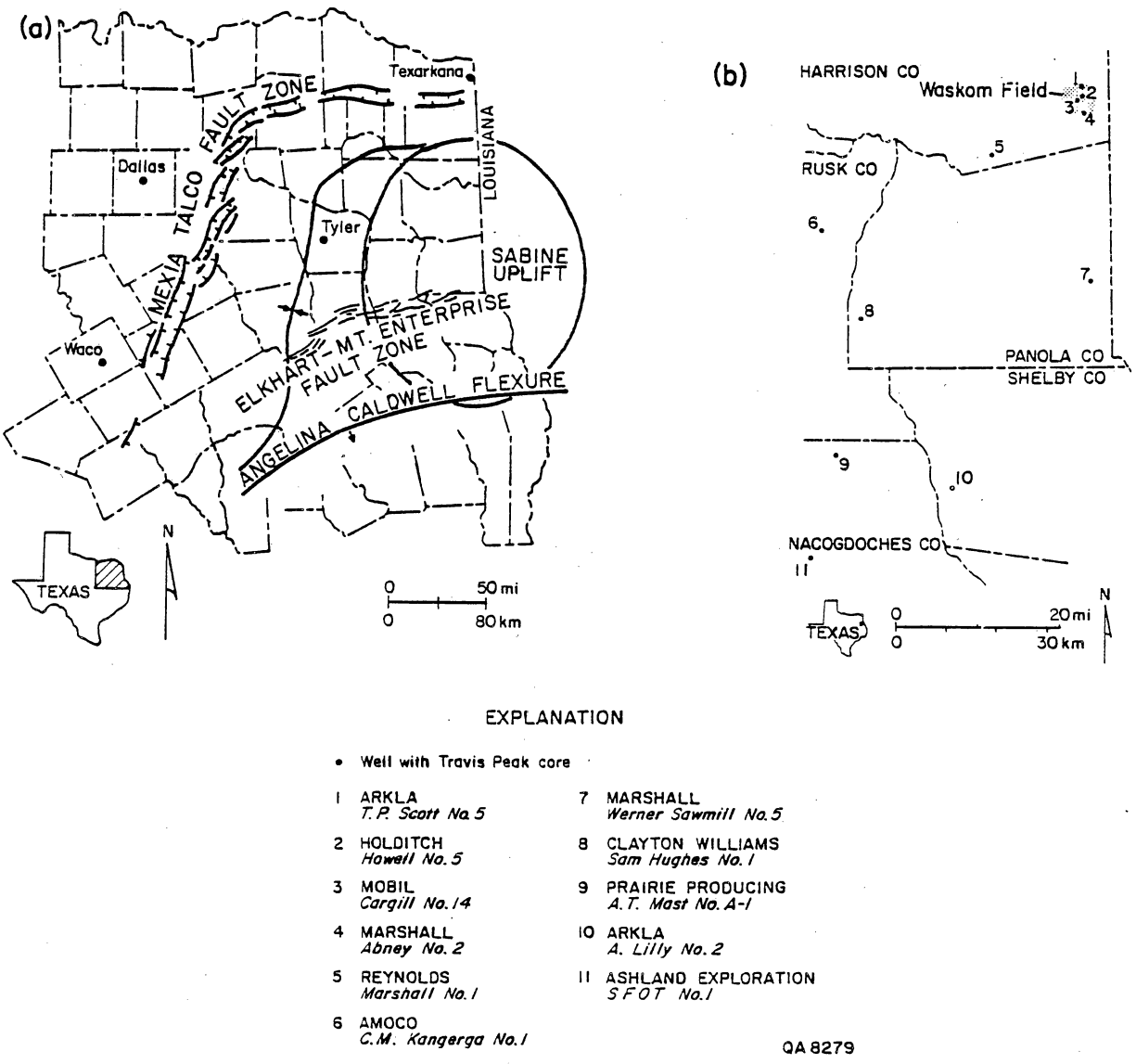

Figure 1. (a) Structural setting of the Travis Peak Formation in East Texas. (b) Location of wells with Travis Peak core.

A group of smaller domal and low-amplitude anticlinal structures is located on the western flank of the Sabine Uplift. Saucier and Finley (1984) and Saucier and others (1985) have interpreted these structures to be salt-cored, low-amplitude anticlines that developed syndepositionally as a consequence of unequal loading of the underlying salt during Travis Peak progradation from the northwest. Deep wells in most of these structures have penetrated salt.

The natural fracture pattern in the study area need not necessarily be simple, despite the relatively simple Cretaceous structural history of the Gulf of Mexico basin. Loading-path models (Voight and St. Pierre, 1974; Narr and Currie, 1982; Engelder, 1985; Warpinski, 1986) that calculate the state of stress for a given rock type by tracing the variations of such factors as rock mechanical properties, temperature, stress, and pore pressure confirm that failure criteria can be met under a variety of conditions and at different times, even during a simple cycle of burial and uplift. Potential causes of fracturing in the Travis Peak include: (1) sediment loading and fluid circulation related to Early Cretaceous basin subsidence and mild extension; (2) deep-seated salt movement and associated faulting (Jackson, 1982); (3) Late Cretaceous and early Tertiary tectonic compression of the Gulf (Jackson, 1986); (4) stretching across the hinges of Gulf-margin-parallel flexures such as the Angelina-Caldwell (Walcott, 1972; Watts and Ryan, 1976); and (5) modern plate-tectonic stresses (Engelder, 1982).

FRACTURE SAMPLING

Fracture descriptions are derived from more than 980 ft of core collected from 7 Travis Peak wells in East Texas (fig. 1, table 1) as part of a comprehensive study of all aspects of the geology and engineering characteristics of the Travis Peak Formation

Table 1. Natural mineralized fractures in seven Travis Peak wells.

Holditch Howell No. 5
Harrison County (571 ft of core)

Core/Fracture	Core Depth	Width	Minerals	Rock Type
7/3	6,208.9 - 09.0	1.0 mm*	Qtz	ss
7/6	6,225.6 - 26.1	1.0*	Qtz + cc	ss
8/4	6,241.5 - 44.6	0.5*	Qtz + cc	ss
9/9	6,303.1 - 03.4	--	Qtz + cc	ss
11/1	~7,438	--	Qtz	ss
11/4	7,442.4 - 42.9	--	Qtz	ss
12/1	7,471.3 - 74.5	1.0*	Qtz + cc	ss
13/5	7,494.7 - 94.8	--	Qtz	ss
13/6	7,495.3 - 95.7	--	Qtz	ss
15/1	7,515.4 - 16.0	--	Qtz	ss
16/3	7,552.1 - 52.4	--	Qtz	ss

Mobil Prod. G. E. Cargill No. 14
Harrison County (200.7 ft of core)

Core/Fracture	Core Depth	Width	Minerals	Rock Type
3/19	6,234.4 - 35.5	1.0 mm	Qtz + cc	ss
4/2	6,270.0 - 72.2	<0.5	Qtz	--

Arkla Expl. T. P. Scott No. 5
Harrison County (244 ft of core)

Core/Fracture	Core Depth	Width	Minerals	Rock Type
1/1	5,823.5 - 23.9	0.5 mm	cc	Lst
1/3	5,830.2 - 30.6	<0.5	--	Lst
1/4	5,832.9 - 33.2	1.0	cc	Lst
1/7	5,839.0 - 39.4	<0.5	--	Lst
2/7	6,177.7 - 78.3	0.5	--	ss
3/2	6,187.3 - 87.8	<0.5	Qtz	ss
3/3	6,189.1 - 96.0	--	--	ss
3/6	6,200.0 - 00.8	<0.5	Qtz + cc*	ss
3/7	6,206.1 - 06.7	<0.5	Qtz + cc*	ss
3/10	6,219.7 - 20.7	<0.5	Qtz	ss
4/5	7,421.1 - 22.3	<0.5	Qtz + cc	ss
4/10	7,440.2 - 40.7	<0.5	Qtz	ss
5/1	7,462.9 - 63.5	<0.5	--	ss
6/2	7,494.4 - 95.2	1.0	Qtz	ss
6/3	7,497.4 - 98.5	0.1	Qtz	ss

Abbreviations:

Qtz = quartz
cc = carbonate mineral
Lst = limestone
ss = sandstone
ms = mudstone
-- = unknown
* = fracture partly open in subsurface

Table 1 continued

Marshall Expl. Werner Sawmill No. 5
Panola County (243 ft of core)

Core/Fracture	Core Depth	Width	Minerals	Rock Type
1/3	6,559.9 - 61.0	2 mm	cc	Lst
3/8	6,883.9 - 84.2	--	cc	ss
4/1	6,890.1 - 90.6	<0.5	--	ss
4/3	6,896.7 - 97.9	<0.5	--	ss
5/3	7,051.0 - 53.0	0.5	Qtz	ss
5/4	7,053.6 - 54.8	<0.5	Qtz	ss

Clayton Williams Sam Hughes No. 1
Panola County (84.1 ft of core)

Core/Fracture	Core Depth	Width	Minerals	Rock Type
2/1	7,047.3 - 49.1	--	Qtz + cc	ss
2/2	7,050.9 - 51.6	--	--	ss
3/4	7,099.5 - 100.0	--	Qtz + cc*	ss
3/5	7,101.1 - 03.4	--	Qtz + cc*	ss

Prairie Mast No. A-1
Nacogdoches County (199.3 ft of core)

Core/Fracture	Core Depth	Width	Minerals	Rock Type
1/7	8,643.1 - 44.7	--	Qtz	ss
1/5	8,662.2 - 62.4	<0.5	--	ss
2/7	9,160.2 - 61.7	<0.5	--	ss
5/7	9,186.8 - 87.3	1.0	Qtz	ss
6/6	9,214.1 - 14.5	0.5	Qtz + cc*	ss
6/7	9,214.9 - 15.6	~0.5	Qtz + cc	ss
6/13	9,227.7 - 28.0	~0.5	Qtz	ss
8/9	9,940.9 - 41.5	~0.5	Qtz	ss
10/8	9,965.9 - 66.9	~0.5	Qtz*	ss
10/10	9,970.8 - 72.0	0.5	Qtz	ss
10/19	9,983.4 - 84.0	0.5	Qtz	ss
11/4	9,990.6 - 91.4	0.5	Qtz	ss

Table 1 continued

Ashland Expl. S.F.O.T. No. 1
Nacogdoches County (180.6 ft of core)

Core/Fracture	Core Depth	Width	Minerals	Rock Type
1/1	9,665.0 - 66.0	--	--	ss
1/2	9,672.0 - 77.6	--	--	ss
1/3	9,679.1 - 88.6	--	--	ss
1/4	9,688.9 - 90.4	--	Qtz	ss
1/5	9,693.1 - 93.5	--	Qtz + cc	ss
1/6	9,694.9 - 95.5	--	Qtz + cc	ss
2/1	9,702.0 - 05.3	--	--	ss
2/6	9,716.8 - 20.4	--	--	ss
3/3	9,736.3 - 37.4	--	--	ms
3/6	9,749.6 - 52.0	--	Qtz + cc	ss
3/8	9,750.2 - 50.9	--	Qtz + cc	ss
5/3	10,090.4 - 92.5	0.5	Qtz + cc*	ss
5/7	10,107.1 - 08.1	--	Qtz + cc*	ss
5/8	10,107.8 - 08.5	<1 mm	Qtz + cc*	ss
5/9	10,107.0 - 111.7	--	Qtz + cc	ss
5/10	10,107.3 - 107.7	--	Qtz + cc	ss
5/11	10,113.4 - 113.7	--	Qtz + cc	ss
6/5	10,131.7 - 138.4	--	Qtz + cc	ss
6/7	10,140.2 - 149.2	--	Qtz + cc	ss
6/8	10,147.5 - 149.2	2	Qtz + cc	ss

(Saucier and Finley, 1984; Holditch and others, 1987a, 1987b). Cores were oriented by standard and digital multishot techniques and paleomagnetic techniques (CER Corporation, written communication, 1987; Ward and others, 1987). Core was reassembled and described in the field. Core fracture descriptions document fracture attitude and length and distinguish between natural and coring-induced fractures based on the criteria described by Kulander and others (1979). The microstructure and crosscutting relations of fracture-filling minerals were studied with petrographic and scanning electron microscope (SEM), and microfracture attitudes were measured on the universal stage in sets of three thin sections, each section being oriented orthogonally to the other two.

Petrographic studies focused on core from three areas in East Texas where most of the oriented fractures were obtained. These areas are (1) Waskom field in Harrison County, (2) Clayton Williams Sam Hughes No. 1 well in Panola County, and (3) the Prairie Mast No. 1-A and Ashland S.F.O.T No. 1 wells in northern Nacogdoches County. The Travis Peak in these three areas differs in present depth of burial and position relative to regional structures (fig. 1). Most information was obtained from Waskom field (fig. 2), where fracture sampling was from a total of 916 ft of core collected from three wells, the Arkla Scott No. 5 (244 ft), the Mobil Cargill No. 14 (201 ft), and the Holditch Howell No. 5 (471 ft) (the GRI Staged Field Experiment No. 1). Of the core recovered in this field, 127 ft, or 14 percent of the core, was successfully oriented by downhole core orientation tools, including 35.6 ft of oriented core from the Mobil Cargill No. 14 well and 91.4 ft from the Holditch Howell No. 5. Oriented core was not recovered from the Arkla Scott No. 5. Additional fractures in the Holditch Howell No. 5 well were oriented with Borehole Televiewer (BHTV), an

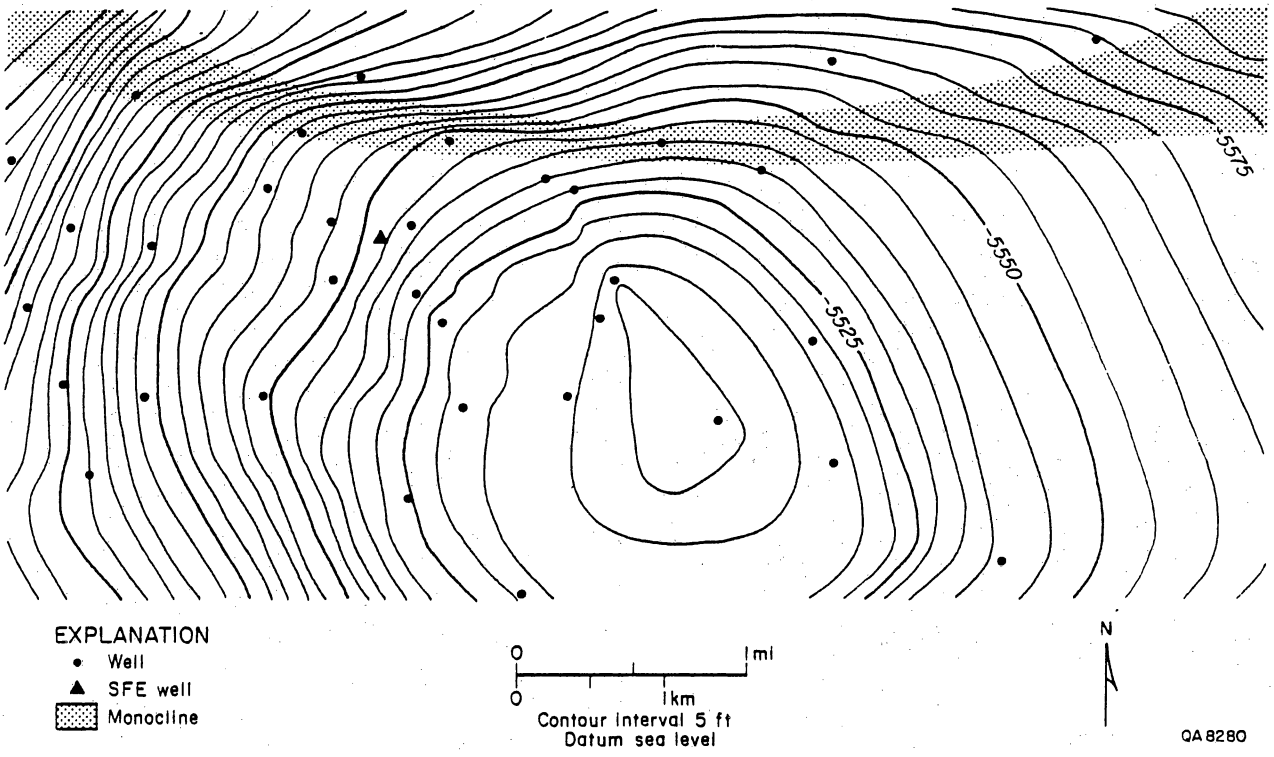

Figure 2. Structural map of a portion of Waskom field drawn on the base of the Sligo Formation. Note the east-trending monocline (stippled).

acoustic logging device used to map the smoothness of the borehole wall (Zemanek and others, 1970), and Formation Microscanner (FMS), a resistivity logging device that examines a small segment of the borehole wall with an array of resistivity sensors located on pads three and four of a four-armed dipmeter tool (Schlumberger Inc., written communication, 1986).

Results from Waskom field provide insight into abundance of natural and coring-induced fractures in the Travis Peak. A total of 197 macrofractures were identified in the 3 cores. Eighty-two of these fractures are natural, 113 are coring-induced, and 2 were produced during hydraulic-fracture stress tests. Only 44 macrofractures are oriented: 19 are from the Mobil Cargill No. 14, of which 14 are natural fractures in mudstone, 1 is a coring-induced petal-centerline fracture, and 1 is a coring-induced petal fracture; 25 are from the Holditch Howell No. 5, of which 4 are natural mudstone fractures, 1 is a mineralized fracture in sandstone, 9 are coring-induced petal-centerline fractures, and 3 are petal fractures. Fifty-four fractures were logged in the Arkla Scott No. 5 core, of which 27 are natural (including 17 mineralized fractures) and 27 are coring-induced.

NATURAL FRACTURES

Natural macrofractures in the Travis Peak Formation can be divided into two major types: (1) mineralized, vertical, dilational fractures produced by net extensional strain perpendicular to fracture strike and (2) gently-dipping shear fractures. The occurrence of each of these fracture types is strongly controlled by rock type; dilational fractures occur predominantly in sandstone, whereas natural shear fractures are restricted to shale and silty mudstone. Quartz-rich sandstone also contains arrays of microfractures.

Sandstone Fractures

Fracture Attitude and Shape

Fractures are typically near vertical. Fractures strike east-northeast to east, but have a wide range of strike within individual wells (fig. 3). Despite the fluctuation of fracture strikes, no direct evidence of multiple fracture sets, such as abutting or crosscutting fractures, has been recovered but data from oriented macrofractures in core are too sparse to draw definite conclusions concerning possible multiple trends or sets. Natural microfractures (fig. 4) also strike predominantly east-northeast, but they have a wide range of strikes.

Fractures in the Holditch Howell No. 5 well were detected with the borehole televiewer (BHTV) and Formation Microscanner (FMS). BHTV fracture trends summarized in figure 5 confirm the east-northeast trend of fractures in Waskom field. Although natural and coring-induced fractures in general cannot be distinguished on logs, preliminary correlation of oriented BHTV and FMS images to core (Part Two) suggests that in Waskom field, natural fracture trends range from approximately 060 to 110 degrees.

In cross section, natural fractures typically follow grain boundaries rather than cut across grains, producing a tortuous microscopic fracture path and contributing to fracture surface roughness (fig. 6). Petrographic inspection of fracture cross sections indicates that 60 to 80 percent of fracture length is intergranular. These observations suggest that the rocks were not tightly cemented when fractures initially propagated; resistance to crack-surface separation was cohesion along detrital grain boundaries rather than fracture of the now ubiquitous quartz cement. Mineralized fracture apertures range between microscopic (<0.1 mm) and 2.0 mm in Waskom field.

Commonly, short branch fractures or sections of fractures that transect grains occur where several grains are stacked in pillars or in tabular grains. These structures or grain shapes may have localized fractures by producing local high stress (e.g., Gallagher and others, 1974). Transgranular fracturing is also associated with variation in fracture dip and strike. Healed microfractures (described in a later section) are locally abundant in narrow (1 to 2 grain diameter), tabular domains that occur parallel to main fractures and along the projection of main fractures in areas where fractures change orientation.

Fractures show various styles of termination. Terminations are either (1) simple tapering, triangular tips (fig. 7), (2) abrupt, blunt tips at lithologic interfaces (fig. 8), or (3) more complex zones of branching, splaying, and microfracturing (fig. 9). Complex splays occur in sandstone with thin, discontinuous mudstone interbeds. These observations suggest that slight lithologic differences arrested natural fracture propagation.

Long fractures are composed of coplanar segments ranging in length from centimeters to tens of centimeters that are commonly arranged in relay and en echelon patterns (fig. 10). Segments are locally separated from adjacent segments by intact rock, or they are connected by short curved or straight transverse fractures. Less commonly, segments follow curved trajectories in the areas where segments overlap, so that in some cases the curving fracture segment abuts an adjoining segment. Continuous fracture segments also contain planar and curved domains that are commonly associated with splays. The curved domains may represent segments of fractures that grew together and that were subsequently connected by throughgoing fractures.

A spectrum of fracture heights (i.e., length in vertical core) is present at any given depth in the Travis Peak (figs. 11 and 12); the tallest fractures are as much as 8 ft high. Regionally, and within individual wells, maximum natural fracture height

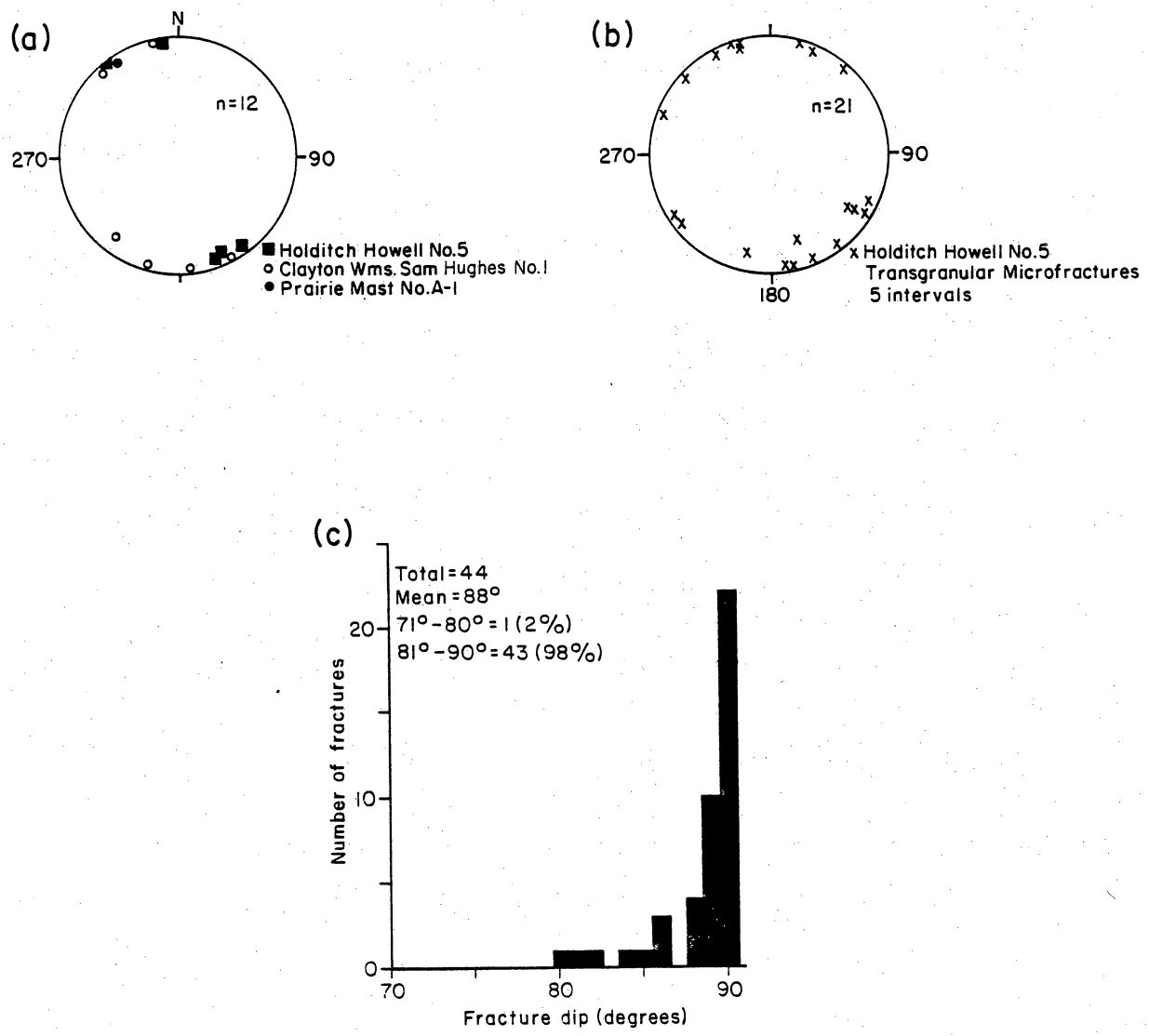

Figure 3. Attitudes of natural sandstone fractures and coring-induced petal-centerline fractures in Waskom field, in Panola County, and in northern Nacogdoches County. (a) Lower hemisphere, equal-area plot of poles to natural fractures. Prairie Mast No. 1-A, Holditch Howell No. 5, and Clayton Williams Sam Hughes No. 1. (b) Lower hemisphere, equal-area plot of microfracture attitude, Holditch Howell No. 5. (c) Histogram of natural fracture dip (5 wells). (d) Strikes of coring-induced petal-centerline fractures. Rose diagrams of sampled East Texas Travis Peak wells (excluding Clayton Williams Sam Hughes No. 1) (two samples per radial division). (e) Strikes of stress-test-induced fractures in the Holditch Howell No. 5 (one sample per radial division). (f) Natural and coring-induced fracture strikes in Prairie Mast No. 1-A core. (g) Strikes of natural and coring-induced fractures in the Clayton Williams Sam Hughes No. 1, Panola County. (h) Natural and coring-induced fractures in Holditch Howell No. 5 core compared with trends of maximum horizontal strain from strain-recovery experiments, from Owen and others (1986). "N" indicates trend of natural fracture; height of lines and boxes indicating fracture and strain relaxation directions is arbitrary.

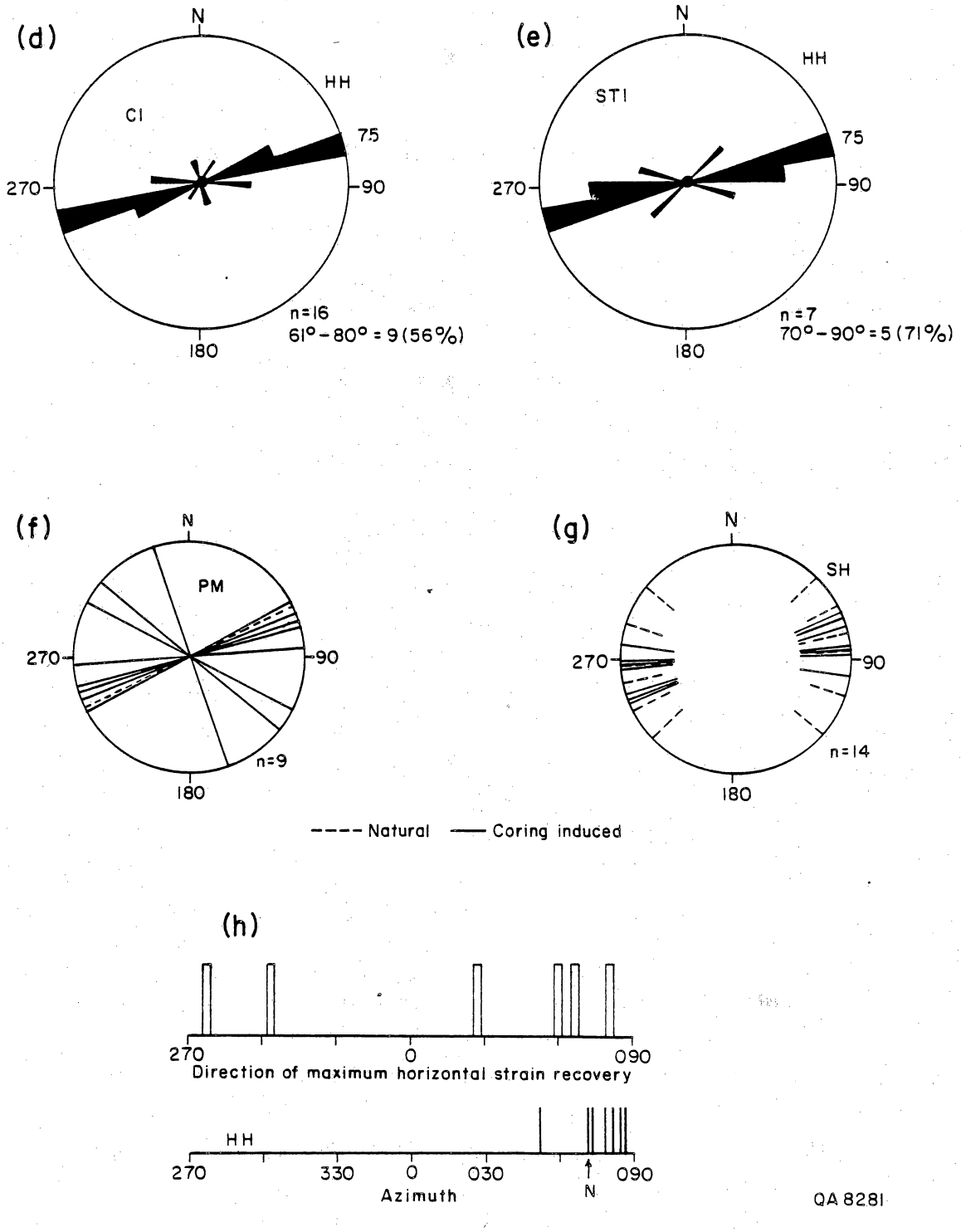

Figure 3 continued

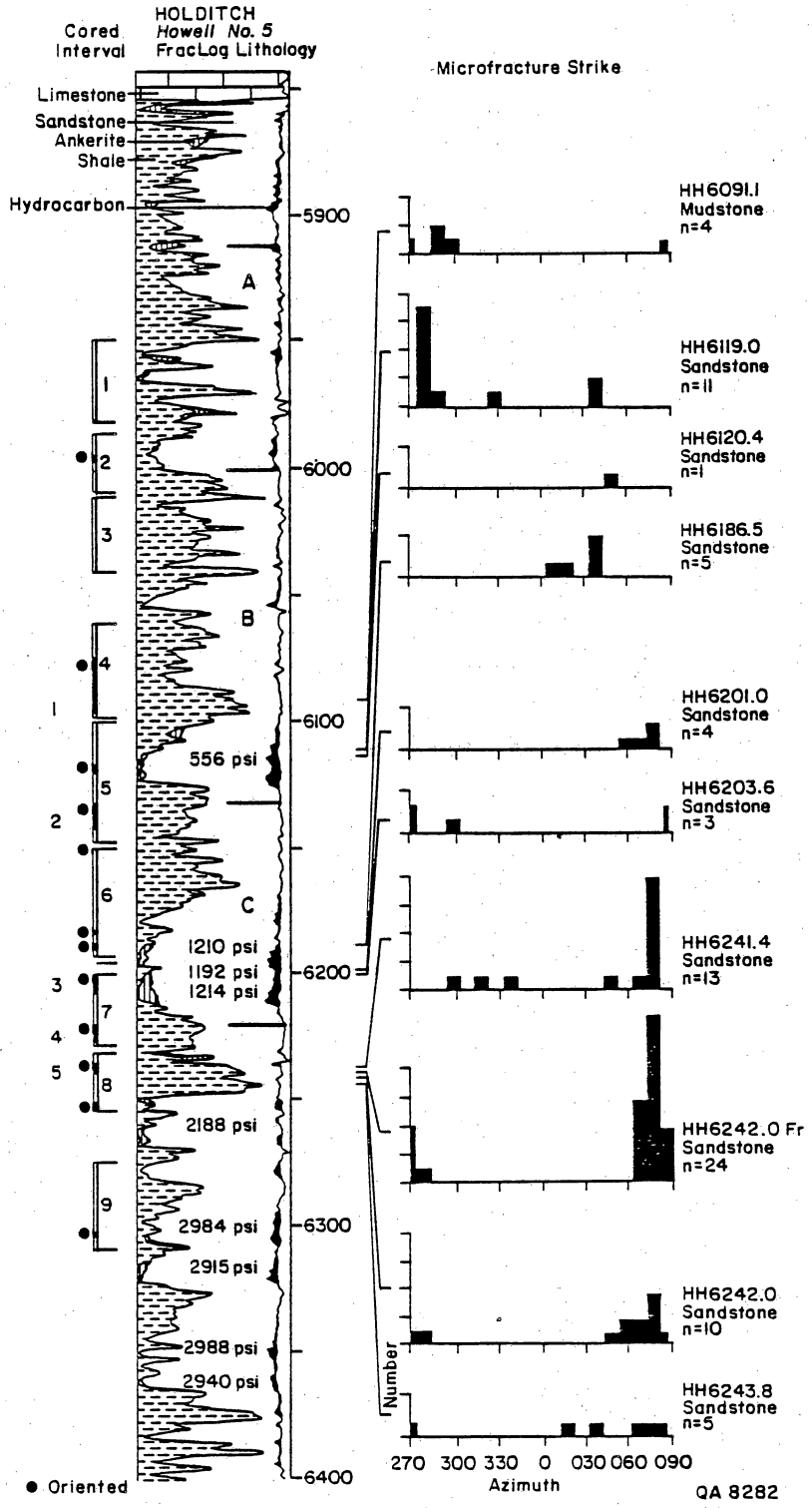

Figure 4. Histograms of natural microfracture trends in Holditch Howell No. 5 core. Each histogram shows the number of transgranular healed microfractures measured in a set of three thin sections from the indicated depth. Locations of the midpoints of oriented macrofractures in this interval are indicated by dots on the left side of the diagram. The A, B, and C sandstone and measured pore pressures are also indicated on the log display, which is simplified from the FracLog display of ResTech.

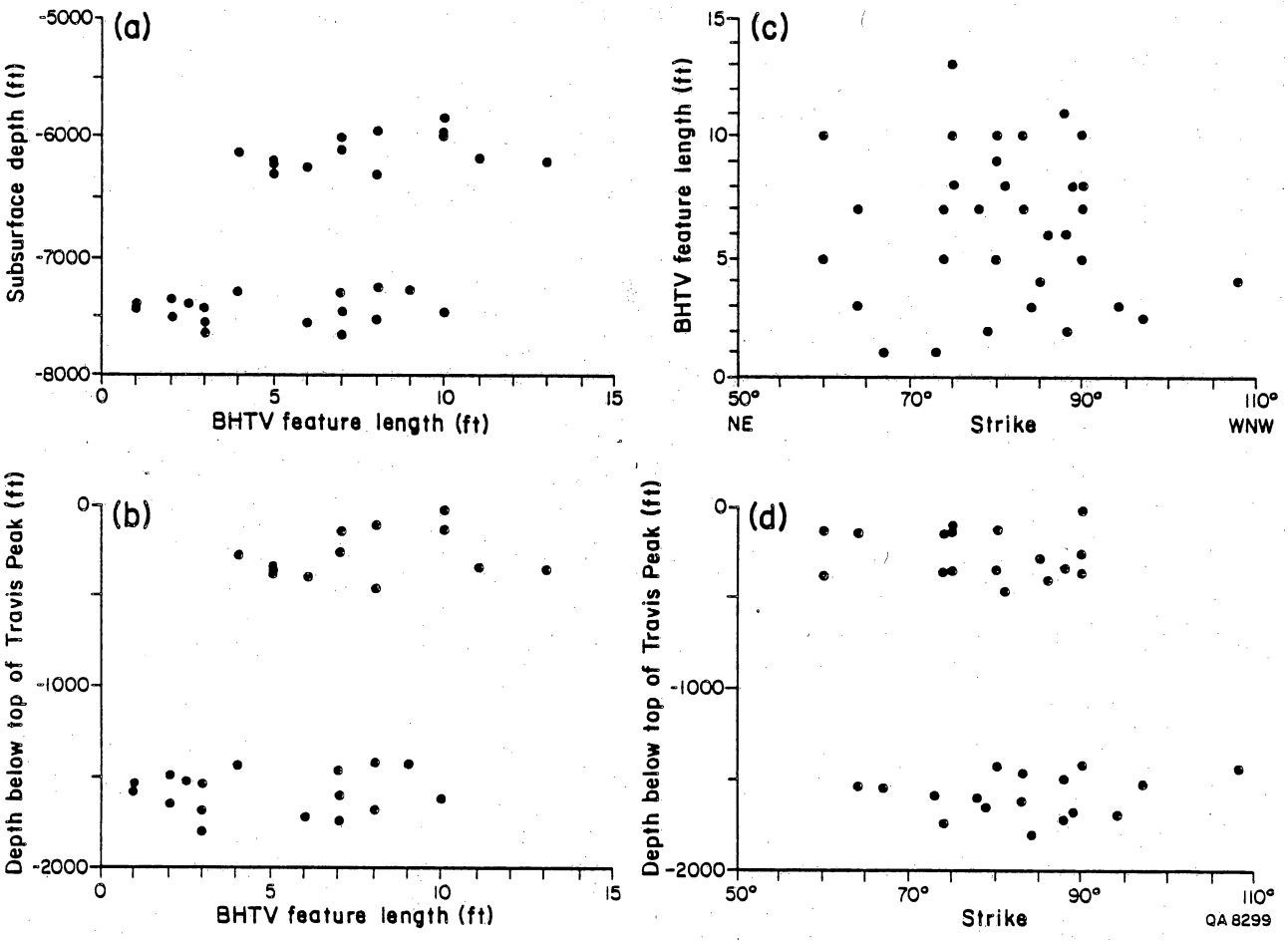

Figure 5. Fracture attitudes and length from BHTV and FMS logs. (a) Fracture length versus depth. (b) Fracture length versus depth below top of Travis Peak. (c) BHTV fracture length versus strike. (d) Depth of fracture midpoint below top of Travis Peak plotted against strike.

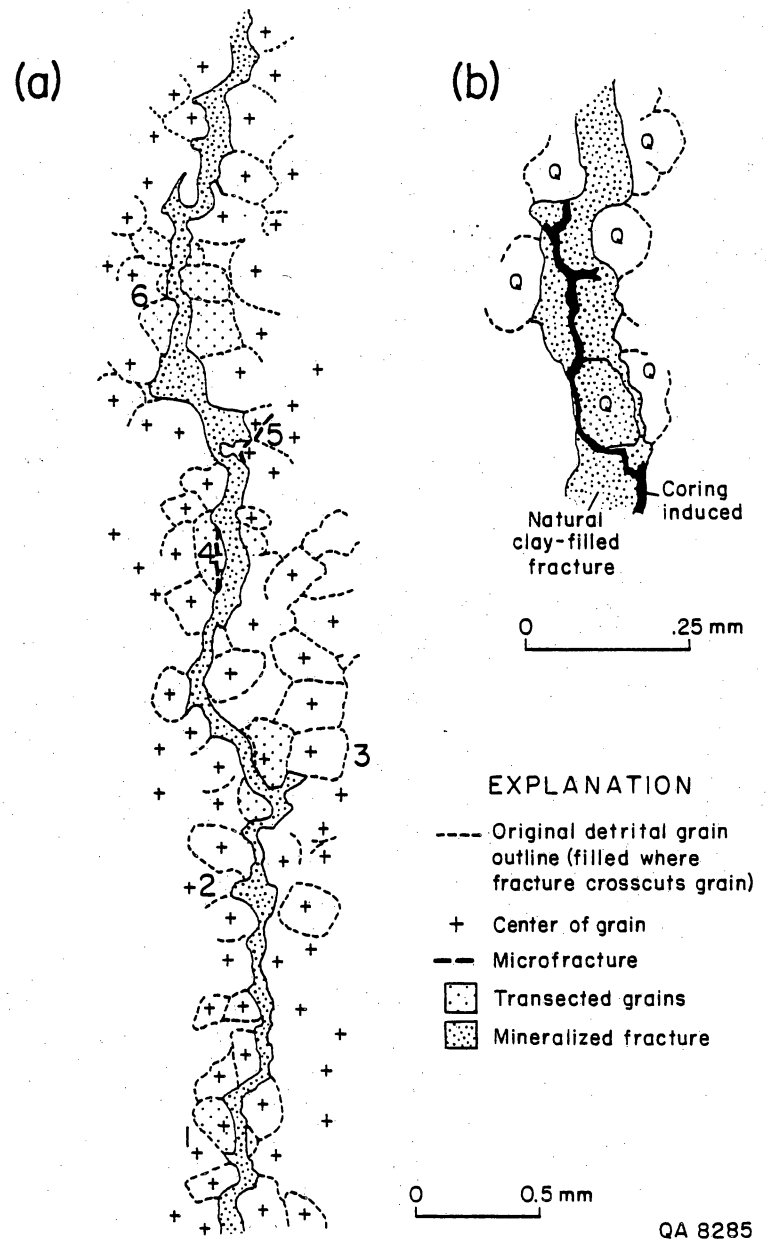

Figure 6. Cross sections of natural fractures showing fracture around and through grains. (a) Fracture from Mobil Cargill No. 14 core showing fracture around grains (labeled 1, 2), variation in fracture dip near grain pillars (labeled 3, 6), and trend of healed microfractures associated with main fracture (labeled 4, 5). Grains crosscut by the fracture are stippled. (b) Detail of Mobil Cargill No. 14 fracture showing reactivation of natural fracture by coring-induced fracture.

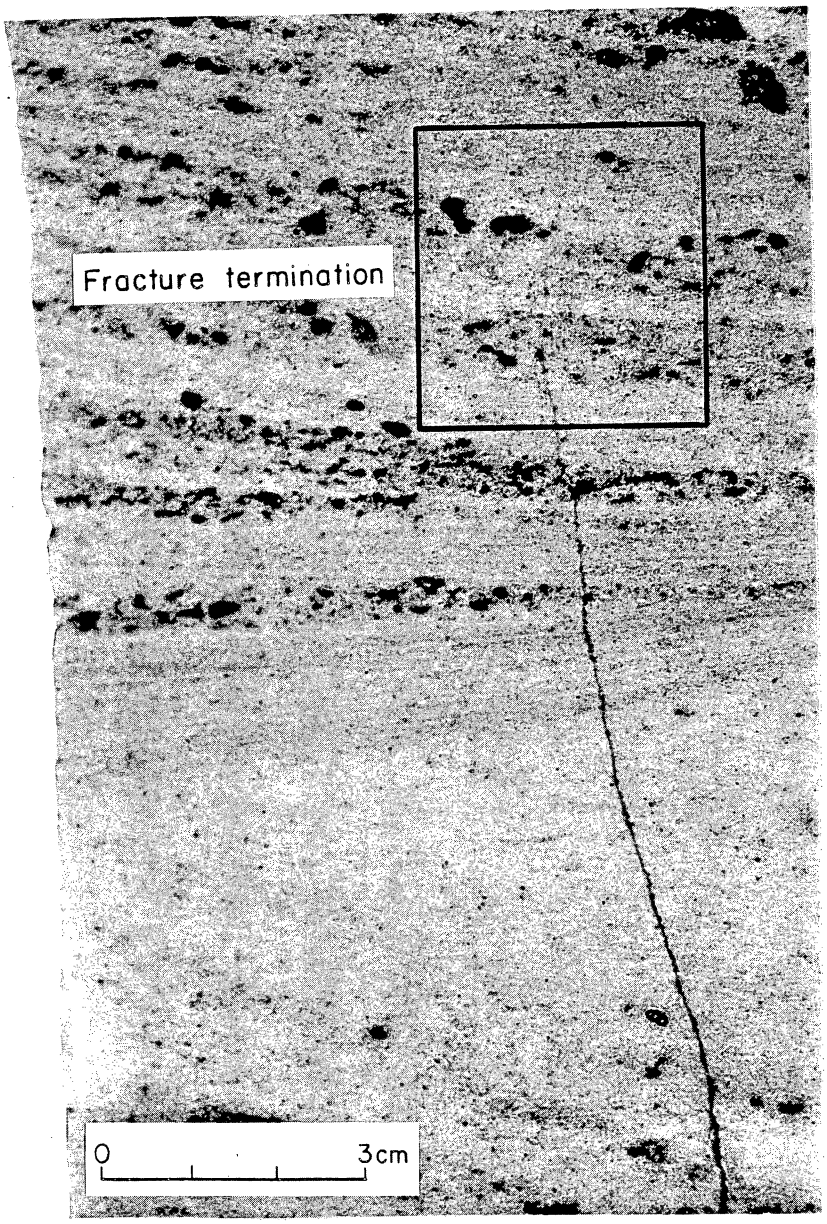

Figure 7. Photograph of simple natural fracture termination. The region of gradually decreasing fracture aperture is outlined (Prairie Mast No. 1-A, 9,958 ft).

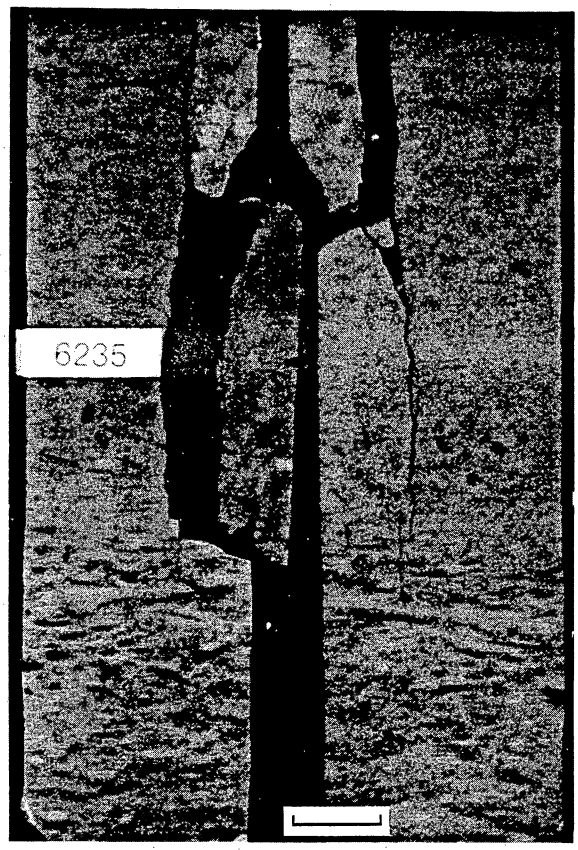

Figure 8. Photograph of fracture termination at shale interbed, Holditch Howell No. 5, 6.235 ft.

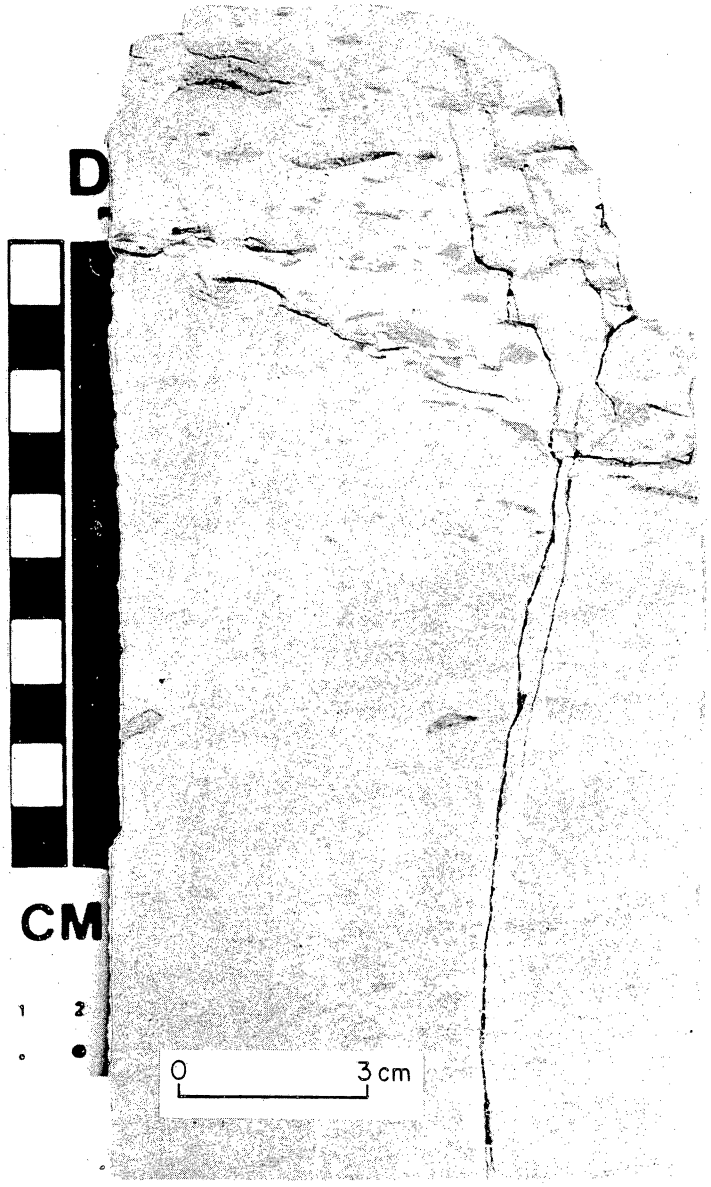

Figure 9. Photograph of complex natural fracture termination in a region of lithologic heterogeneity. Prairie Mast No. 1-A. 9,983.4 ft.

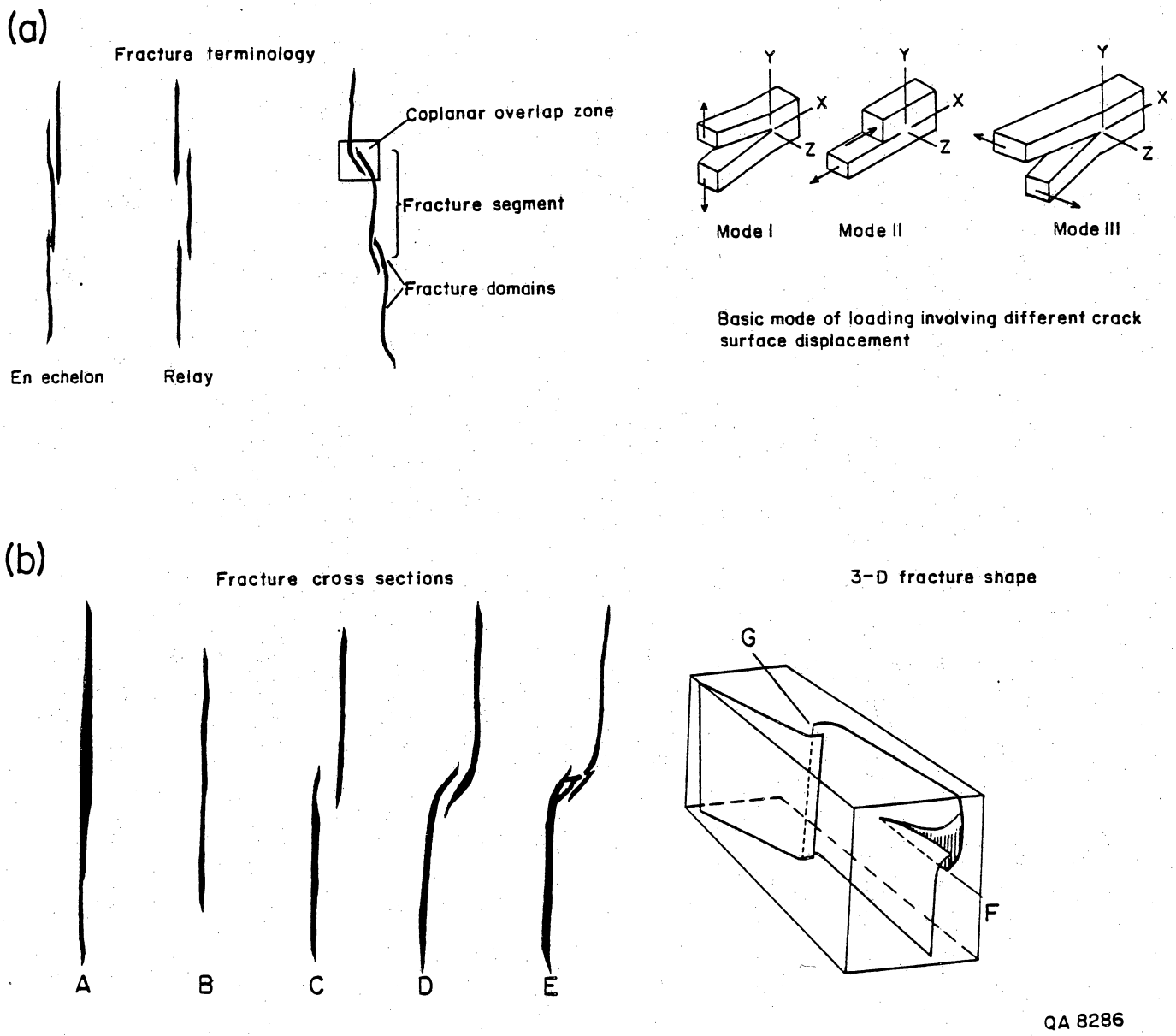

Figure 10. Shape of natural fractures in the Travis Peak Formation. (a) Terminology describing the interrelationship of fracture segments and different crack surface displacement. Sandstone fractures have both en echelon and relay patterns and were opened by Mode I displacement. Mode I, opening or tensile mode, where crack surfaces move directly apart. Mode II, sliding or in-plane shear mode, where crack surfaces slide over one another perpendicular to the leading edge of the crack; Mode III, tearing or antiplane shear mode, where crack surfaces move relative to one another and parallel to the leading edge of the crack. (b) Representative fracture cross sections (labeled A-E). F and G illustrate a possible 3-D shape of an individual fracture extrapolated from cross-sectional pattern.

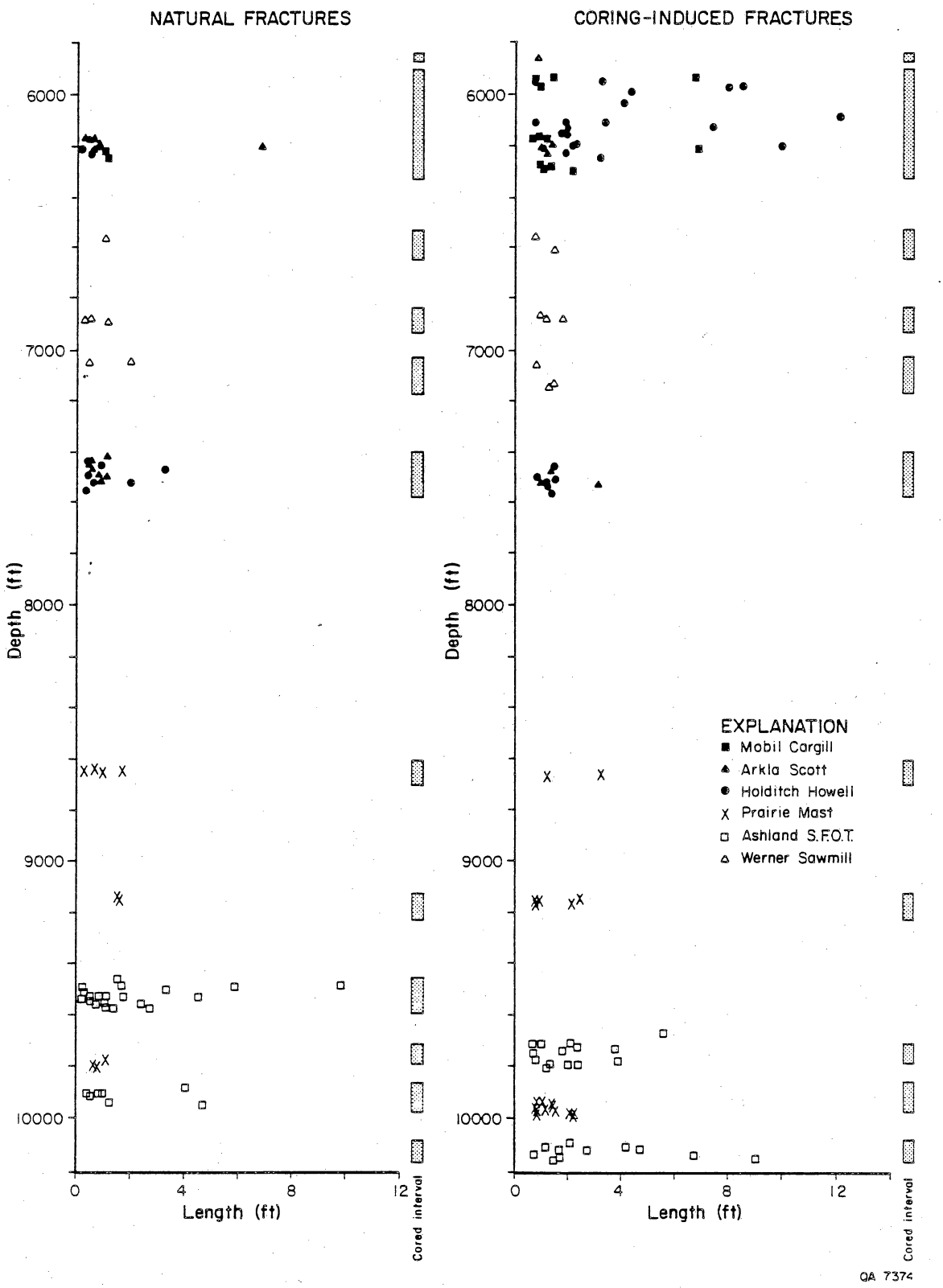

Figure 11. Graph of natural and coring-induced fracture length versus depth. Data from CER Corporation, 1984, 1985a, 1985b, 1986a, 1986b, 1987a, 1987b, and written communication, 1987.

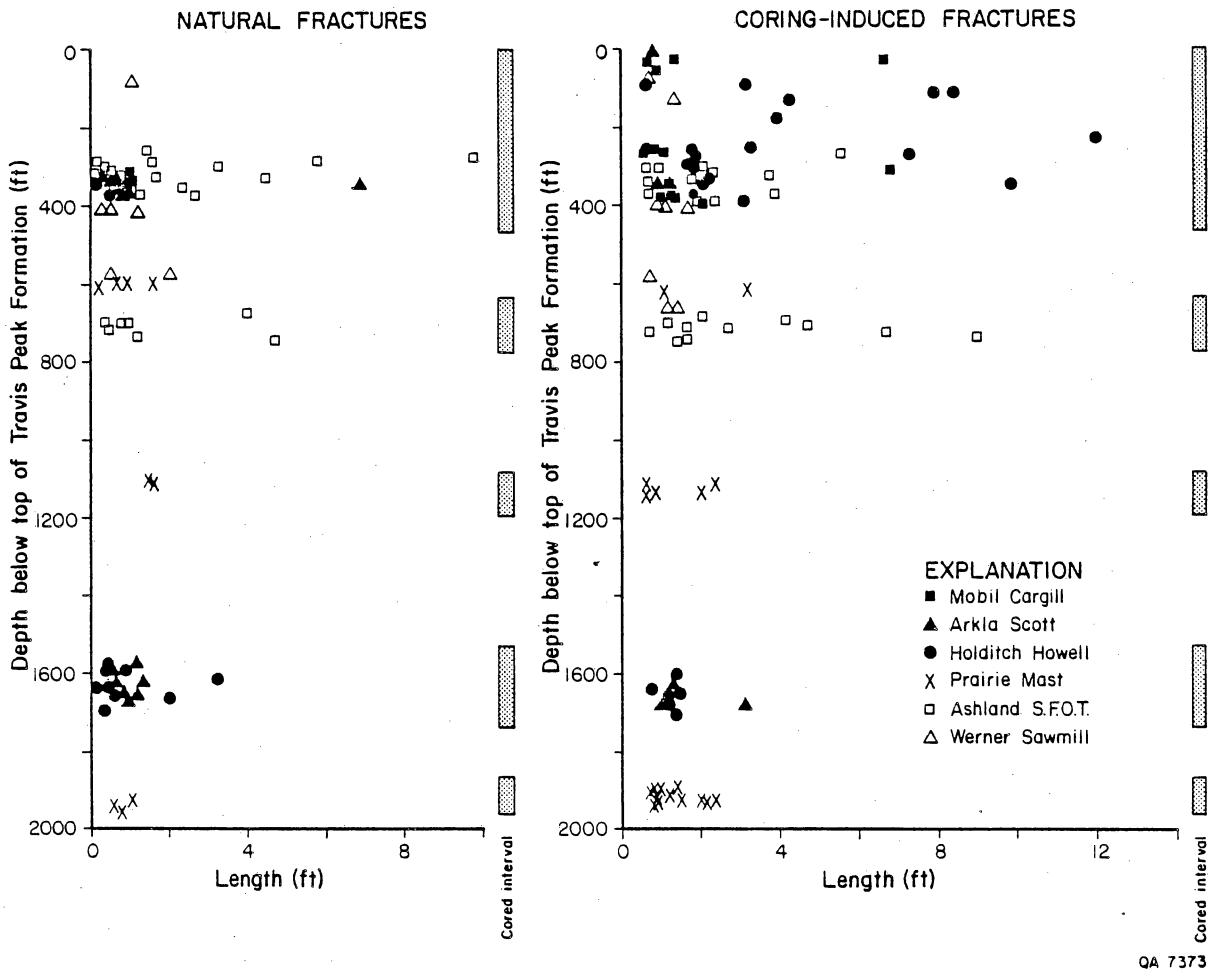

Figure 12. Graph of natural and coring-induced fracture length versus depth below the top of the Travis Peak Formation.

decreases with depth below the top of the formation, but no consistent pattern is evident in natural fracture length with subsurface depth (figs. 11 and 12). Decreasing fracture height with increasing stratigraphic depth parallels trends of increasing quartz cementation and decreasing porosity with depth, but no trend is evident in sandstone bed thickness with stratigraphic position that could account for the variation in the fracture-length pattern (Dutton, 1987; Fracasso, 1987). The spacing of natural fractures in the Travis Peak could not be measured because the diameter of the 4-inch core is less than fracture spacing.

Cumulative fracture length in core and number of natural and coring-induced fractures vary in one 100 ft interval that was cored in all three Waskom field study wells (fig. 13). Rock type and bed thickness are comparable in this interval. The greatest number of natural fractures occurs within a subtle monoclinal flexure that is parallel to the fracture trend (figs. 2 and 13), suggesting that intensity of fracturing varies with position in the structure.

Petrology of Fracture-filling Minerals

Most sandstone fractures are lined by both quartz and ankerite, but some fractures contain only quartz, and some small fractures in clay-rich rocks are filled entirely with clay minerals. Locally, natural fractures are associated with hydrocarbon fluorescence, hydrocarbon odor, mud gas shows, and some contain oil. Fracture filling quartz occurs as faceted crystals and thin (50 to 100 μm) overgrowths in optical continuity with adjacent quartz grains (figs. 14 and 15). Ankerite occurs as yellowish-white to yellowish-brown, blocky, rhombohedral crystals that are commonly widely spaced (1 to 5 mm) on fracture surfaces and have diameters between 100 μm and 1 mm. Less commonly, ankerite occurs on fracture surfaces as coalescent masses or

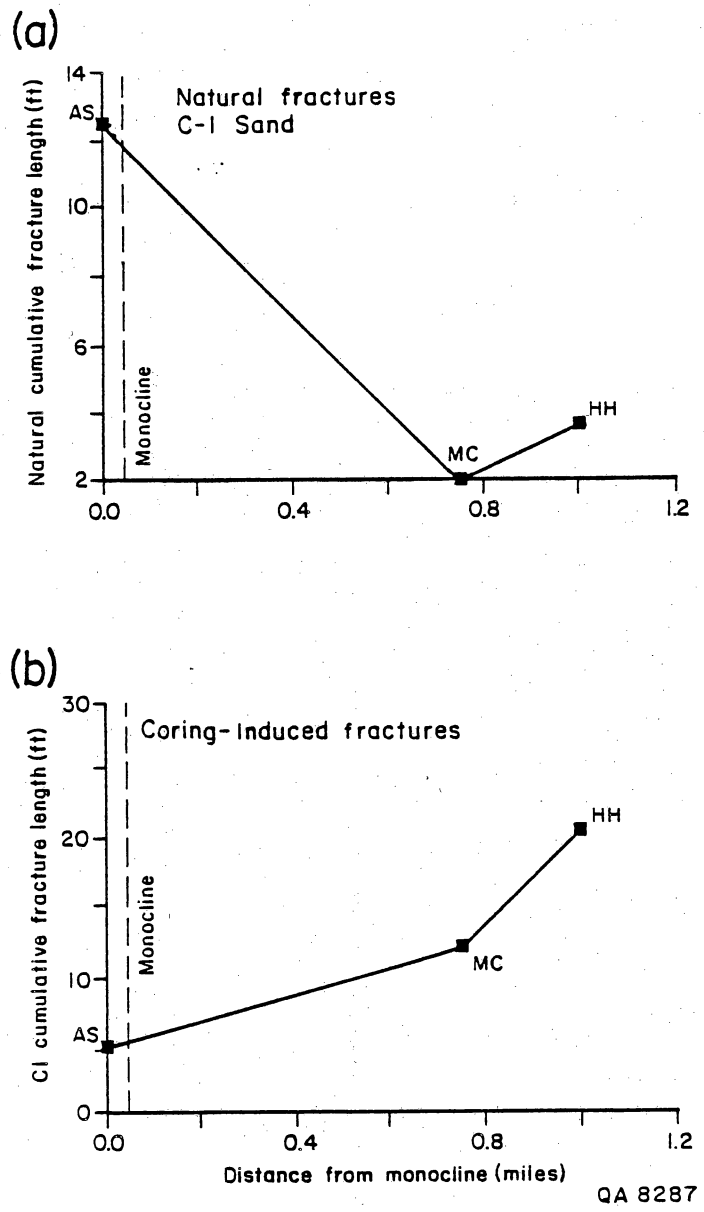

Figure 13. Variation in cumulative fracture length (e.g., total measured vertical length of fractures) versus distance from Waskom field monocline in stratigraphically equivalent intervals. (a) Cumulative length of natural fractures in correlative 100-ft-thick sections of the Travis Peak versus distance from the east-trending monocline shown in figure 2. (b) Cumulative coring-induced fracture length in the same interval. Differences could reflect the influence of enhanced fracturing in monocline. HH, Holditch Howell No. 5; MC, Mobil Cargill No. 14; AS, Arkla Scott No. 5 (within monocline).

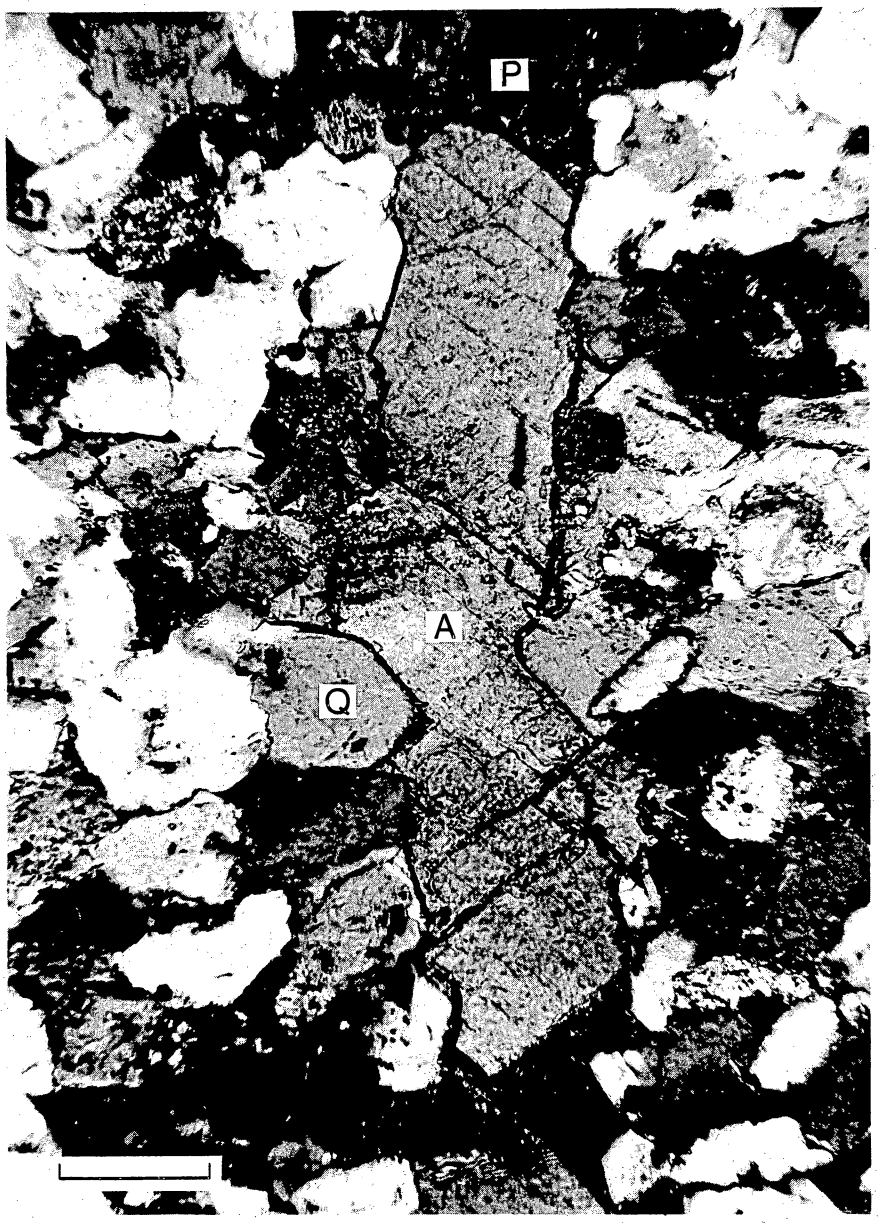

Figure 14. Evidence of open natural fractures from Holditch Howell No. 5 core at a depth of 6,241.5 ft. Photograph of ankerite crystal bridging natural fracture. Note minor fractures and narrow twin lamellae within ankerite and faceted quartz overgrown by ankerite. Ankerite occupies only about 10 percent of the volume of this fracture; the rest of the fracture volume represents open subsurface porosity.

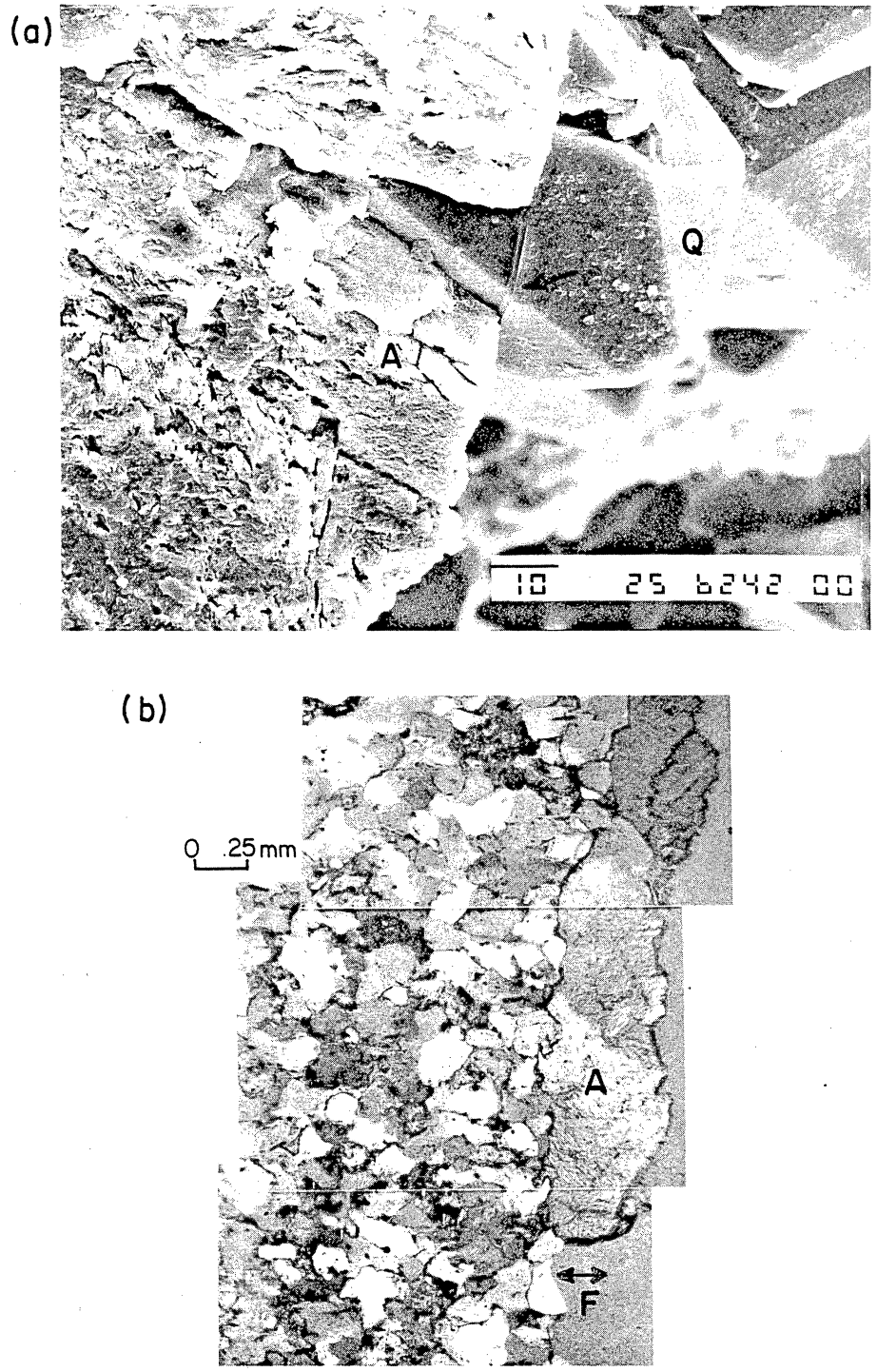

Figure 15. Evidence of the precipitation sequence quartz → ankerite. (a) SEM image of faceted quartz and ankerite on fracture surface, Holditch Howell No. 5, 6,242.3 ft. (b) Photomicrograph showing cross-sectional view of fracture and quartz-ankerite mineralization. Note the faceted quartz overgrown by ankerite.

ankerite completely fills fractures. Ankerite does not occur in all natural fractures. Ankerite is the most conspicuous fracture filling mineral because of its relatively large crystal size. However, quartz is more abundant because it is uniformly distributed over fracture surfaces. The fine-grained clay minerals locally filling fractures are morphologically similar to diagenetic illite elsewhere in the Travis Peak. The zeolite analcime ($NaAlSi_2O_6 \sim H_2O$) occurs as rare, isolated, white 0.5-mm-diameter crystals at 1,901 m in the Holditch Howell No. 5 well, where it is closely associated with ankerite. It was identified on the SEM on the basis of cubic crystal morphology and qualitative EDS spectra (fig. 16). The possible presence of analcime could indicate low silica concentrations in contemporary fracture-filling fluids (Sand and Mumpton, 1978).

Crosscutting relations establish the sequence in which fracture-filling minerals precipitated. Quartz precipitated first; it shows euhedral growth faces against both ankerite and clay minerals (figs. 14 and 15). Where quartz and ankerite occur together, the sequence of precipitation is quartz followed by ankerite. Feldspar exposed on fracture surfaces has a pitted or skeletal appearance that indicates partial dissolution of feldspar following fracture opening and quartz precipitation. Detailed observations of ankerite-quartz relations suggest that quartz could have continued to grow during early ankerite precipitation, or alternatively, that an episode of ankerite growth was followed by a minor episode of quartz precipitation (fig. 15), but these relationships are ambiguous. Clay-mineral precipitation followed ankerite precipitation, on the basis of clay coating on ankerite-quartz contacts in fractures. Some clay minerals may also have coated fracture-filling quartz prior to at least some ankerite precipitation, but this relationship has not been demonstrated by clear cross-cutting relations. Timing of fracture-filling mineral precipitation is best documented from

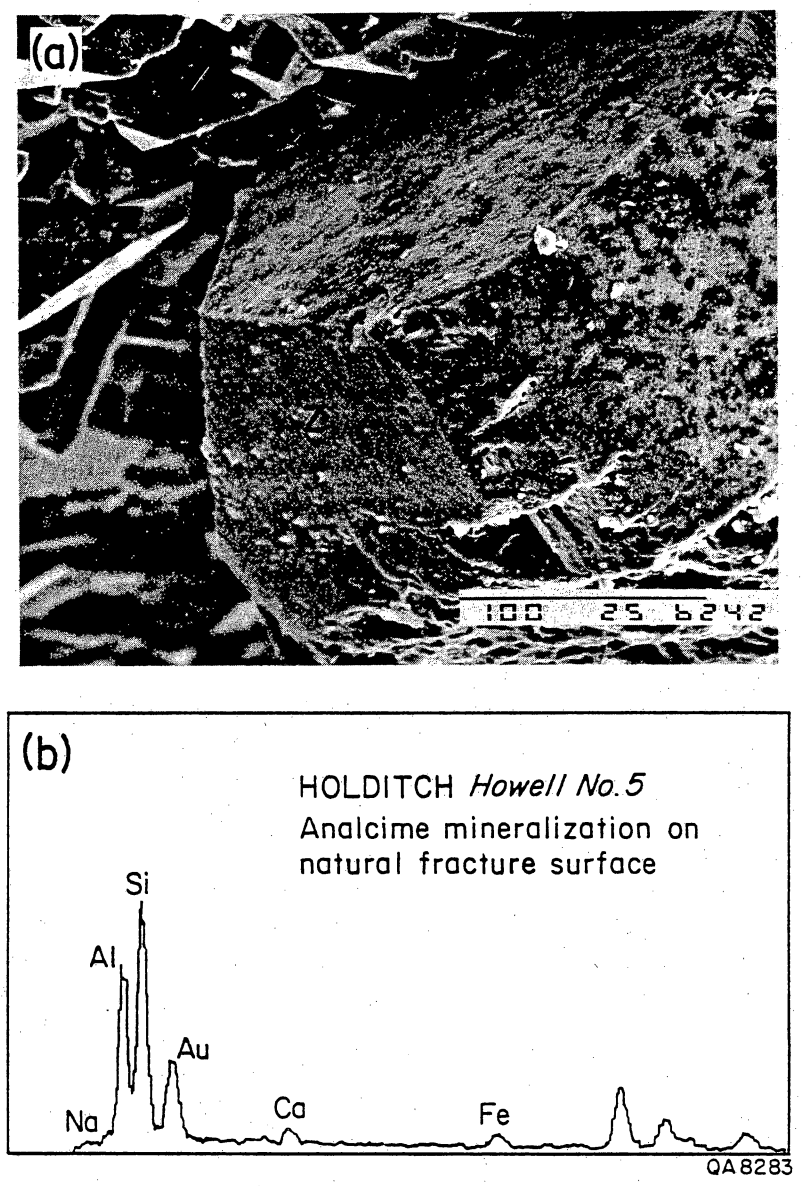

Figure 16. Zeolite fracture mineralization. (a) SEM image of the zeolite analcime on fracture surface. (b) Representative EDS spectra from this sample.

fractures in the upper Travis Peak in Waskom field, but it is also evident in samples from other areas of East Texas.

Some natural fractures are partly open (that is, open to pore fluid and not mineral filled) (figs. 14 and 15); the maximum aperture of open fractures is 2 mm, but open fractures typically have apertures of less than 0.5 mm. Preservation of delicate fracture-bridging minerals in unbroken open fractures demonstrates that these fractures were open in the subsurface. Quartz crystals on opposite sides of open fractures shows no sign of fracturing, abrasion, or dissolution (fig. 17). Since fracture closure would have damaged crystal faces on fracture walls, these fractures have probably remained open after precipitation of quartz cement.

Fracture-filling quartz in the upper Travis Peak contains planes of fluid inclusions that parallel fracture walls and are symmetric about the centerline of the fracture (fig. 18a). These structures are indicative of the process known as crack-seal deformation (Ramsay, 1980a). The alternation of inclusion planes and clear quartz indicates that each matched pair of fluid inclusion planes represents an increment of quartz growth into a partly open fracture; subsequent reopening of the fracture occurred preferentially along the fracture centerline. As many as five episodes of crack-seal deformation are recognized in Travis Peak fractures on the basis of symmetric planes of fluid inclusions. Quartz with crack-seal structure is developed discontinuously along fractures. Planes commonly occur within irregularly shaped pillars and patches of fracture bridging quartz (fig. 18). Fluid-inclusion planes within mineralized macrofractures differ from the transgranular fluid-inclusion planes in that the inclusions are larger and less closely spaced in vein quartz than in the healed microfractures.

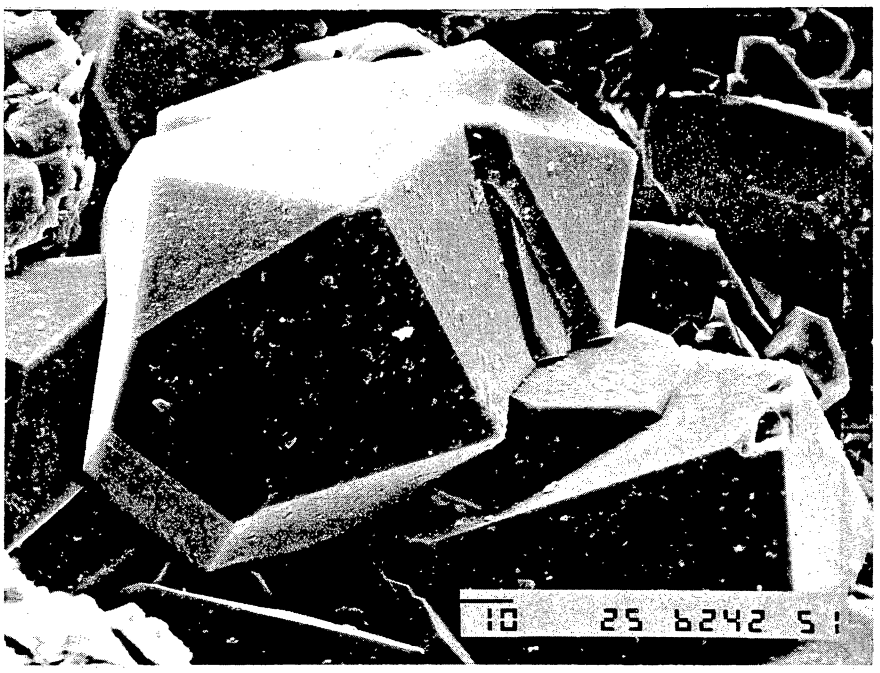

Figure 17. Fracture-lining quartz (SEM image). Bar is 10 microns. Holditch Howell No. 5, 6,242.1 ft.

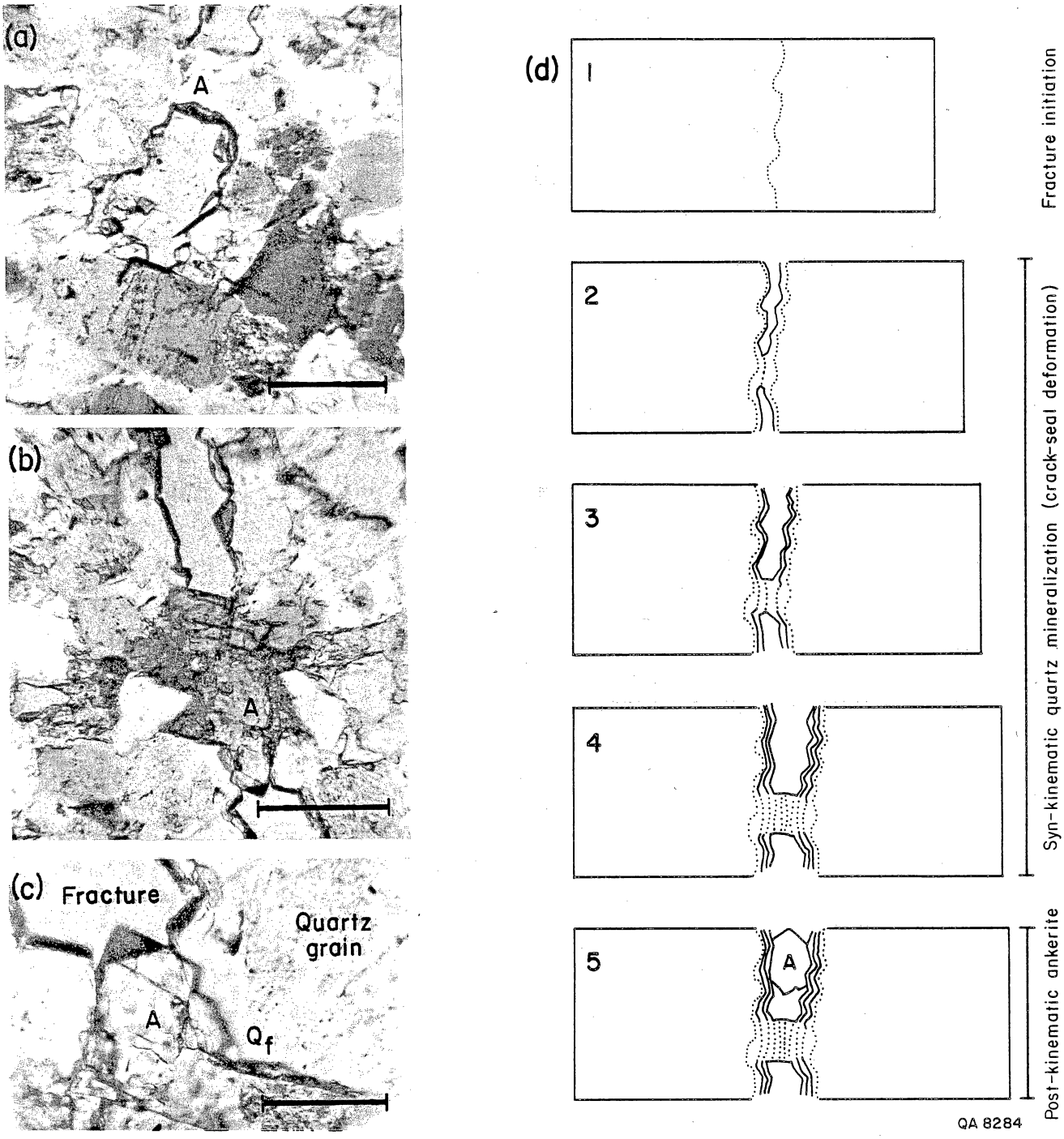

Figure 18. Evidence of crack-seal deformation and mineralization sequence. (a) Multiple, parallel, symmetric fluid-inclusion planes parallel to main fracture within vein-filling quartz. Note unfractured ankerite bridging fracture. (b) Post-kinematic, unfractured ankerite. Simple crystallographic terminations facing open fracture demonstrate that ankerite did not form by crack-seal mechanism. (c) Fractured quartz grain with fracture-filling quartz overprinted by post-kinematic ankerite. (d) Crack-seal model of fracture evolution based on mineral relations in Travis Peak fractures. Each stage in the diagram represents a cross section of the fracture at the end of a crack-seal cycle. The last sketch illustrates the relations shown in (a).

In contrast to quartz, ankerite shows no evidence of crack-seal deformation; it is post-kinematic in origin (fig. 18). Ankerite typically occurs as single crystals with subhedral terminations aligned parallel to the fracture plane. Internally, ankerite has sparse thin twin lamellae and narrow, rare intragranular fractures striking across, rather than parallel to, the main fractures (fig. 14).

Microfractures

Different types of microfractures in rocks have been described by various workers (Tuttle, 1949; Simmons and Richter, 1976). Some microfractures are open cracks with no secondary alteration or mineralization, some are partly or completely filled with secondary minerals, and some remain only as planes of fluid inclusions. Three types of microfractures are evident in Travis Peak rocks: (1) planes of fluid inclusions that represent closed, healed, microfractures; (2) open transgranular microfractures; and (3) open grain-boundary cracks. Only fluid-inclusion planes and grain-boundary cracks are described here. Open transgranular microfractures are interpreted as having resulted from drilling and core handling.

Quartzarenites contain planes of transgranular and intragranular fluid inclusions 0.5 to 2 mm long (fig. 19). Transgranular inclusion planes crosscut grains and quartz cement with no deflection at grain boundaries or evidence of crystallographic control. They are composed of closely spaced, small ($<10\mu m$) fluid inclusions that locally show transitional shapes between tubes and spheres. Locally, regions of unhealed microcrack and plate-shaped pores grade laterally into coplanar cylindrical or spherical inclusions. The quartz between fluid inclusions is in optical continuity with host grains and appears to have the same luminescence as the host grain. Multiple planes composed of two outer planes of minute fluid inclusions symmetric about an inner plane of

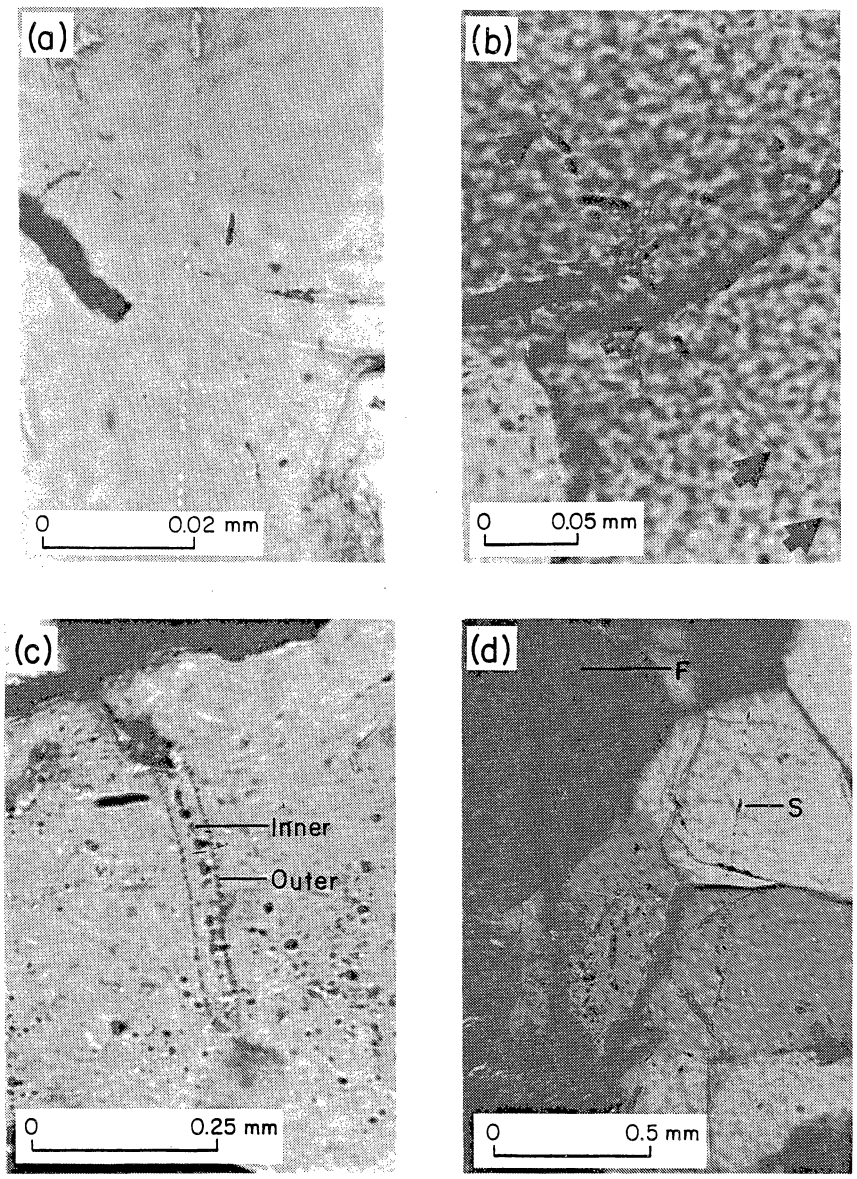

Figure 19. Photomicrographs illustrating healed microfractures. (a) Transgranular fluid-inclusion plane. Clayton Williams Sam Hughes No. 1, Panola County, 7,095.3 ft. (b) Transgranular plane (indicated with arrows). Note tabular aspect of fluid inclusions, Prairie Mast No. 1-A, 9,161.0 ft. (c) Plane composed of several planes arranged in a symmetric pattern (possible crack-seal vein), Mobil Cargill No. 14; arrows indicate inner and two outer planes. (d) Plane S transecting several grains, and cement, Arkla Scott No. 5, 7,454.9 ft. Note associated, parallel fracture, F.

coarser inclusions (fig. 19c) are rare, except where planes occur within sealed macrofractures (fig. 18). The small size of many inclusions (1 to 5 μm) hinders analysis; they appear to be composed of a single phase, possibly a brine. Locally, discontinuities in inherited features such as disseminated impurities within quartz grains show that transgranular planes are associated with reprecipitation of quartz. Intragranular fluid-inclusion planes, in contrast to transgranular planes, commonly consist of widely spaced, irregularly shaped, unequal-sized inclusions in randomly oriented planes. Commonly, planes emanate from grain-grain contacts and pass through or near grain centers. The longest planes occur where grains are arranged in vertical pillars.

Previous experimental studies (Lemmlein and Kliya, 1960; Smith and Evans, 1984) and observations of deformed rocks (Tuttle, 1949; Sprunt and Nur, 1979; Lespinasse and Pecher, 1986) show that fluid-inclusion planes with characteristics identical to the planes in the Travis Peak Formation are closed microfractures. Intragranular planes could be healed fractures inherited from source rocks that ultimately provided clastic grains for the Travis Peak Formation, but planes that are continuous across cement or several sedimentary grains must have formed after sandstone deposition, and they record fracture propagation and healing in the diagenetic environment.

Transgranular fluid-inclusion planes in Travis Peak sandstone show an east-northeast preferred orientation (figs. 4 and 20) that is parallel to natural fracture trends. Fluid-inclusion-plane attitude was measured in sets of three orthogonal thin sections on the universal stage. One section was always cut parallel to bedding. Because of the small size of the planes, it was not possible to identify the same fracture in different thin sections to check orientation estimates. Samples were cut from core containing natural macrofractures and from oriented core that lacked

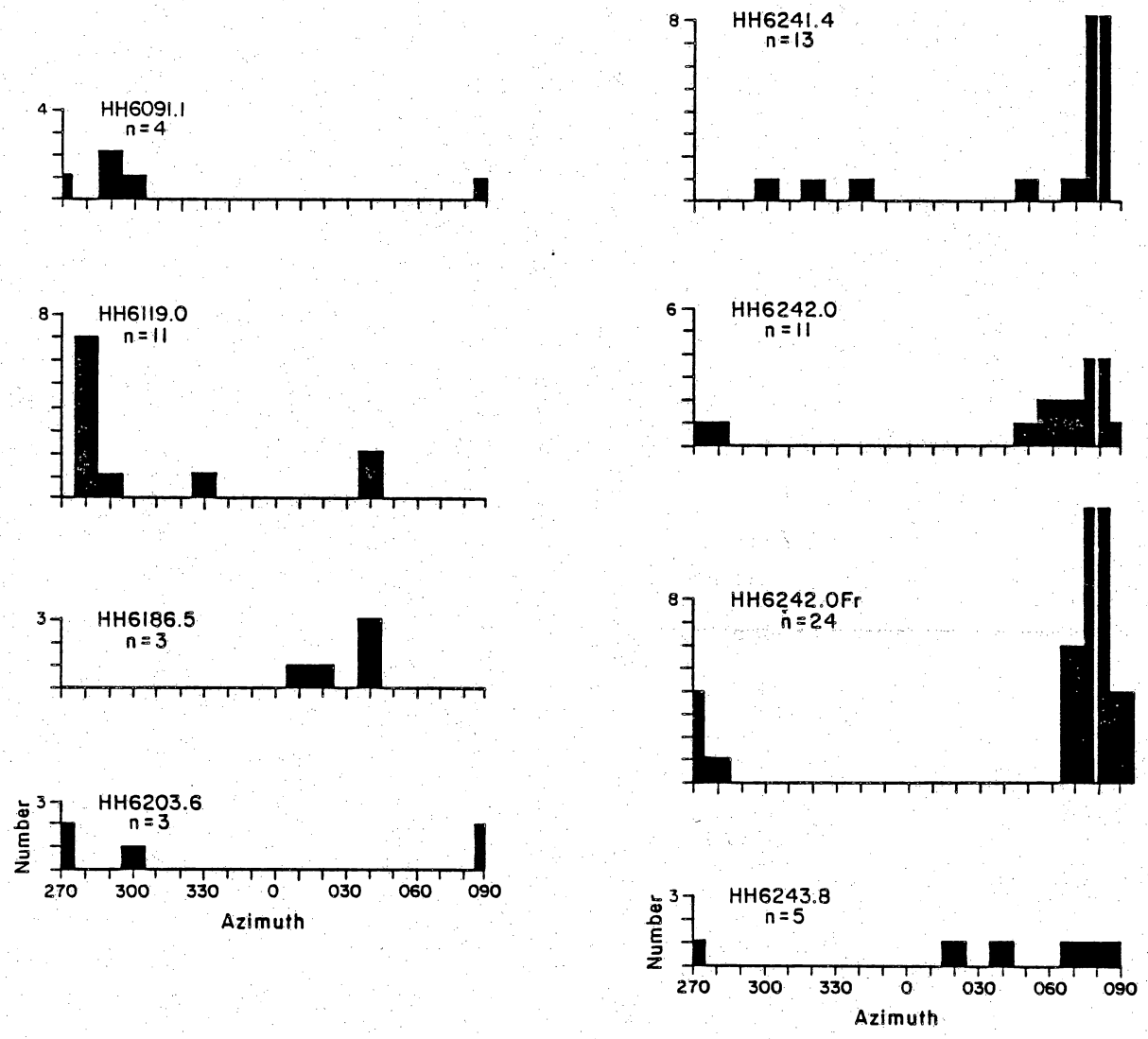

Figure 20. Histograms of the strike of transgranular planes at various depths, from Holditch Howell No. 5 core.

macrofractures; both yielded consistent microfracture trends. The dips of transgranular planes are also regular; steep dips are most common, but inclinations as gentle as 50 degrees are present. Microfracture attitudes are therefore comparable to macrofracture attitudes.

Transgranular planes are most common in quartz-rich rocks and are less abundant in rocks with clay matrix, abundant clay cement, or significant proportions of feldspar or calcite (fig. 21a). Planes are most abundant adjacent to macrofractures, but also occur in low concentrations distant from large fractures in quartz-rich rocks. Coarser, more poorly sorted rocks tend to contain more transgranular planes than do very fine grained, well-sorted rocks. Systematic counts indicate that as many as 10 to 20 transgranular planes per cm^3 occur in quartz cemented quartzarenites, and planes are more abundant near mineralized macrofractures. The abundance of transgranular planes was estimated by scanning a thin section for 20 minutes. Measured in this way, microfracture abundance does not show significant variation with depth, log-derived mechanical properties (fig. 21b), original porosity (fig. 21c), or stratigraphic position (fig. 21d). Because of the small size of the transgranular planes, point counting techniques tend to underestimate fluid-inclusion plane abundance. Furthermore, the preferred orientation of planes also introduces potential variability in apparent abundance since counts were made on randomly oriented thin sections.

Under SEM grain-boundary microcracks are also visible in Travis Peak sandstone (fig. 22). These microcracks have been observed at contacts between domains of quartz cement. They are shorter and narrower than the healed microfractures described previously. These cracks are too small to be visible with the petrographic microscope, and their orientation was not measured. Because they are open and unhealed, they could have formed by core expansion at the surface after core retrieval.

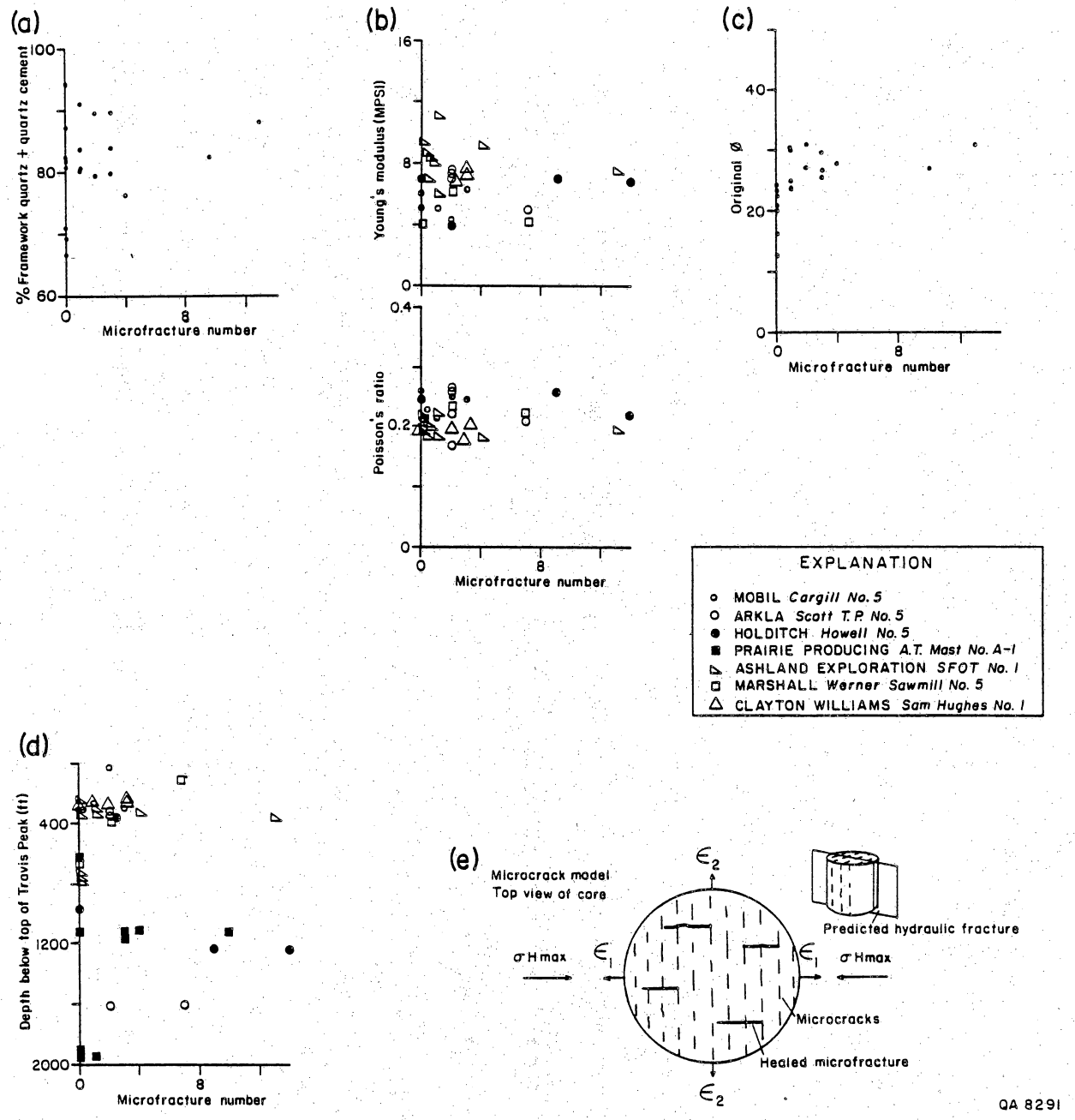

Figure 21. Relation of healed microfractures to other rock properties, burial depth, and other microstructures. Except for dependence on rock composition, microfracture abundance has little relation to other factors. (a) Comparison of microfracture number to volume of quartz cement (n/cm^3); the wide range of values at high quartz content is partly a consequence of sampling bias: planes that have a preferred orientation are not uniformly sampled with randomly oriented vertical thin sections. (b) Microfracture number and rock mechanical properties derived from FracLog (Hunt, 1986). (c) Original porosity (present/primary porosity, plus total cement). (d) Depth below top of the Travis Peak. (e) Microcrack model for strain recovery and sonic velocity anisotropy of core. Healed microfractures in Travis Peak sandstone do not correspond to the microcracks of this model.

(a)

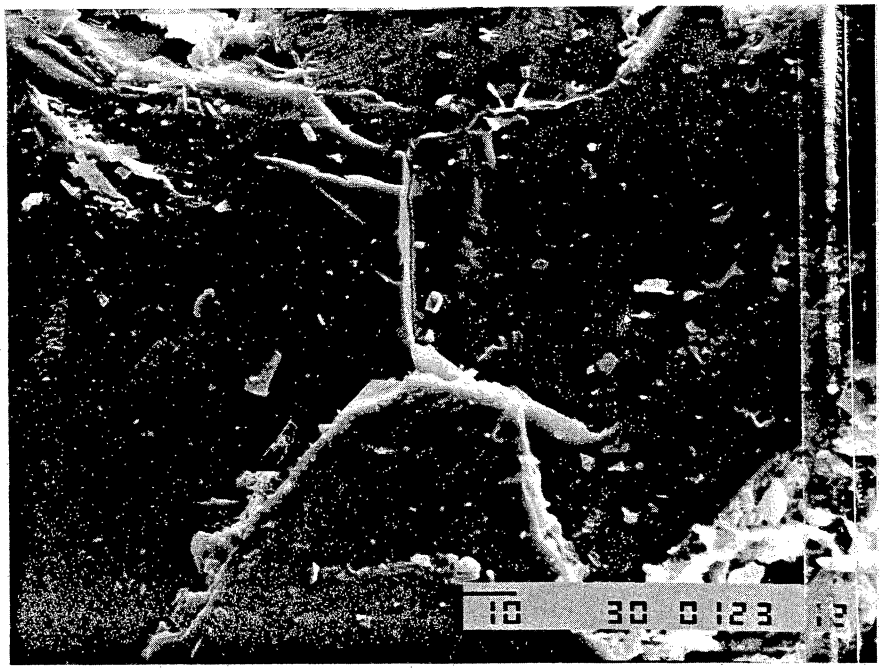

(b)

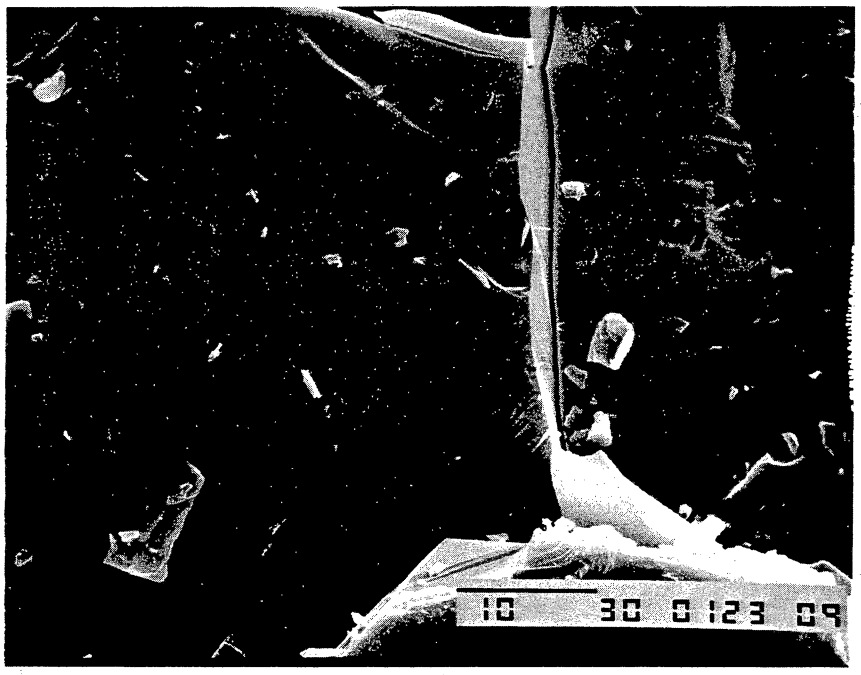

Figure 22. SEM images (a, b) of grain boundary crack, Arkla Scott No. 5, 7,453.3 ft.

Regional Trends

Waskom field and the wells in northern Nacogdoches County differ in structural setting. In northern Nacogdoches County, the top of the Travis Peak is approximately 2,000 ft deeper than in Waskom field, and regional bedding dip is to the southwest rather than the northwest, as a result of Tertiary regional gulfward tilting. Recent activity on the Elkhart-Mount Enterprise fault zone (Collins and others, 1980), a north-facing, east-trending normal fault system, suggests that the state of stress in northern Nacogdoches County could differ from the stress state in Harrison County, where there are no active faults.

Despite the differences in structural setting, the appearance and mineralization of natural fractures are similar in all core examined so far, and significant differences in fracture trend between these two areas have not yet been detected. There is some indirect evidence of multiple fracture trends in northern Nacogdoches County; small mineralized fractures with orientations differing by more than 40 degrees occur in one slabbed, continuously fitted section of unoriented Prairie Mast No. 1-A core, and similar relations are present in Ashland S.F.O.T. No. 1 core. In contrast, microfracture trends and BHTV fracture trends in the Waskom field are somewhat more uniformly oriented (figs. 3 and 5). However, the seven natural mineralized fractures in the Clayton Williams No. 1 Sam Hughes also show a wide range of trends, from 045 degrees (northeast) to 310 degrees (northwest)(fig. 3). These comparisons are limited by sparse data on natural fracture orientation.

Differences in fracture and microstructural style are apparent between the Waskom field wells and the Prairie Mast No. 1-A and Ashland S.F.O.T. No. 1 in northern Nacogdoches County. Natural fractures in Prairie Mast No. 1-A sandstone are short,

have small apertures, and are commonly tightly cemented with quartz and contain little or no carbonate. In contrast, in Waskom field natural fractures in sandstone include fractures with height exceeding 2 m and that locally have large (2 mm) apertures. However, the variability of fracture length and width within Waskom field suggests that local, field-scale contrasts in natural fracture patterns arising from variations in the degree of quartz cementation and from differences in structural position may be as great as these apparent regional differences.

Mudstone Fractures

Physical Characteristics

Natural fractures in mudstone are randomly oriented, gently dipping shear fractures with downdip linear surface marks ("slickenside striations") (figs. 23 and 24). Only one short calcite-filled dilational fracture in mudstone was observed. In addition to slickenside striations, fracture surfaces commonly show long wavelength (>5 cm) undulations transverse to the striation trend. Apart from striations, fracture surfaces are smooth and highly polished. Identical fractures have been produced experimentally by Means (in press) who demonstrated that they form by shearing. Fractures show no systematic geometric relationship to the core and were therefore not produced by coring. Fracture dips range from 40 degrees to subhorizontal (fig. 25), most fractures having gentle dips. Strikes of shear planes and trends of slickenside striations have a wide orientation range (fig. 25).

The striations are straight ridges and grooves that are matched on opposed fracture surfaces so that fracture surfaces fit together precisely. In cross section, the ridges and grooves are not smooth curves, but instead are composed of planar

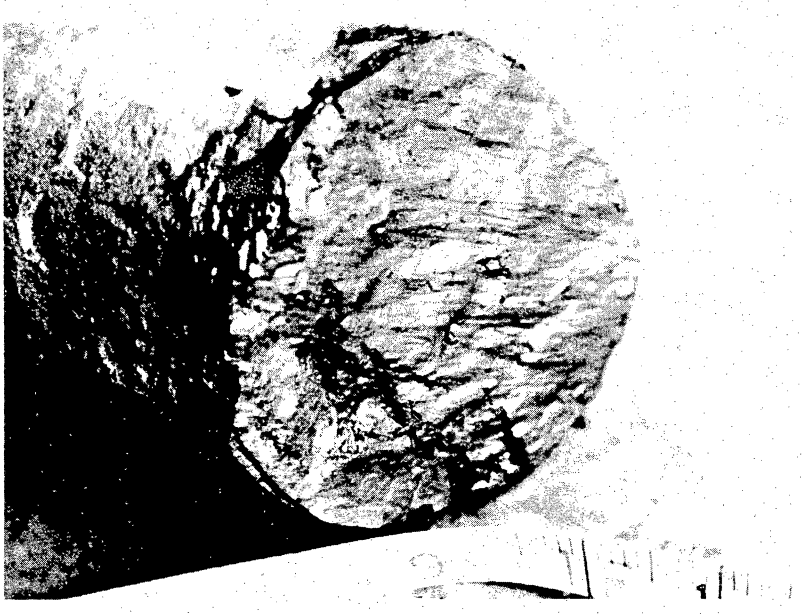

Figure 23. Core photograph of shear fracture, Holditch Howell No. 5 core, 6,024 ft.

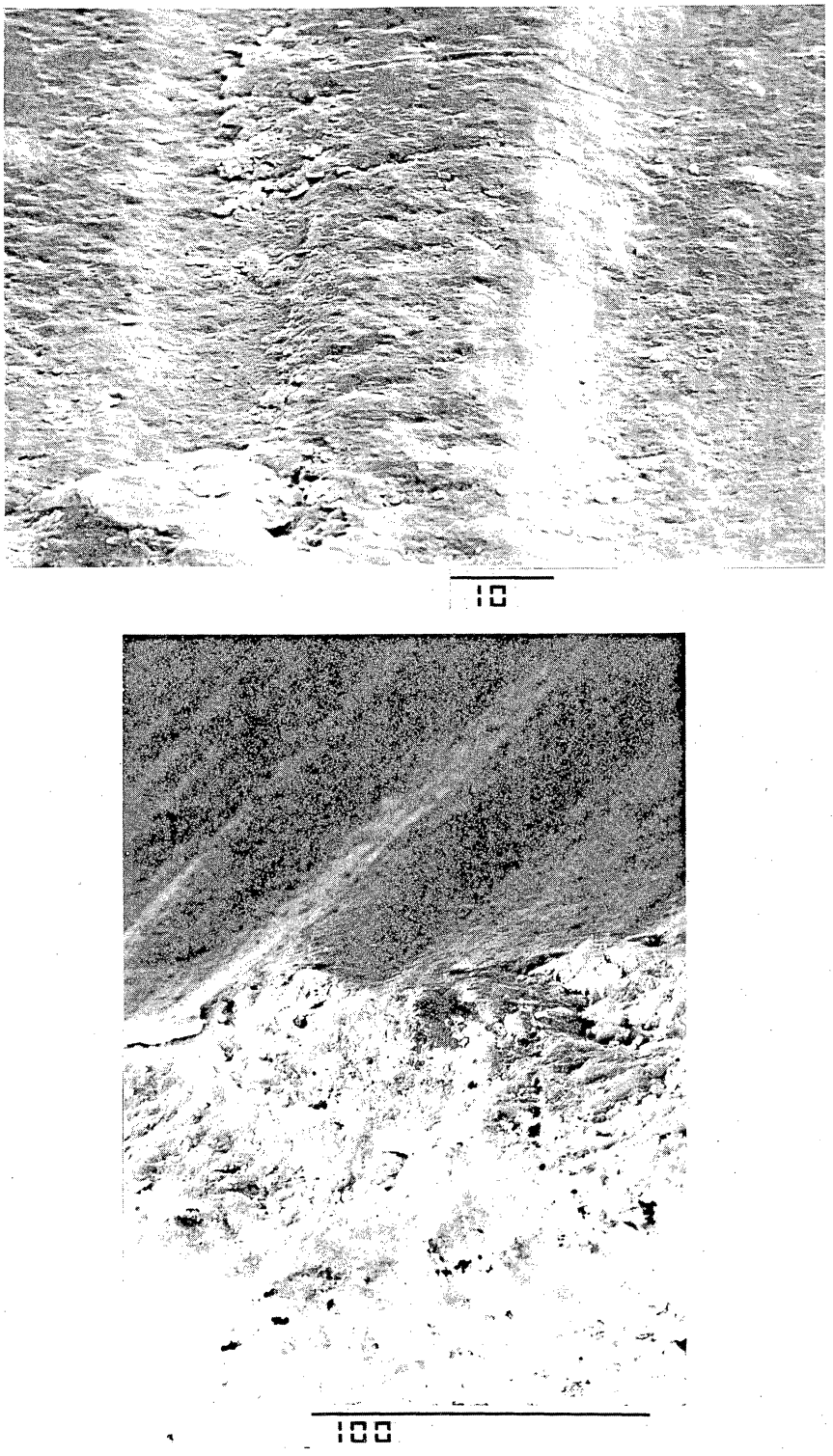

Figure 24. SEM images of shear fracture slickenside striation shape, Prairie Mast No. 1-A, 8,626 ft. The upper photograph shows views of both fracture surface and fracture cross section. Bar scale is in microns.

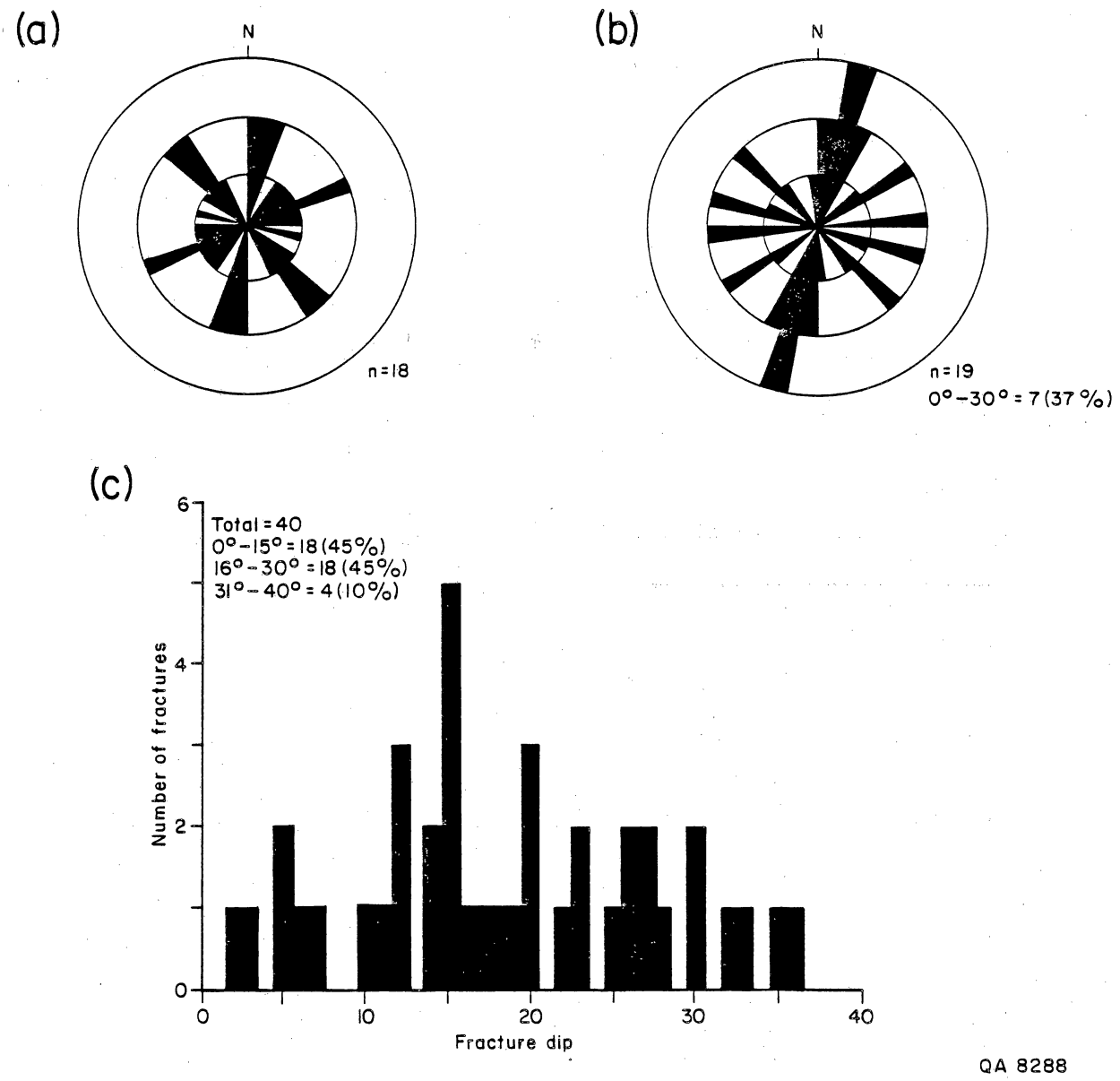

Figure 25. Rose diagrams and histograms of shear fractures and slickenside striation attitude. (a) Strike of fractures in mudstone. Mobil Cargill No. 14. (b) Trend of slickenside striations. Mobil Cargill No. 14. (c) Histogram of mudstone fracture dips. all East Texas wells.

surfaces (figs. 23 and 24). Striations have similar shapes at all scales and commonly extend across entire exposed fracture surfaces (up to 20 cm) with little change in shape. Offset on these shear fractures cannot be estimated because offset marker horizons are absent within core; it is therefore impossible to rule out some shortening across these surfaces. By analogy with similar structures exposed in outcrop (Means, in press; Laubach and Griffiths, 1986) the striations are probably longer than the total displacement along the polished surfaces in the direction of the striation trend. The striations are undulations on the fracture surface; no rigid inclusions, asperities, debris trails, or fibrous mineral growths that could cause the striations or that could be used to measure sense of movement are evident on fracture surfaces.

Cross sections of shear fractures in mudstones show that the polished, striated fracture surfaces are actually the upper parts of tabular deformation zones with thicknesses approximately equal to twice the height of slickenside striations (50 to 100 μm) (fig. 26). Within these zones, the rock appears finer grained, and is denser, more strongly indurated, and presumably less permeable. These domains of reduced grain size do not correspond to bedding. In some samples, domains of progressively reduced clay-mineral particle size are visible parallel to the fracture zone itself (fig. 26), supporting the inference that grain-size reduction was produced by deformation associated with fracturing.

Interpretation of Mudstone Fractures

If the mudstone fractures are the result of vertical loading and compaction, the acute angle between brittle shear fractures should face the greatest shortening direction (Anderson, 1951), and therefore should have steep dips (fig. 27a). Two

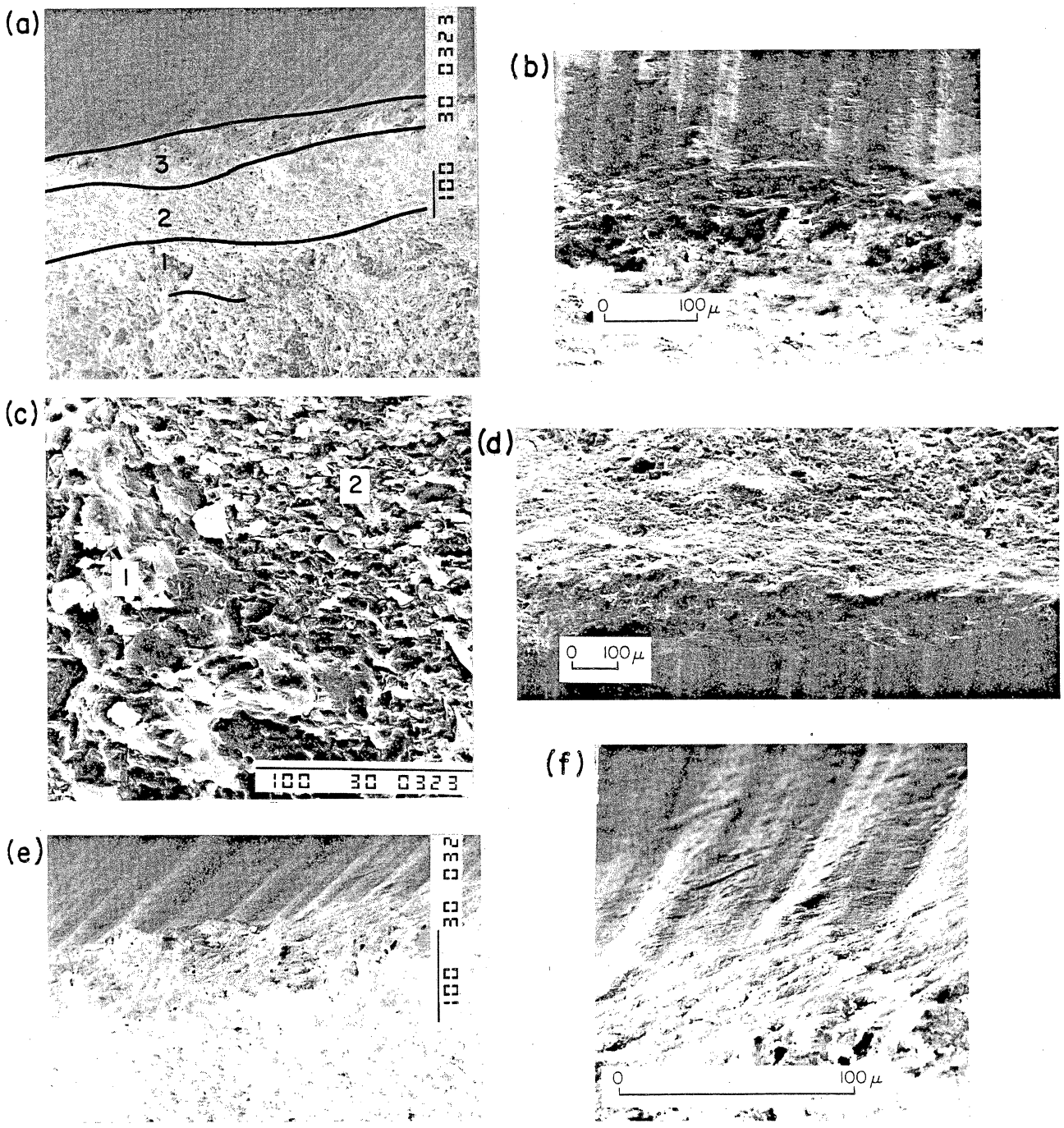

Figure 26. SEM of grain-size reduction domains parallel to shear fracture. Prairie Mast No. 1-A, 8,626 ft. (a) Domains of apparent reduced grain size. (b) Apparent grain-size differences adjacent to fracture. (c) Detail of grain-size reduction from zone 1 to zone 2 (boundary runs from upper left to lower right). (d) Possible development of preferred orientation near shear fracture. (e) Domainal character of mudstone fabric near shear fracture. (f) Detail from (e) of foliation development. Bar scale on all photographs is in microns.

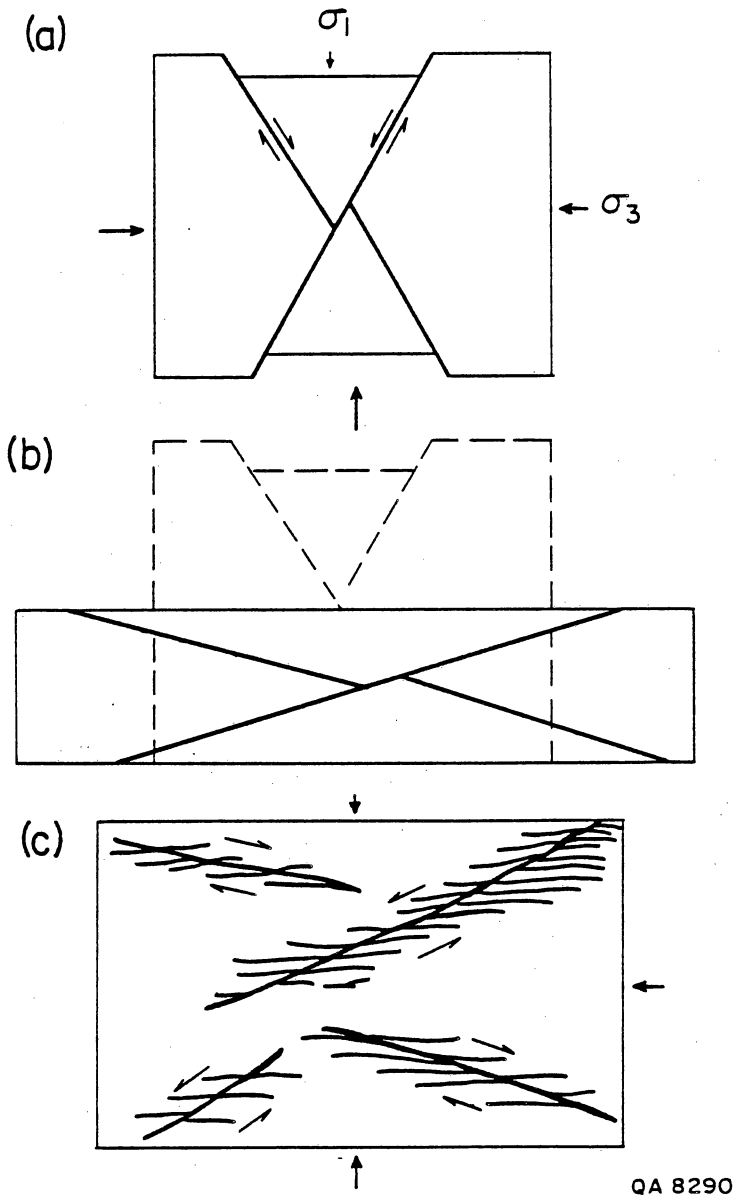

Figure 27. Alternative models of mudstone shear fracture development by compaction. Horizontal lines in (c) represent clay mineral preferred orientation caused by shearing. See text for discussion.

possibilities could explain the observed gentle dips. Fractures may have formed with steep initial dips and then rotated as material planes during subsequent penetrative flattening (compaction) of intervening mudstone (fig. 27b). Alternatively, shear fractures and the associated zones of grain-size reduction may be ductile rather than brittle shear zones (fig. 27c). Surface structures on mudstone fracture slip surfaces and zones of deformed mudstone parallel to the slip surfaces suggest a ductile, rather than brittle, deformation mode. This interpretation in consistent with the experimental observations of Means (in press) and with the gentle dips of the fractures. For ductile shear zones, the obtuse angle between shears faces the greatest shortening direction (Ramsay, 1980b). Some steeply-dipping shear fractures and bedding-parallel flattening fabrics in mudstone provide some support for the first interpretation.

If motion on mudstone fractures is assumed to be normal dip-slip, the orientation of shear fractures and their respective striations can be used to infer the principal directions of discontinuous bulk deformation by Arthaud's (1969) M-pole method (fig. 28). Ideally, the M-pole plot can resolve directions of greatest and least horizontal finite strain, which appear as concentrations of M-poles on the diagram, and the results could be used to infer the orientation of horizontal paleostresses. The results obtained are consistent with formation of shear fractures by bulk flattening perpendicular to bedding as a result of burial compaction, but the pattern is not sufficiently well defined or asymmetric to resolve any horizontal variation that may exist.

The timing of shear fracturing is unknown. Apparently, similar structures are present in a variety of structural settings, including some soils (see references in Means, in press). As a consequence, the relationship of these structures to sandstone fractures is uncertain. Perhaps the most significant observation concerning these

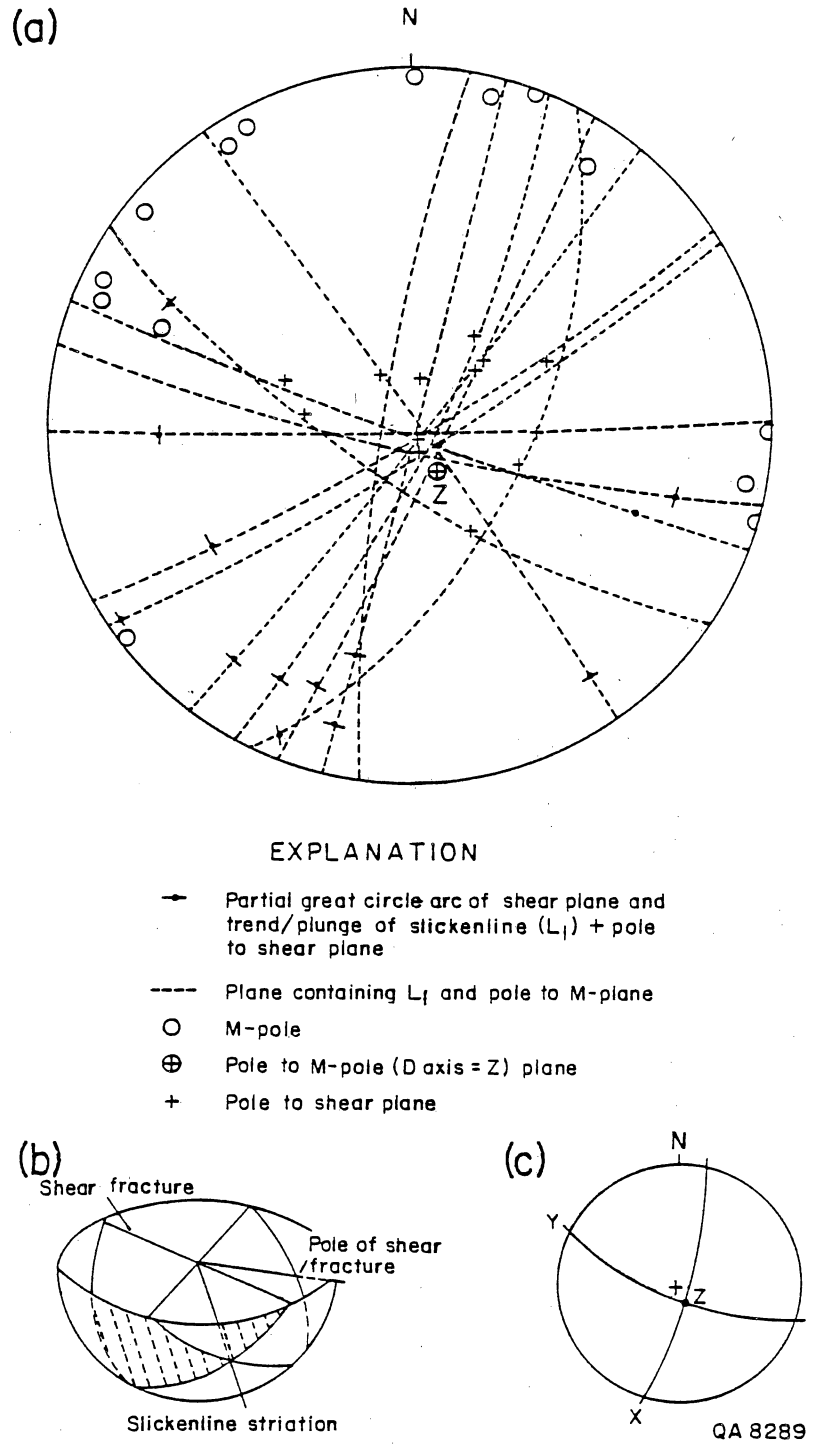

Figure 28. Shear fracture attitudes. Mobil Cargill No 14, 6,213.2 to 6,226.6 ft. (a) M-pole plot for defining the principal planes of anisotropy of the finite-strain ellipsoid in mudstone, a technique that could help predict natural extension fracture patterns in adjacent sandstone. Insets illustrate derivation of plot (b) and one possible interpretation of M-pole pattern (c) for finite-strain ellipsoid attitude (see Arthaud, 1969; Bles and Feuga, 1986). X, Y, and Z represent principal axes of finite strain ($X \geq Y \geq Z$).

features is the lack of associated mineralization, suggesting that they did not act as conduits for the transfer of fluids across shale layers.

CORING-INDUCED FRACTURES

Fractures produced by the coring or drilling procedure possess unique geometries directly related to, and often symmetrical with the core (Kulander and others, 1979). Previous studies have shown that coring-induced petal-centerline fractures tend to have a preferred orientation that may be controlled by rock fabric or contemporary stress (Kulander and others, 1979), a result consistent with observations of petal-centerline fractures in Travis Peak core (fig. 3).

Petal-centerline fractures (Kulander and others, 1979) are coring-induced fractures that are composed of a short, smoothly curving concave downward petal fracture that gradually merges in the down-core direction with a long planar centerline fracture that commonly bisects the core (fig. 29). Fracture inclination ranges from approximately 45 degrees to vertical, whereas the fracture maintains a constant strike. Petal-centerline fractures eventually terminate within the core, and in the Travis Peak cut smoothly across grains and locally display surface markings such as plumose structure typical of rapid fracture propagation in indurated material (Hertzberg, 1983). In contrast to open natural fractures, coring-induced fractures are unmineralized.

Petal-centerline fractures are common in Travis Peak core (figs. 11 and 12; CER Corporation, written communication, 1986) and occur in approximately equal proportions in both sandstone and mudstone. The planar and relatively smooth appearance of fracture surfaces is similar to that of fractures produced during

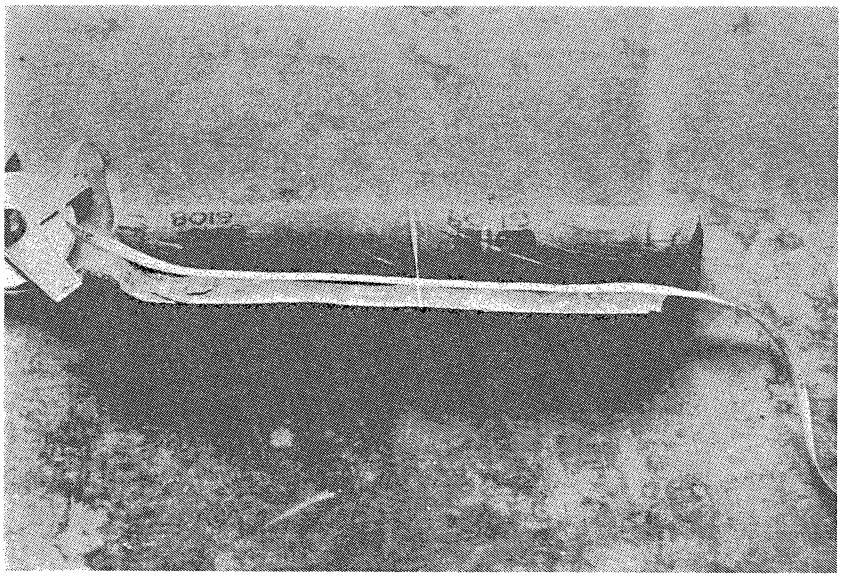

Figure 29. Photograph of coring-induced petal-centerline fracture. Holditch Howell No. 5 well. 6,108 ft.

hydraulic fracture stress tests in the Holditch Howell No. 5 Travis Peak (CER Corporation, 1987a). Petal-centerline fractures have east-northeast strikes in both the upper and lower Travis Peak in Waskom field (figs. 3 and 5). In northern Nacogdoches County, some northwest-trending petal-centerline fractures were observed. Strikes of natural and coring-induced fractures deviate by as much as 30 degrees where centerline fractures and dilational mineralized fractures occur in the same core. In some cases, coring-induced fractures reactivate natural fractures (fig. 6), but generally petal-centerline fractures are not parallel to macroscopic anisotropy in core. Coring-induced fractures have a smaller degree of variation than natural fractures, both regionally and within individual wells in all areas. For example, eight petal-centerline fractures in the same interval of the Clayton Williams No. 1 Sam Hughes ranged between 055 degrees and 280 degrees, but have a mean trend of 070 degrees (fig. 3).

Locally, centerline fractures emanate from lithologic heterogeneities within core, or are coincident with core orientation scribe lines, suggesting that some petal-centerline fractures may have nucleated on core scribe knives after core was separated from surrounding rock. On the other hand, paleomagnetic directions in core segments that contain petal-centerline fractures but that are broken up by horizontal spinoff fractures can be aligned by fitting the core together along the centerline fracture (Van Alstine, 1986), showing that some petal-centerline fractures in the Travis Peak predate spinoff fractures. Petal-centerline fractures that predate spinoff fractures probably propagated in front of the drill bit (Kulander and others, 1979), an interpretation supported by observations of local scoring of petal-centerline fractures by the bit and fractures crosscut by scribe lines.

Petal-centerline fracture length varies with stratigraphic position (figs. 11 and 12) in a pattern that resembles the pattern of natural fracture length with stratigraphic

depth; that is, petal-centerline fractures are longest in the upper Travis Peak and shorter in the lower Travis Peak (figs. 5 and 12), indicating that the ease with which fractures propagate vertically varies in the Travis Peak with stratigraphic position. Abundance of coring-induced fractures across the Waskom field monocline in the same stratigraphic horizon, however, is inversely related to abundance of natural fractures (fig. 13), suggesting that natural fractures may have relieved stresses in the monocline.

In the Holditch Howell No. 5 there is agreement between mean petal-centerline strike (60 to 80 degrees) and the direction of maximum horizontal anelastic strain relaxation (fig. 3). Petal-centerline fractures are not necessarily parallel to natural fracture trends (figs. 3 and 20) and therefore may reflect in situ stress rather than rock anisotropy, a conclusion consistent with the observation that coring-induced petal-centerline fractures trend subparallel to the east-northeast direction of hydraulic fracture propagation in Waskom field (Holditch and others, 1987b).

DISCUSSION

Fracture Timing

Crack-seal structure in fracture-filling quartz indicates that quartz precipitated episodic fracture opening. The predominance of intergranular fracture pathways suggests that fracturing was initiated before quartz cementation was far advanced because transgranular fracturing is favored in highly indurated, quartz-cemented rock (Hamil and Sriruang, 1976). Transgranular microfractures in quartz cement, together with crack-seal structures, indicate continued fracture growth in quartz-cemented rock. Post-kinematic ankerite indicates that fractures had ceased to widen prior to ankerite precipitation.

The genetic sequence of fracture-filling minerals can be used to link the timing of fracture propagation to the diagenetic history described by Dutton (1987) (fig. 30). The diagenetic sequence consists of (1) quartz precipitation, (2) feldspar dissolution, and (3) ankerite precipitation. The same mineralization sequence is indicated by crosscutting relationships among fracture-filling minerals. The close relationship between diagenesis and fracture propagation is also possibly reflected in the parallel variation in the extent of quartz cementation and natural fracture length with depth below the top of the formation.

Dutton (1986, 1987) showed that $\delta^{18}O$ values of quartz cement range between +20 and +24 o/oo (SMOW). The $\delta^{18}O$ composition of quartz overgrowths indicate that they precipitated from meteoric fluids at temperatures between 55° and 75°C, or depths of approximately 3,000 to 5,000 ft at geothermal gradients consistent with current models for the thermal evolution of the Gulf and with vitrinite reflectance data (Dutton, 1986)(fig. 30). If the assumptions involved in specifying the timing of diagenesis are correct, then the conditions and timing of fracture growth are also fixed. The inferred conditions are indicated in figure 30.

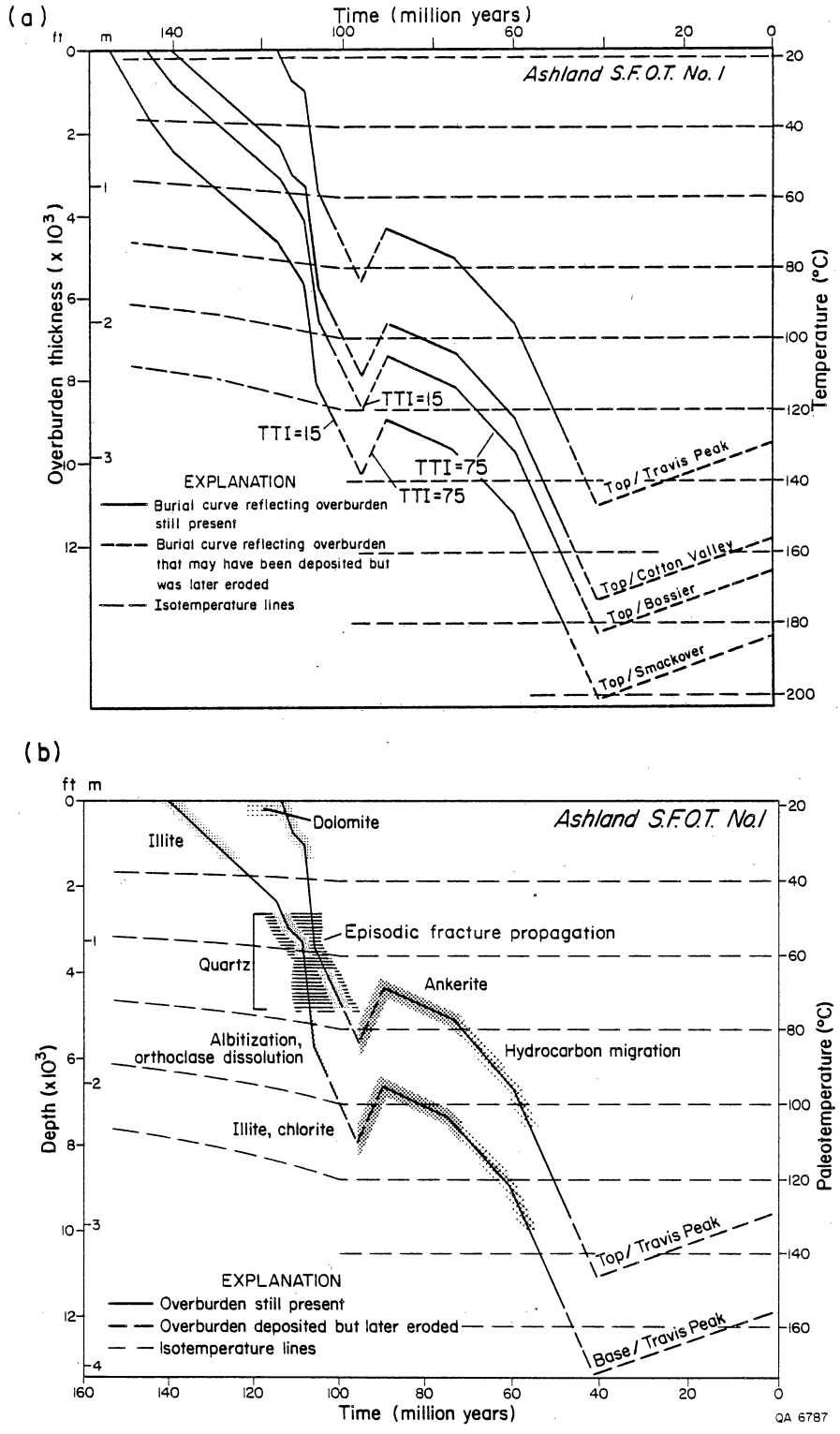

Figure 30. Burial history of the Travis Peak Formation (from Dutton, 1987). Correlation of diagenetic and fracture mineralization sequence specifies (a) timing and (b) conditions of fracture propagation.

Fracture Mechanism

Extension fractures in Travis Peak sandstone are interpreted to be natural hydraulic fractures resulting from fluid pressure in excess of the minimum principal confining stress (σ_3) by at least the tensile strength of the rock (fig. 31) at the time of fracture formation. The close relationship observed between natural fractures and cementation suggests that decreasing permeability, fracturing, and fluid migration are genetically linked. The fractures are unlikely to be the result of thermal-elastic contraction resulting from erosional unloading and cooling because the Travis Peak has never been uplifted by more than a small percentage of its burial depth (Engelder, 1985). Furthermore, the relationship between fracture-fill and diagenetic mineral sequence suggests that fractures propagated during burial rather than during uplift. Moreover, crack-seal fractures provide direct evidence of natural hydraulic fracture, as described below. The regionally developed preferred orientation of fractures indicates that east-southeast-directed tectonic extension accompanied fracture formation.

Hydraulic and tectonic fractures can form at depth in response to near lithostatic fluid pressures (Secor, 1965; Price, 1974; Engelder, 1985). Several mechanisms, coupled with restricted pore-fluid escape, can cause increased fluid pressure, including: compaction, thermally-induced expansion of water, generation and migration of hydrocarbons, and fluid flow induced by regional tectonism or other causes (Smith, 1971; Magara, 1975, 1981; Di-ckenson, 1974; Bethke, 1985; Oliver, 1986). The 1.6- to 3.2-mi depths of overpressure inferred for the Travis Peak are somewhat shallower than the 4.8- to 8-mi depths to overpressure observed in Cenozoic rocks of the Gulf of Mexico basin (Magara, 1975, 1981), but depth of burial does not place a restriction on development of overpressure if pore-fluid escape is sufficiently restricted

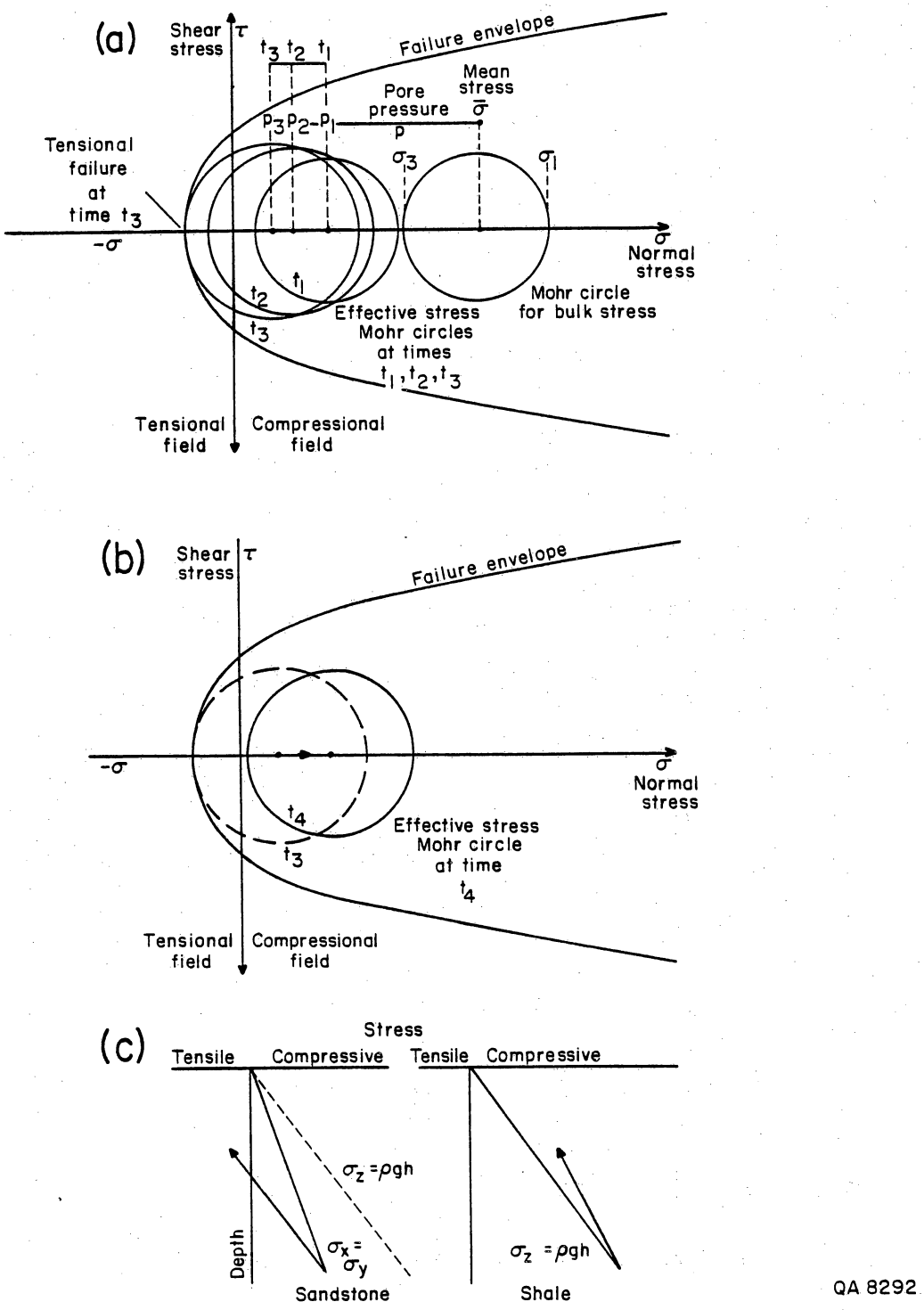

Figure 31. Mohr circle representation of part of the stress history of the Travis Peak Formation. (a) Pore pressure increase drives the effective stress circle down the normal stress axis of the Mohr diagram toward the failure envelope. (b) Uplift and erosion reduce vertical load but also reduce pore pressure. (c) Idealized stress versus depth of burial for sandstone and shale based on Poisson's ratio and thermal effect but neglecting tectonic stress. Lithification and mechanical property changes are shown occurring at maximum burial depth, an assumption that is invalid for the Travis Peak Formation. See text for details.

and large fluid influxes occur.

The conditions that typify overpressure in the Cenozoic of the Gulf Coast, however, are not applicable to the sandstone-rich Travis Peak. In shale-rich Cenozoic rocks, continuous compaction produces a normal hydrostatic vertical fluid-pressure gradient, and undercompaction due to entrapped water produces an abnormal, overpressured trend. As a result, overpressured shale is commonly highly fractured. In contrast, the sand-dominated Travis Peak must have been highly permeable (compared with shale) prior to quartz cementation, and although the mudstone-rich upper Travis Peak and dense carbonate in the overlying Sligo Formation might have hindered fluid expulsion, delayed compaction of the Travis Peak probably was not a significant influence on fluid pressure. The absence of significant mineralized or dilatant fractures in Travis Peak mudstone suggests that effective stresses in these rocks were not sufficiently reduced to produce tensile fractures. The origin of the inferred episode of overpressure in the Travis Peak therefore must differ from that of the Gulf Coast Cenozoic.

An episode of mid-Cretaceous fluid-assisted fracturing in the Travis Peak Formation is consistent with the existence of two factors that would have promoted excess fluid pressure; an elevated geothermal gradient and continuous influx of water from outside the formation. An elevated Cretaceous geothermal gradient may be inferred from thermal-mechanical models of Gulf basin evolution (Nunn and others, 1984; Dutton, 1987). A large influx of extra-formational water may be inferred from the large volume of quartz cement in the Travis Peak (>17 percent) and the low solubility of SiO_2 in water (Land and Dutton, 1979; Dutton, 1987). For example, at 200°C and 200 MPa confining pressure, the solubility of SiO_2 in H_2O is approximately 10^{-4} by weight (Fournier and Potter, 1982), indicating that 10^4 cm^3 of water is required for the deposition of 1 g of quartz. Larger volumes of fluid would

be required to deposit the quartz cement in the Travis Peak because the transporting water was probably in the 75° to 100°C range.

Origin of the hydrologic conditions causing migration of the quartz-precipitating fluids into the Travis Peak is unknown. Dutton (1987) suggested that heat flow resulting from the decay of a rift-related thermal anomaly may have driven convection of meteoric water. Direction of fluid migration is also unknown, although development of a natural fracture array could have produced an east-northeast-trending preferred fluid migration pathway.

The proposed cause of fracture in Travis Peak sandstone involves local pore pressure in excess of hydrostatic developed within individual shale-bounded sand bodies as a result of the introduction of large volumes of water from outside the formation coupled with gradually decreasing permeability due to quartz cementation. This model implies that the least permeable, most highly cemented sandstones in the Travis Peak could have the widest and longest fractures. Overpressure in this case may be primarily a consequence of the large fluid input rather than ineffective fluid expulsion. Water movement may have been restricted locally by the shape of permeable sandstone beds.

Hydraulic fracturing under the influence of episodically varying fluid pressure is thought to be the mechanism for the propagation of crack-seal fractures (Ramsay, 1980a; Engelder, 1987). Following Ramsay (1980a) and Etheridge and others (1984), the stress state prior to fracture is interpreted to have been close to one of brittle failure. An increase in fluid pressure by a small amount leads to the initiation of an extension fracture (fig. 31). Dilation of the fracture causes a local drop in fluid pressure, and mineral phases that are saturated in the fluid will tend to precipitate. Mineral growth from the introduced fluid in pores adjacent to the fracture or in the fracture itself causes decreasing permeability, and thereby contributes to renewed fluid

pressure increase. Such isothermal pressure drops can promote quartz precipitation, but cooling of the migrating fluid is more likely to govern quartz precipitation in the diagenetic environment (Fyfe and others, 1978; Fournier and Potter, 1982; Helgeson and Lichtner, 1987).

The role of tectonism in the formation of the Travis Peak fractures is difficult to specify, and without more information on fracture spacing, the total strain associated with the fractures cannot be assessed. Tectonic extension is necessary for the regional development of systematically oriented fracture sets (Segall and Pollard, 1982; Segall, 1984). Moreover, recent viscoelastic burial/stress models suggest that high fluid pressures alone may be insufficient to cause extensive tensile fracturing in sedimentary basins (Warpinski, 1986). The east-northeast trend of natural fractures is consistent both with formation under the influence of mild gulfward extension that characterized Gulf tectonics in the Early Cretaceous (Jackson, 1982) and with the postulated east-northeast compression involved in formation of the Sabine Uplift (Jackson and Laubach, 1987). However, the timing of fracture propagation in the Travis Peak evidently predates formation of the Sabine Uplift, suggesting Early Cretaceous south-directed extension governed fracture trends. In Waskom field, fracturing is apparently more intense in east-trending monoclines. The timing of quartz precipitation does not correspond to any specific tectonic or structural event in the northern Gulf Basin. Fracture propagation could instead have been the result of changes in fluid circulation patterns superimposed on a uniform extensional regime.

A question that is not yet resolved is whether fractures vary in aperture or trend over gentle salt structures. Preliminary comparison of fractures in the Waskom field structure, which overlies a salt anticline, with fractures in northern Nacogdoches County that are distant from salt structures shows no apparent difference in fracture style or trend.

The termination of fracture growth in the Travis Peak preceded movement on the Sabine Uplift. The termination of fracture propagation may have been the result of decreasing fluid pressure caused by disruption of regional hydrologic systems and the effects of uplift. Fluid pressure decreases as the height of the fluid column is reduced and as cooling occurs, and on a Mohr diagram (fig. 31) the effective stress circle shrinks and moves up the normal stress axis, away from the failure envelope. Uplift and erosion can promote fracture growth because the magnitude of horizontal stresses is reduced through thermal-elastic contraction, but the approximately 1,500 ft of uplift was evidently not sufficient to produce new breaks in mineralized fractures. High-pressure water trapped in isolated fractures may have contributed to keeping fractures open during subsequent burial, but some fractures are in contact with permeable beds that could have bled off excess fluid pressure. The survival of open fractures through the later history of Travis Peak burial was probably the result of propping by discontinuous quartz and ankerite bridges, coupled with the inherent strength of the quartz-cemented rock surrounding the fracture and low horizontal stresses.

Implications for Stress History Models

Stress-history models of sedimentary basins are methods for estimating current stress state and stress contrasts between different lithologies from the inferred geologic history of a basin. These models can also be used to predict fracture patterns. Typically, models consider the combined effects of (1) sedimentary loading and unloading, (2) pore-pressure changes, (3) changes in rock mechanical properties due to diagenesis and compaction, and (4) tectonic strains (Price, 1974; Voight and St. Pierre, 1974; Prats, 1981; Narr and Currie, 1982; Engelder, 1985; Warpinski, 1986). For example, following Voight and St. Pierre (1974), the horizontal

stresses (σ_x and σ_y) can be calculated in terms of the vertical stress (σ_z), thermal expansivity (α), and mechanical properties (Young's modulus, E; Poisson's ratio, ν; temperature, T):

$$\sigma_x = \sigma_y = (\nu/1\text{-}\nu)\sigma_z + \alpha E \Delta T/(1\text{-}\nu). \quad (1)$$

With a knowledge of burial depth and estimates of mechanical properties at different times, plots can be constructed of depth of burial versus magnitude of horizontal principal stress. To test more sophisticated models that incorporate tectonic stresses, pore pressure variations, and viscoelastic deformation (for example, Warpinski, 1986), knowledge of the evolution or history of the following is desirable: (1) magnitude and direction of horizontal and vertical strains ($\epsilon_x, \epsilon_y, \epsilon_z$); (2) pore pressure history, including the relation of fracturing to fluid migration; (3) history of mechanical property changes, (4) timing of fracture propagation; and (5) current stresses.

The relation of fractures to diagenetic patterns in the Travis Peak has two implications for generalized stress history models. First, fluid migration and intermittent hydraulic fracture can govern fracture propagation in sandstone in passive margin basins. Porosity-reducing sealing of fractures and episodic fracture propagation represent episodic changes in fluid pressure and highlight the time-dependent nature of porosity, permeability, and pore pressure. The evolution of these properties may be critically affected by the movement of fluids that are not locally derived.

Second, the timing of changes in rock mechanical properties in the Travis Peak is not the one generally envisioned in most models. Stress history models commonly assume that rock properties change gradually during burial and that rock achieves

maximum diagenetic alteration and compaction at maximum burial (Narr and Currie, 1982; Warpinski, 1986). This is an important assumption because diagenetic changes greatly affect the evolving mechanical properties of rock. In the Travis Peak, however, the mechanical properties and natural fracture pattern were evidently established at an early stage in the burial history. The timing of mechanical property changes with respect to burial influences the potential stress contrasts that may exist between sandstone and shale (fig. 31c). Maximum stress differences are predicted if lithification and changes in mechanical properties of sandstone and shale occur at the maximum depth of burial (Voight and St. Pierre, 1974; Prats, 1981). Whitehead and others (1986) have found only small stress differences between contrasting rock types in the Travis Peak. Implications of the timing of mechanical property changes and fracturing for vertical stress contrasts and fracture height growth are a subject of continuing investigation.

A further implication concerns the possible presence of residual stresses in the Travis Peak. The decrease in the average height of both natural and coring-induced fractures (figs. 5, 11, 12) and changes in the style and trend of borehole ellipticity with stratigraphic depth (Part Two) suggest that the geologic history of the basin could be influencing present stresses. The dependence of the length of induced structures that reflect current stresses, such as coring-induced fractures and borehole ellipticity, on the extent of quartz cementation and paleo-depth (rather than current burial depth) and the near parallelism of natural and induced fractures raises the possibility that the modern horizontal stress anisotropy of the Travis Peak is influenced by a residual elastic strain (Price, 1966; Friedman, 1972; Holzhausen and Johnson, 1979; Hoskins and Russell, 1981) perhaps locked in by the quartz cement, which increases with stratigraphic depth in the Travis Peak. The influence of lithologic heterogeneity on the fracture-height pattern is currently unknown, but the lower Travis

Peak is more sand rich than the upper Travis Peak (Dutton, 1987; Fracasso, 1987), suggesting that there could be fewer natural barriers to height growth in the lower Travis Peak. These possibilities remain to be tested by more extensive coring of the middle and lower Travis Peak.

Origin and Significance of Healed Microfractures

Networks of healed or sealed microfractures have not previously been recognized in sedimentary rocks outside orogenic belts. Experimental studies (Smith and Evans, 1984; Brantley and others, 1986) demonstrate rapid fracture healing at temperatures greater than 200°C in the presence of a pore fluid. Studies of natural examples of healed fractures have generally interpreted deformation temperatures to be at least this great (Sprunt and Nur, 1979). Results from the Travis Peak show that microfracture closure by healing at shallow depths (<8 mi) and low temperatures (<170°C) is more common in sedimentary rock than previously thought. The existence of closed postdepositional microfractures may have been overlooked because they are easily observed only at higher magnifications than are commonly employed in petrographic studies and because in sedimentary rock, fluid-inclusion planes are commonly assumed (correctly) to have been derived from the sedimentary source terrain.

Two mechanisms to account for closing the microfractures are (1) dissolution and reprecipitation of minerals on a local scale by diffusive mass transfer ("healing"), and (2) precipitation of material transported over distances greater than grain scale ("sealing"). Vitrinite reflectance data and burial history curves (Dutton, 1986, 1987) show that the maximum temperatures reached by the Travis Peak Formation in East Texas were less than 170°C and that the maximum burial depth was less than 13,120 ft, which is outside the reported range for healing. The rapidity of experimental

healing in the 200°C range suggests, however, that this process may operate more slowly at the lower temperature of the diagenetic environment (Smith and Evans, 1984).

Sealing by quartz precipitation could also close fractures under low-temperature, low-confining-pressure conditions. The parallel, axial, paired fluid-inclusion planes in quartz-filled macrofractures (fig. 18) were formed by sealing. Matched fluid-inclusion planes (fig. 19) suggest that at least some microfractures also formed in this way. However, cathodoluminescence studies suggest that the detectable variation in trace-element composition of quartz in closed microfractures is not significantly different from that of the quartz grains, suggesting that most microfractures have healed rather than sealed. Nevertheless, healing and sealing are not mutually exclusive, and in these rocks the evidence in favor of one process or the other is not conclusive.

The ramifications of the existence of low-temperature microfracture healing and of closed microfractures in general are far-reaching. Microfractures affect many physical properties of rocks, including strength, permeability, and seismic-wave velocity (Simmons and Richter, 1976; Krantz, 1983). Fluid-inclusion planes are material discontinuities that can serve as stress concentrators promoting crack nucleation and growth. Healing could play an important role in the evolution of sandstone mechanical properties during burial, because healing counteracts microfracture creation and propagation, causing rocks to be stronger under geological strain rates than is predicted by the results of brittle fracture experiments. Microfracture healing also may play a role in governing the geochemical evolution of fluids in sedimentary basins. Healing reduces porosity and the proportion of rock that is in contact with a given volume of fluid, and thus affects the capacity of a volume of rock to interact chemically with transient fluids.

Syn-cementation microfracturing and crack sealing, in conjunction with networks of macrofractures, provide a mechanism for introducing into low-permeability sandstones the large water volumes that are necessary (Land and Dutton, 1979) for pervasive quartz cementation where no local silica source is present. Transgranular microfractures alone may not have been sufficiently abundant to provide a significant fluid conduit, but transgranular microfractures may be only one manifestation of microfracturing that occurred primarily along grain boundaries, a possibility supported by the observation that macrofractures propagated along, rather than across, grain boundaries over most (>75 percent) of their length (fig. 6). Alternatively, microfractures may not necessarily have been fluid conduits if they closed primarily by healing.

The healed microfractures observed in Travis Peak sandstone probably do not correspond to the microcracks that have been invoked to explain strain relaxation, thermal expansion of oriented core, and sonic velocity anisotropy (see Teufel, 1982). Results from Waskom field show that anelastic strain recovery directions (Owen and others, 1987) and thermal expansion (Jeffrey and others, 1987a) predict microcrack arrays at high angles to the observed transgranular plane trend. Furthermore, transgranular microfractures predate elastic relaxation due to core retrieval and are not abundant enough to account for the strains observed by Owen and others (1987) in Travis Peak core. Although elastic changes in transgranular microfractures probably do occur as a result of stress relief, the influence of these changes on the behavior of core at the surface is apparently less than the effect of smaller but much more common grain boundary cracks (fig. 22). At depth, where grain-boundary cracks are presumably closed, transgranular microfractures may have a more important influence on mechanical and seismic anisotropies.

Implications for Hydraulic Fracture Treatment

Low permeability (tight) gas-bearing sandstone reservoirs are important economic resources that are often difficult and costly to exploit. Research supported by the Gas Research Institute (GRI) under the Tight Gas Sands project is designed to increase understanding of tight gas sandstone reservoirs and to facilitate their utilization. In 1986, GRI-supported research was focused on evaluation, hydraulic fracture treatment, and production of the first GRI Staged Field Experiment (SFE 1) well in the Travis Peak Formation, the Holditch Howell No. 5, in Waskom field (figs. 1 and 2).

Natural fractures in Waskom field have several characteristics that suggest that they could potentially affect hydraulic fracture treatment: (1) some fractures in the Travis Peak locally have significantly greater porosity, and potentially greater permeability, than the surrounding sandstone matrix; (2) natural fracture trends deviate from the trend of current stress trajectories. During hydraulic fracture treatment, these characteristics may tend to promote leakoff and pressure fluctuations through opening of natural fractures, fracture branching, and development of auxiliary fractures; potentially, these effects may result in screenout (Lamont and Jessen, 1963; Nolte and Smith, 1981; Blanton, 1982; Warpinski and Teufel, 1987)(fig. 32). Results of experiments in volcanic rocks in Nevada in which hydraulic fractures were created and subsequently mined out confirm that natural fractures may be dilated and multiple fracture strands may form during hydraulic fracture treatment (Warpinski and Teufel, 1987; fig. 32). Whitehead and others (1986) report patterns of pressure decline during stress tests in the Travis Peak that could be the result of fluid leakoff into natural fractures. Predictions of the results of massive hydraulic fracture treatment and interpretation of minifrac stress tests are based on the assumption that induced

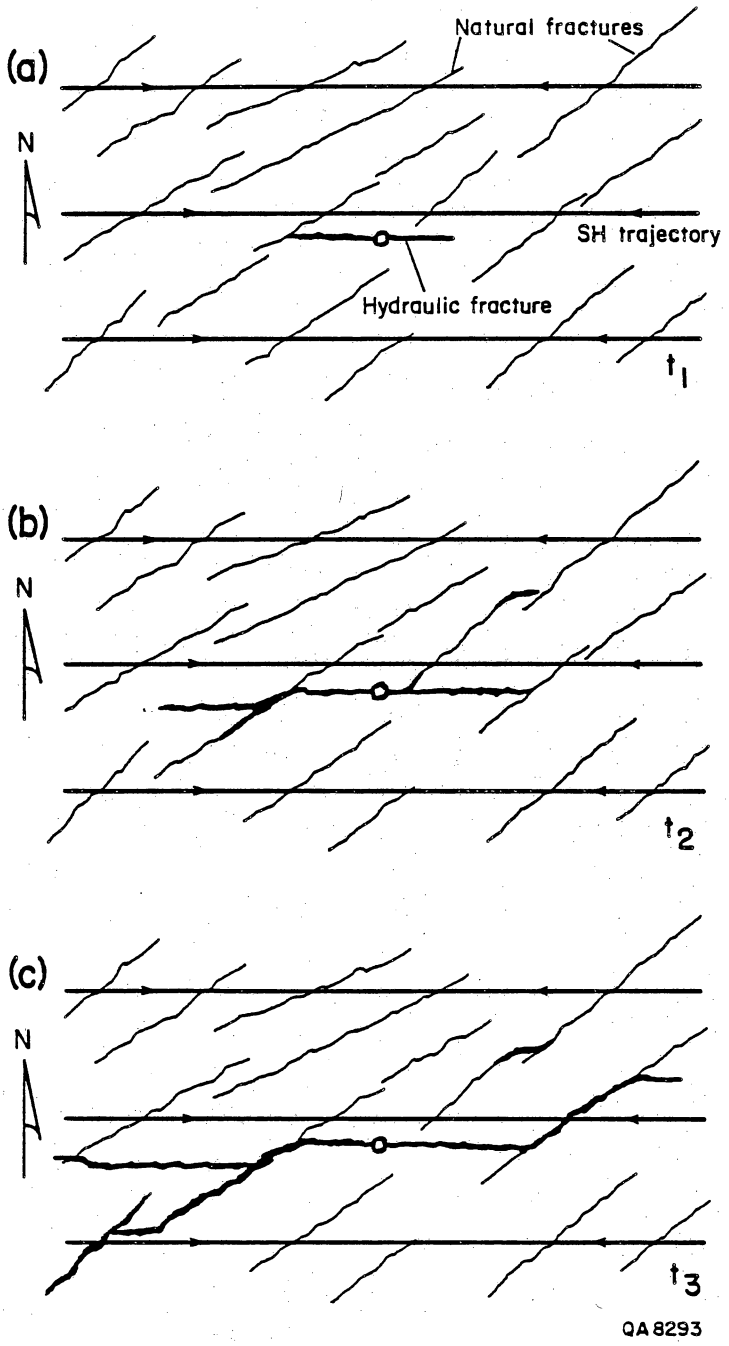

Figure 32. Map view of hypothetical interactions between natural fractures and hydraulically-induced fractures propagating along stress trajectories (SH = maximum horizontal compressive stress). Natural fractures in Waskom field probably vary in shape, trend, and length distribution to a greater extent than is shown here. (a) Hydraulically-induced fractures may propagate at an angle to natural fracture trends. In Waskom field this angle is probably small. (b) Dilation of natural fractures may contribute to development of non-planar engineered fractures. Because some natural fractures are open, induced fractures will tend to follow curved trajectories toward them. (c) Interactions between natural and induced fractures could contribute to evolution of a composite natural and induced fracture network during fracture treatment.

fractures propagate in a plane perpendicular to the least horizontal stress, but in fractured rock this may not be the case if preexisting fractures are reopened by the fracturing fluid (Barton, 1986; Warpinski, 1986).

High-pressure fracturing fluids tend to penetrate natural fractures with effects that depend on fracture orientation and cohesion, stress, and the pressure and viscosity of the fracturing fluid at the zone of interaction. Closely spaced, permeable fractures normal to the least principal stress tend to be opened most readily by high pressure fracturing fluid, but fractures that are inclined to the least principal stress, such as those in Waskom field, can also be opened. Moreover, fracturing along grain boundaries and mineralization along fracture surfaces combine to produce a poor fit between opposed natural fracture walls in the Travis Peak; consequently, these natural fractures would tend to preserve some porosity even if large fracture-bridging crystals were removed and opposing fracture walls were brought in contact.

An induced fracture tends to realign normal to the least principal stress, but as a result of the interaction with the natural fracture array, the induced fracture tends to be more tortuous. The fracture zone may be wider and shorter than if a single induced fracture had been produced and may have a trend governed by the pattern of interaction between in situ stress and natural fracture spacing (fig. 32). Segmentation and curvature of natural fractures in the Travis Peak (figs. 6, 9, 10) suggest some small scale fracture patterns that could result from the interaction between engineered fractures and natural fractures (see Segall and Pollard, 1982) (fig. 32). Fracture interactions that occur naturally in the Travis Peak are also significant because the narrow, low-permeability overlap zones between segments may regulate flow in the fracture network and overlap zones could potentially be damaged by stimulation procedures. The possible presence of interacting natural fractures may be detectable

through analysis of hydraulic fracture treatment results, post-fracture production and pressure buildup data (Jeffrey and others, 1987b; Holditch and others, 1987b; Branagan and others, 1987).

Natural fracture spacing may have an important influence on reservoir quality and the growth of engineered fractures, but without deviated (non-vertical) borehole for fracture sampling, specifying fracture spacing in flatlying sedimentary rocks is rarely possible (Lerche and Narr, 1986), and fracture spacing has not been determined for the Travis Peak. Some fracture models predict wider fracture spacing at greater depth (Nur, 1982; Kemeny and Cook, 1985). Surface studies in other rocks (Ladeira and Price, 1981; Verbeek and Grout, 1982) show that fracture spacing varies with bed thickness, lithology, and structural position (for example, more fractures might be predicted in the hinge of the Waskom monocline). In a recent study, Grout and Verbeek (1987) recognized a pre-uplift fracture set in surface exposures, but clear evidence of the timing of fracture propagation available in their exposures is rare. It has been suggested that the relation between fracture spacing and bed thickness in surface exposures can be used to infer fracture spacing in the subsurface (Narr and Lerche, 1984), but surface fracture spacing patterns are of limited value for rocks that have never been uplifted and unloaded, because many outcrop exposures contain unloading and release fractures that do not exist at depth (Engelder, 1985). Conclusions based on fractures observed at the surface therefore cannot be used at present to predict subsurface fracture spacing.

SUMMARY AND IMPLICATIONS

Natural and coring-induced fractures in the Travis Peak trend east-northeast, but the strike of fractures varies and is poorly known at present (fig. 3). Because coring-

induced petal-centerline fractures are parallel to hydraulically-induced fractures they may prove useful for predicting fracture propagation direction. Natural fracture porosity is locally only partly occluded by quartz and ankerite mineralization and primary fracture porosity remains in some Waskom field fractures. The fractures could potentially influence gas production and the propagation of hydraulically-induced fractures in this reservoir. Studies of natural fracture mineralogy and microstructure, combined with results of previous diagenetic studies, provide evidence of natural hydraulic fracture propagation during the Cretaceous, and provide constraints for stress history models of the northern Gulf basin.

Petrographic studies show that healed microfractures can be used to determine subsurface natural fracture trends. Microfractures are more common than macrofractures, so they can be used to define subsurface trends in a more systematic and reproducible way than can be accomplished by sampling widely spaced macrofractures by coring. Observations of healed microfractures may provide a key tool for diagenetic studies of sandstone in sedimentary basins because fluid inclusions trapped in post-depositional microfractures provide a record of the evolution of fluid chemistry and temperature. Primary fluid inclusions in quartz cement have been used in combination with basin subsidence studies to estimate the conditions and timing of diagenesis and hydrocarbon migration (Haszeldine and others, 1984). Further documentation of healed microfracture morphology and distribution should be sought in petrographic studies of sandstone so that their significance can be assessed more fully.

Future work on Travis Peak fractures will be designed to answer several questions that have been raised by this petrographic study. What is the regional trend of natural fracture sets and how do the trends vary? Do fracture patterns vary regionally and with depth? How are fracture patterns and distribution of diagenetic

minerals linked, and can one be used to predict the other? Do the width and abundance of natural fractures increase with an increasing degree of quartz cementation? Do residual elastic strains govern hydraulically-induced fracture propagation in the Travis Peak? Does a systematic, scale independent (fractal?) relationship exist between microfractures and macrofractures that can be used to predict subsurface fracture spacing? Documentation of regional variations in fracture patterns through the collection and examination of oriented core will provide the evidence needed to test these results. Studies of fracture mineralogy and fluid-inclusion chemistry will provide better estimates of the timing and environmental conditions of fracture propagation. Evidence of the timing of fracturing provides a key element that can be used to refine and quantify models of basin stress and natural fracture propagation history necessary for predicting natural fracture distribution and the origin of vertical stress contrasts important for containment of hydraulically-induced fractures.

PART TWO:

ANALYSIS OF FRACTURING AND WELLBORE ELONGATION BASED ON BOREHOLE TELEVIEWER, FORMATION MICROSCANNER, AND ELLIPTICITY LOGS

ABSTRACT

Three types of wireline logs were used to evaluate borehole features. Formation microscanner (FMS) and borehole televiewer (BHTV) logs were used to document distribution and types of vertical features in the borehole of the Holditch Howell No. 5 well. BHTV fractures range from 2 to 13 ft long. Their orientation ranges from about 60 to 100 degrees, consistent with fractures observed in core. BHTV fractures in the upper Travis Peak are significantly longer than those in the lower Travis Peak. Where log and core overlap most vertical features detected on FMS logs correlate with fractures in core. Further work is required to establish criteria for distinguishing between natural and drilling-induced fractures.

Ellipticity logs from seven wells were examined. Two significant azimuths of wellbore elongation were defined on the basis of 574 elliptical zones: 344 degrees and 74 degrees. The northwest azimuth coincides with the orientation of the regional minimum horizontal principal stress. The northeast azimuth coincides with the trend of fractures detected in BHTV logs and core. The orientation of borehole ellipticity in upper Travis Peak is predominantly northeast, whereas in the lower Travis Peak ellipticity is mostly northwest. This change in orientation with increasing stratigraphic depth corresponds to a decrease in BHTV fracture length, suggesting that northeast-trending ellipticity is caused by erosion along fractures in the borehole. Northwest-trending ellipticity is probably caused by stress-induced spalling of the wellbore parallel to least horizontal principal stress.

INTRODUCTION

The purpose of this study was to analyze three different types of logs, to compare them with core, and to determine their effectiveness in detecting fractures and other stress-induced features in the borehole. Borehole televiewer and formation microscanner logs can detect fractures and borehole elongations. They provide useful information for establishing fracture trends and lengths and for distinguishing stress-induced borehole breakouts from fracture-induced elliptical zones. Ellipticity logs were used to determine predominant directions of wellbore elongation.

These studies are important for the description of subsurface stress because fractures and borehole elongations can be used to determine the orientation of horizontal stresses (Gough and Bell, 1982; Plumb and Hickman, 1985; Plumb and Cox, 1987) and to predict the orientations of hydraulically-induced fractures. Plumb and Hickman (1985) used BHTV and four-arm caliper logs from a single well to show that wellbore breakouts developed parallel to least horizontal principal stress. Later, Plumb and Cox (1987) analyzed wellbore elongation data from a large area of the Appalachian Basin and found that the orientation of borehole elongations, coring-induced petal-centerline fractures, and hydraulic fractures was controlled by the contemporary regional stress field. Wellbore elongations were consistently perpendicular to hydraulically-induced fractures, and aligned with least horizontal principal stress in the region.

DESCRIPTION OF BOREHOLE TELEVIEWER AND FORMATION MICROSCANNER LOGS

Continuous BHTV log covers the intervals from 5,940 to 6,320 ft and from 7,240 to 7,665 ft of the Holditch Howell No. 5 well (fig. 33). Core is available for

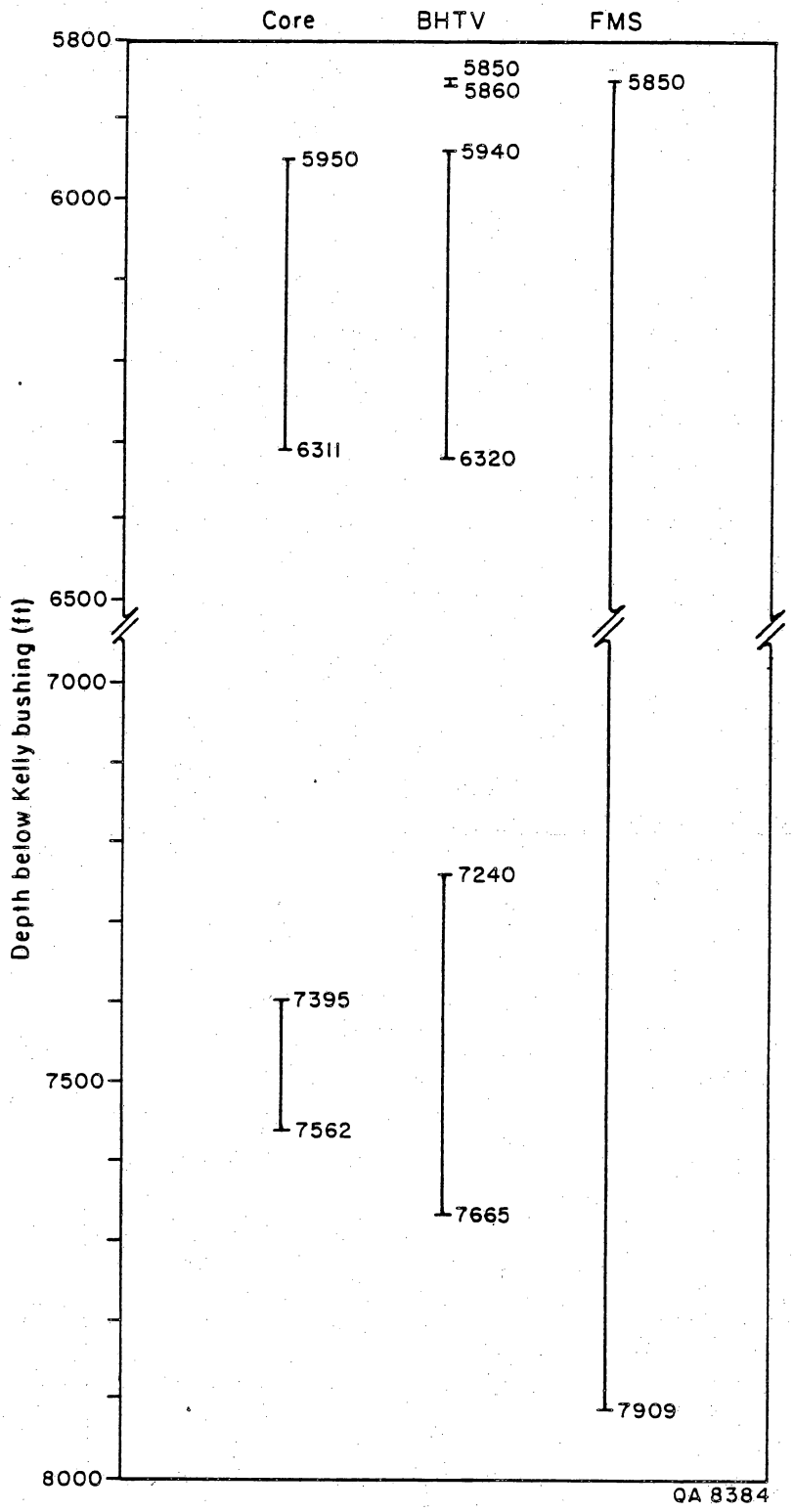

Figure 33. Chart showing well depths cored and well depths surveyed by the borehole televiewer (BHTV) and formation microscanner (FMS) logs. Holditch Howell No. 5 well.

most of this interval. FMS logs provide continuous coverage of the borehole from 5,850 to 7,909 ft. Several logging runs were made with the FMS over some intervals providing images of the same intervals with the tool oriented in different directions.

Borehole Televiewer

The Borehole Televiewer (BHTV) is an acoustic device used to map the smoothness of the borehole wall. Principles of its operation and use have been described by Zemanek and others (1970). The BHTV measures the reflectivity of the borehole wall and plots the amplitude of the reflected signal as a function of azimuth and depth. Low reflectivity features such as fractures and borehole breakouts appear as dark areas on the log. Data are plotted at 1 inch = 2.5 ft (1:30) vertical scale, and the circumference of the borehole = 2.0 in horizontal scale. The resulting plot is an "unwrapped" image of the borehole wall, with south at the center and north at the left and right edges (fig. 34b).

Fractures are discernible as dark, pencil-thin, linear, vertical features where they intersect the borehole wall (fig. 34b). Natural fractures are detected by the BHTV only if they are open wider than 0.03 in (Nelson, 1985) or have been modified by drilling to produce a topographic feature on the borehole wall. Fractures were identified on the log and measured for length and orientation (fig. 5). BHTV fracture trends and lengths were confirmed where possible by fracture orientation data from the FMS log (fig. 34a).

The BHTV was also used to identify the locations and orientations of elliptical sections of the borehole. Elliptical sections are recorded on the BHTV log as dark, irregular, relatively wide (0.1 to 0.3 inches) vertical bands. They usually appear in pairs or groups of four (fig. 34b, d).

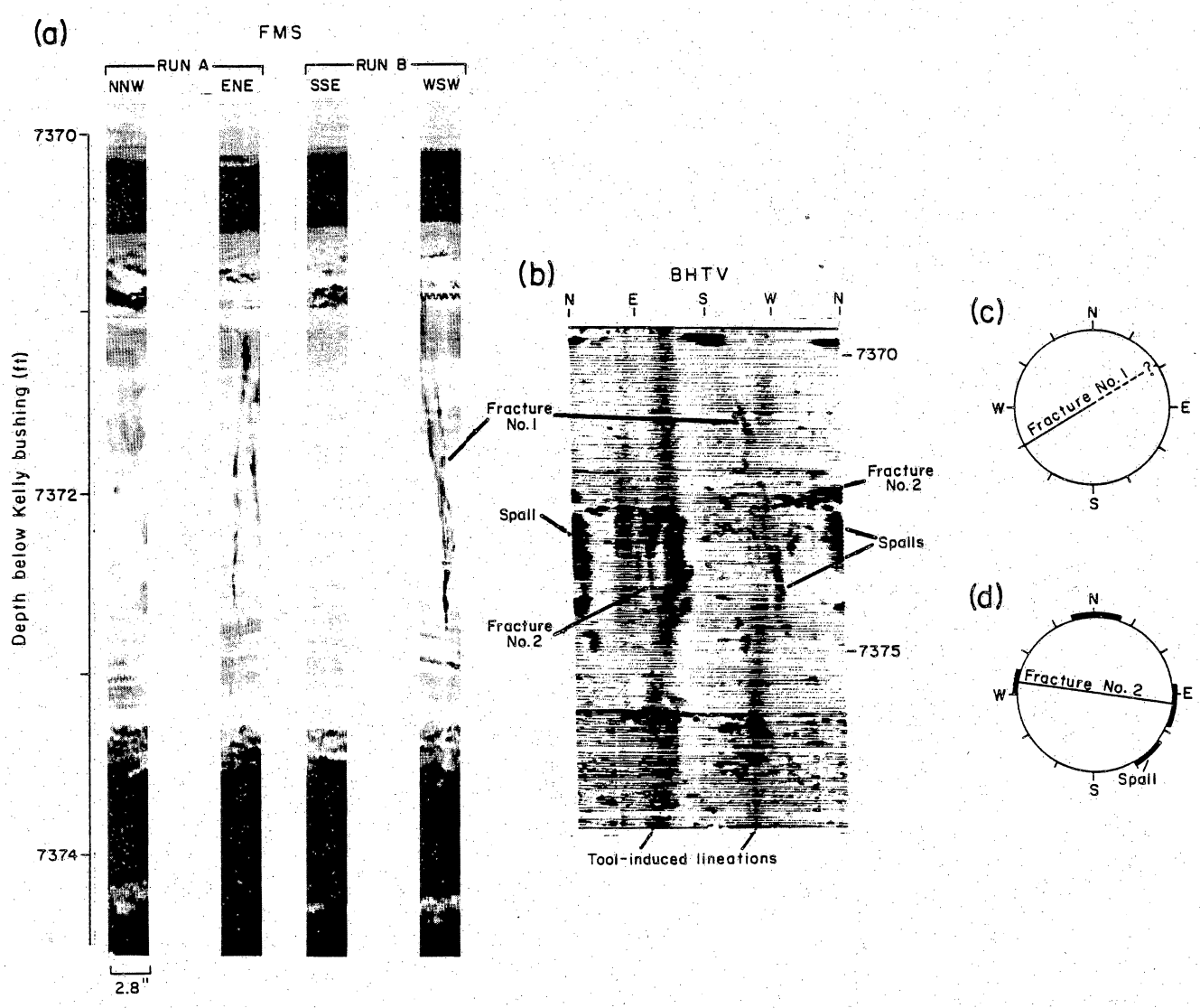

Figure 34. Comparison of fractures and spalls on FMS and BHTV logs. Holditch Howell No. 5 well. (a) Two FMS runs over the same interval. Linear vertical feature on pads oriented east-northeast and west-southwest is a fracture. Dipping beds are visible at 7,372.7 ft. (b) BHTV log over same interval. Fractures are visible at 7,371 and 7,374 ft. Fracture no. 1, at 7,371 ft, corresponds to fracture on FMS log. Fracture no. 2, at 7,374 ft, is not visible on FMS log because neither FMS logging pass sampled the fracture. Dark, irregular areas in the east and west quadrants are spalls that intersect fracture no. 2. Dark bands in the north and southeast quadrants are spalls that do not intersect fractures. Straight, parallel, dark vertical bands extending the length of the section in the east-southeast and west-southwest quadrants are toolmarks. (c) and (d) Directional plots of borehole features illustrate orientation of fractures and spalls on BHTV log.

Formation Microscanner

The Schlumberger Formation Microscanner (FMS) is a resistivity tool that examines two 2.8-inch-wide segments of the borehole wall. Arrays of 27 resistivity sensors are located on pads 3 and 4 of a four-arm dipmeter tool (Schlumberger, 1987). The azimuth of pad 1 is recorded on the log. Data are plotted at horizontal and vertical scales of 1:5 (Steve Grayson, Schlumberger, personal communication, 1987). FMS images are conductivity maps of portions of the borehole wall. The high resolution of the FMS makes it a valuable tool for looking at small features and for distinguishing borehole spalls from fractures at a high angle to the borehole wall. Fractures must produce resistivity anomalies to be detected. Plumb and others (1985) report vertical resolution of better than 0.4 inch for sedimentary structures and detection of fractures with apertures of less than 0.04 inch with the FMS tool. Comparison of core and FMS logs from the Holditch Howell No. 5 in this report confirms their results but shows that the size of conductive features is somewhat larger on the FMS log than in core. Unlike the BHTV, which surveys the entire borehole wall, each FMS pad covers only two narrow strips (fig. 34a). Multiple tool passes with pads in different orientations are therefore required to determine fracture orientation. Generally, in the Holditch Howell No. 5, multiple tool passes did not result in adequate coverage of the borehole because the irregular borehole shape causes the tool to track the same axes of the borehole.

Variable vertical offset of 0 to 5 ft between the FMS and core limited the correlation of specific fractures from log to core. However, many small sedimentary features such as crossbedding, bioturbation, and lithologic boundaries (fig. 35) were distinguished on the FMS log and provided depth control for log-to-core correlations.

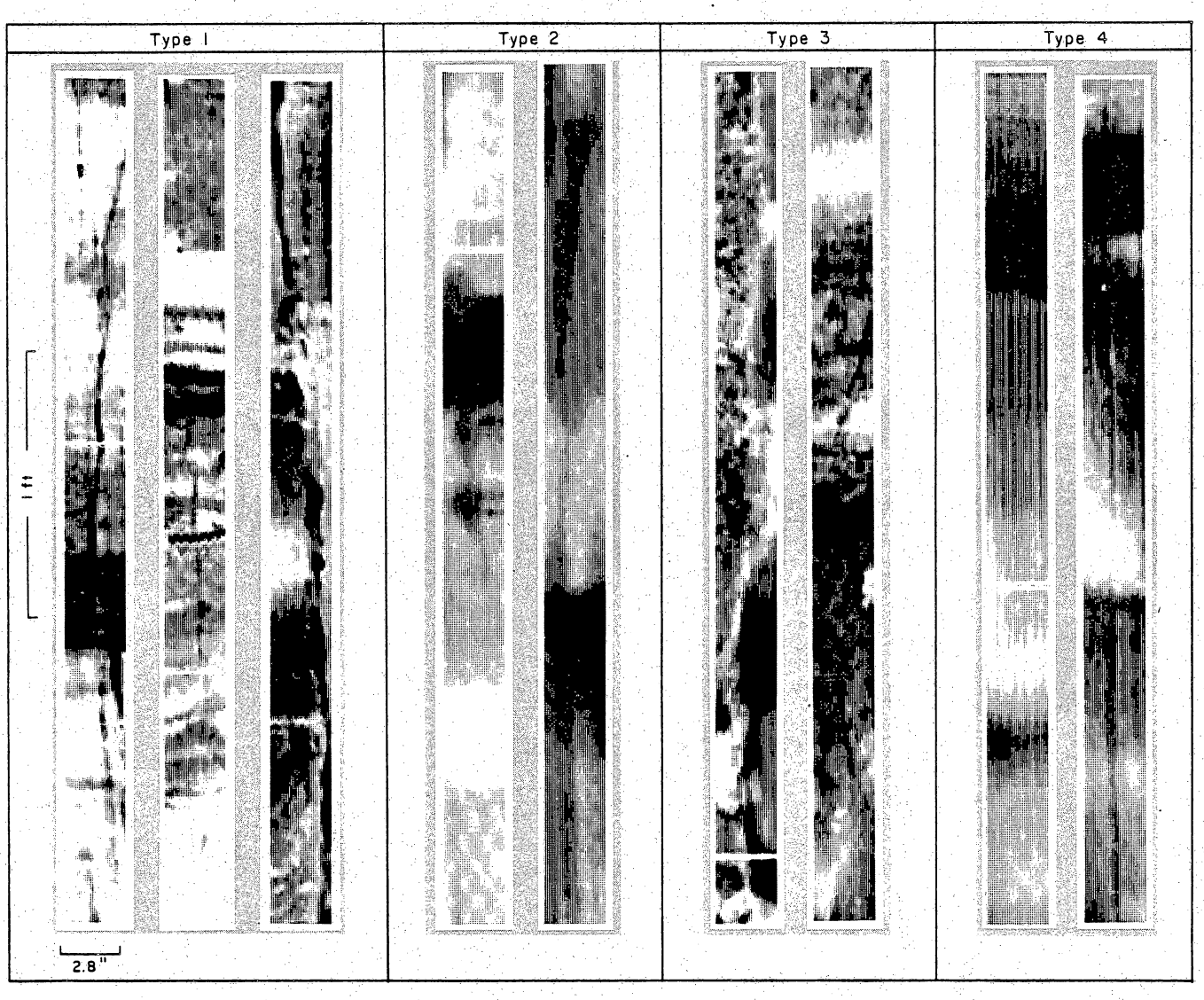

Figure 35. Range of linear vertical features seen on the FMS logs, classified into four types. Type 1 features are dark, anastomosing lineations of varying lengths (1 to 10 ft) and widths (0.3 to 0.9 inch). Features have clearly defined boundaries and are easily distinguished from their background due to high contrast. Type 2 features are more subtle lineations. Type 3 lineations are contacts between mottled areas and more uniform areas of the log. Type 4 lineations are regular, straight-sided, parallel lineations ranging from a hairline width to 0.5 inch wide. Type 1, 2, and 3 features correspond to fractures and borehole spalls.

ANALYSIS OF FEATURES DETECTED ON BOREHOLE TELEVIEWER AND FORMATION MICROSCANNER LOGS

Borehole Televiewer

More than 70 narrow, vertical features interpreted as fractures were detected by the BHTV in 815 ft of the Holditch Howell No. 5 well. These vertical features were confirmed to be fractures by comparison with the core and FMS features. Length and/or orientation data were obtained for 42 fractures (fig. 34).

BHTV fracture length varies with depth. The length of BHTV features is similar to that observed in core and includes a marked decrease in average fracture length of 4.9 to 7.7 ft from the upper to the lower Travis Peak (fig. 5a, b). Linear features terminate at bedding planes on the BHTV log as do fractures in the core.

Fractures 0 to 500 ft below the top of the Travis Peak show preferred orientations of 60 to 90 degrees, are nearly vertical, and have apparent lengths of 4 to 13 ft (fig. 5c, d). From 1,400 to 1,800 ft below the top of the Travis Peak fractures strike from approximately 70 to 100 degrees. Apparent lengths range from 2 to 10 ft (fig. 5a, b). Apparent length is the length visible on the BHTV log and is less than the actual length of the fracture when the fracture is subvertical. In the Holditch Howell no. 5 well, all of the BHTV fractures are subvertical to vertical (fig. 34b). The apparent length of dipping fractures is much less than actual fracture length.

Two types of spalls were identified on the BHTV log. One type of spall occurs around the fracture trace and slightly to one side of it on the BHTV logs. Another type of spall occurs at an angle to the fracture trace and in unfractured zones. Figure 34b shows two spalls, one in the same direction as fracture no. 2 and one

oriented approximately 90 degrees to it toward the north. The elongation that is in direct contact with the fracture appears to be caused by a natural fracture intersecting the borehole and spalling off at the edge of the fracture trace. Spalls on the north and southeast section of the BHTV log are not associated with BHTV fractures. Analysis of spall dimensions, orientations, and frequency will help to determine the relationship between spalls, fractures, and stress.

Borehole elongations are easily confused with tool-induced features that appear on the log as thick (0.25 to 0.5 inch), spiraling, parallel lines (figs. 34b and 36). However, tool-induced features are continuous through 25 to 200 ft intervals, and borehole elongations are only 1 to 10 ft long.

Formation Microscanner

More than 100 narrow, vertical features were detected in the cored interval (571 ft) of Holditch Howell No. 5 well. These vertical linear features on the FMS log were classified into four types based on their shape, vertical continuity, shading, and width (fig. 35), and they were compared to the core. Feature types 1 through 3 could be correlated to natural and coring-induced fractures and fracture zones (fig. 37); type 4 features are artifacts of logging and data processing procedures.

Type 1 linear features are the most prominent and most easily distinguished. They exhibit a very high contrast to their background and range in shading from black to gray. Two varieties of type 1 features include continuous, dark (conductive) features and features composed of discontinuous, dark (conductive) segments separated by light (resistive) segments. Feature lengths vary from short, discontinuous 0.3-ft segments to 10-ft anastomosing strips. Apparent widths of the features vary from approximately 0.3 to 1.0 inch. Most type 1 features were correlated to fracture zones

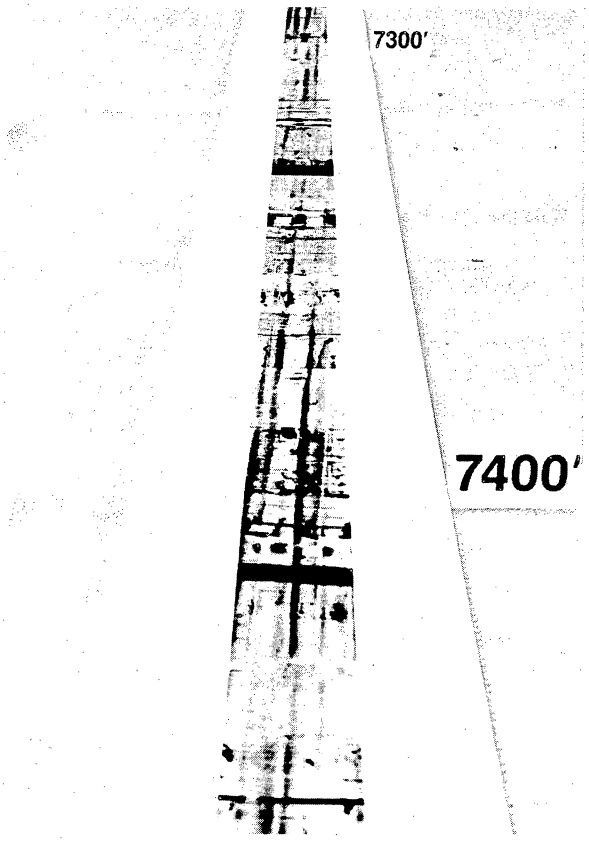

Figure 36. Oblique photograph of BHTV log showing diffuse, spiraling vertical bands. These features are too long and continuous to be natural features. Systematic spiral pattern suggests that these features (which can be mistaken for spalls locally) are the result of tool marks on the borehole wall or BHTV tool eccentricity.

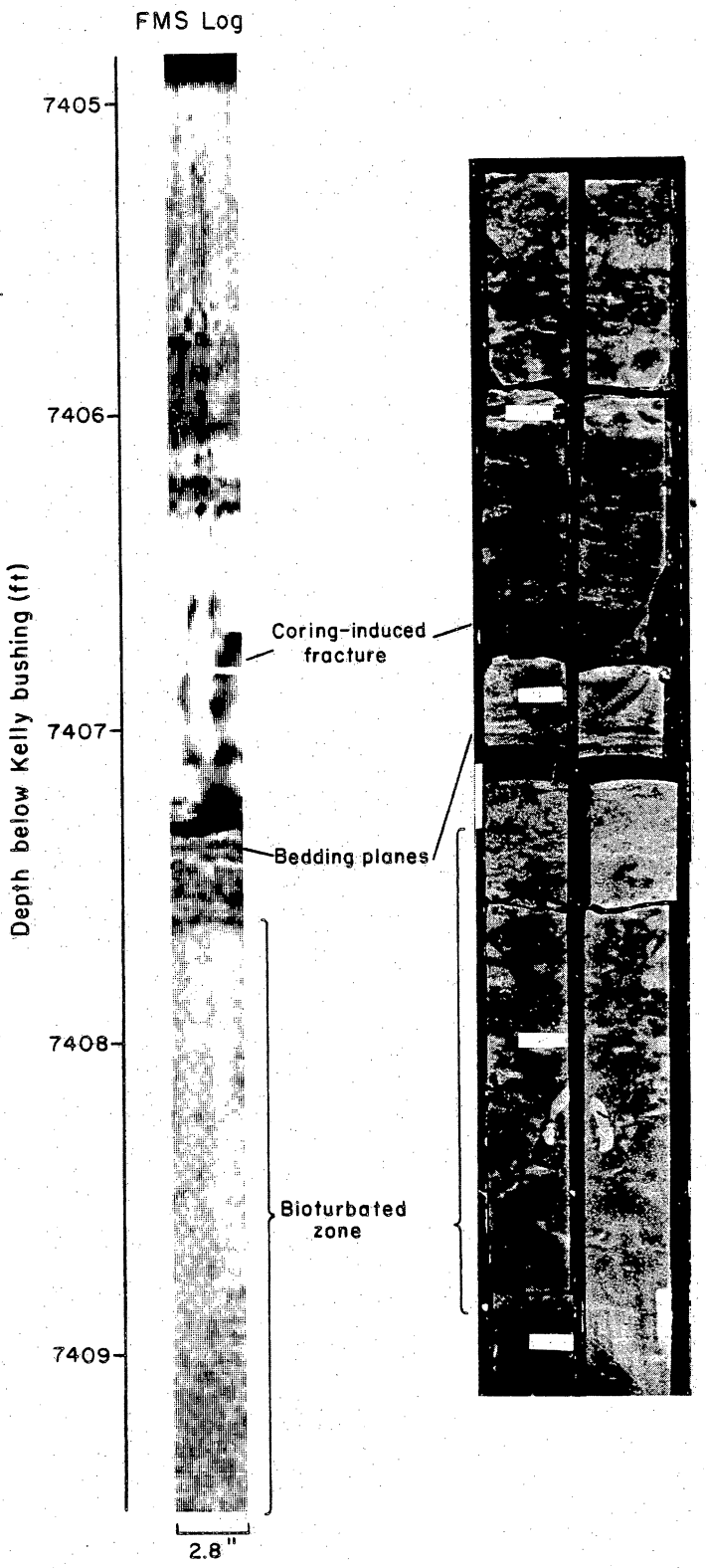

Figure 37. Comparison of features seen on the FMS log to features identified in the core. Fracture at 7,407 ft hooks out the side of the core and is the same length (1 ft) as the feature on the FMS log. Horizontal and dipping bedding planes are visible at 7,407.4 ft. A zone of heavily bioturbated sandstone in the core corresponds to a mottled interval on the FMS log starting at 7,407.6 ft.

in the core. The majority of natural fractures detected on the FMS log were type 1 features. In some instances, segmented features with alternating conductive and resistive segments corresponded to partly open mineralized fractures. Discontinuous conductive features cannot always be used to distinguish natural fractures because coring-induced fractures also occur in discontinuous segments in the core (Part One). Often, natural fractures are faint and difficult to detect. The most prominent type 1 features are coring/drilling-induced. Some small fractures not observed during visual inspection of the core were detected on the FMS log because the FMS tool is sensitive to small differences in resistivity that are not visible on the core.

Type 2 features have lateral boundaries that are more diffuse and irregular than Type 1 features (fig. 35) and average 0.5 to 1.0 ft long. Type 2 features are generally lighter than type 1 features. Less than half of these features correlated to fractures in the core. Other type 2 features corresponded to zones of bioturbation. A few individual burrows visible in the core correlated to Type 2 features. Some natural fractures are type 2 features.

Type 3 features are characterized by sharp vertical contacts between mottled and more uniform log patterns; they are elliptical, resistive zones elongate parallel to the borehole. Some type 1 features pass vertically into type 3 features (fig. 35). Type 3 features are interpreted to be spalls.

Type 4 linear features are straight, continuous, parallel features, with apparent widths of 0.2 to 0.5 in. These features do not correspond to features in the core, and they may be artifacts of logging procedures. Some type 4 features (fig. 35) superficially resemble some type 2 or type 3 features, but are straighter and have sharper edges.

WELLBORE ELLIPTICITY--DEFINITION, MEASUREMENT, AND COMPILATION

Wellbore elongation has been studied as a means of determining the directions of horizontal principal stresses. Previous work by Plumb and Hickman (1985) on wellbore ellipticity distinguished between elongations caused by intersection of the wellbore with natural fractures and those caused by spalling of the wellbore in a stress field with unequal horizontal stresses (breakouts). Studies by Gough and Bell (1982), Plumb and Hickman (1985), and Zoback and others (1985) show that breakouts develop parallel to the minimum horizontal principal stress. Near-vertical, tension fractures that form in response to the present stress regime will be perpendicular to the minimum horizontal principal stress. If wellbores elongate along these fractures, the largest diameter will be aligned with the maximum horizontal principal stress, at right angles to breakouts. However, natural fractures that formed under a previous stress regime cannot be used for understanding present stress orientations.

This study concerns the relation among in situ stress, fracture patterns, and wellbore ellipticity in seven wells in East Texas (fig. 38). Zones of wellbore elongation were measured on ellipticity logs produced by ResTech, Inc. (fig. 39). Ellipticity is defined as follows (B. Ward, ResTech, personal communication, 1987):

$$\text{ellipticity} = |C1\text{-}C2|/\text{bit size} \qquad (2)$$

where: C1 = reading from caliper 1-3 (in)

C2 = reading from caliper 2-4 (in)

bit size = diameter of drill bit as recorded on well log (in)

Diameters of drill bits for these wells ranged from 7-7/8 in to 9-7/8 in.

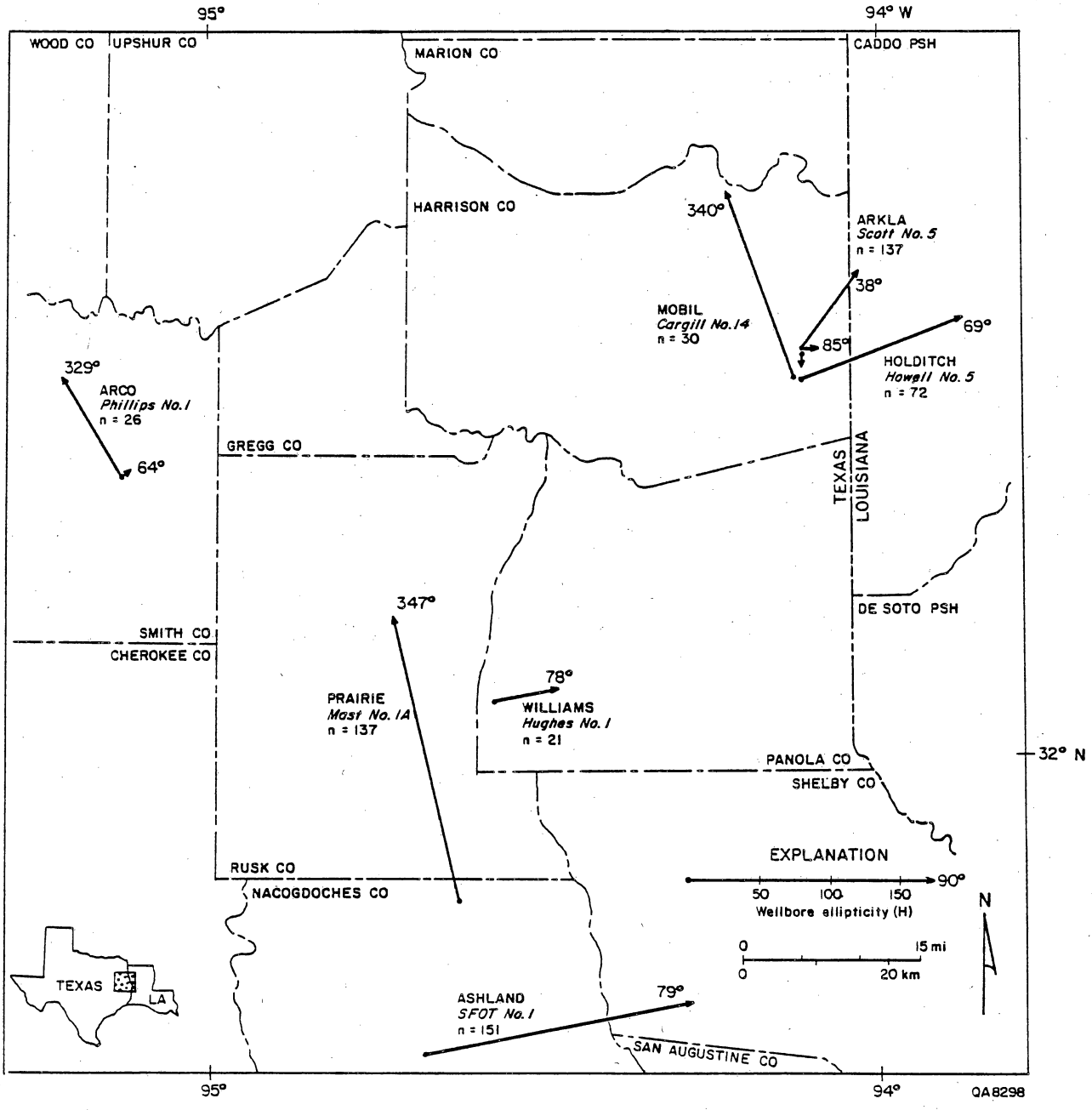

Figure 38. Map of seven wells with polar plots of H for wellbore ellipticity. Distribution of wellbore ellipticity is strongly bimodal, with northwest- and northeast-trending peaks.

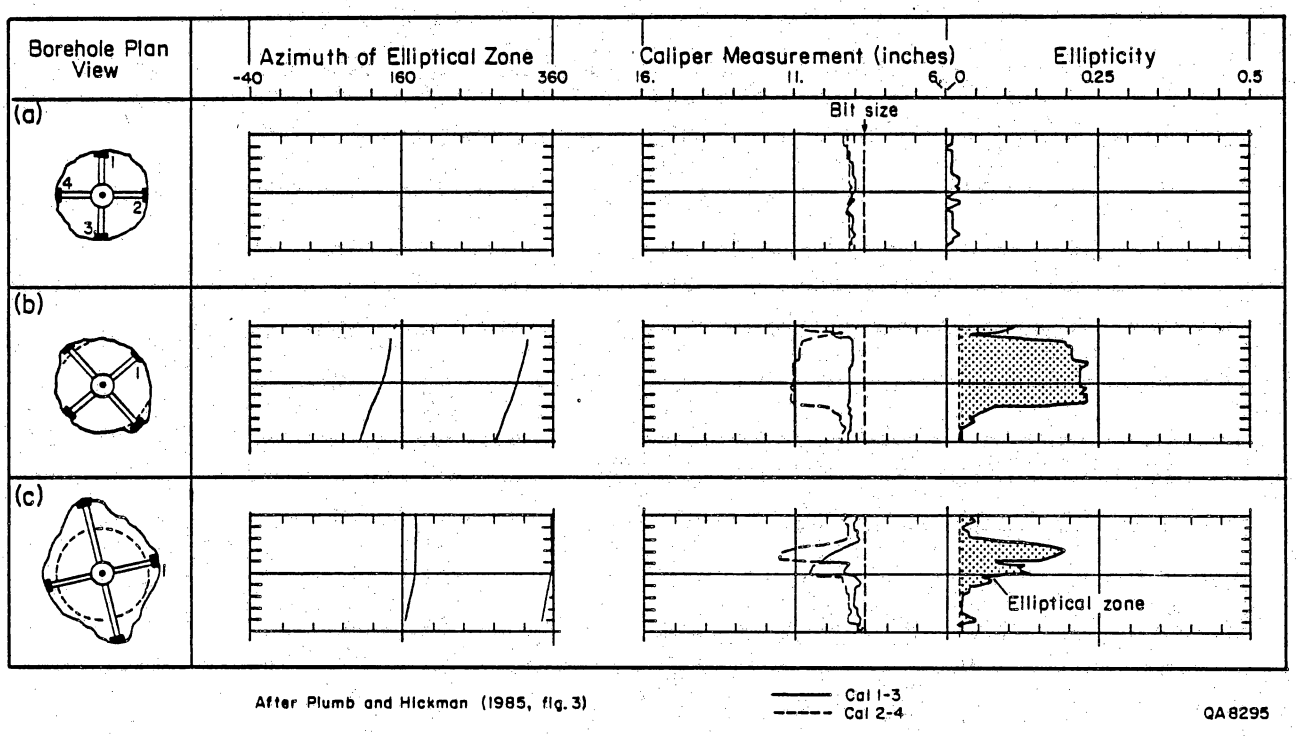

Figure 39. Plan views and ellipticity log sections for in gauge borehole, borehole breakout, and washout. (a) Caliper readings for in gauge hole are near bit size; hence no azimuth of elliptical zone is recorded. (b) Caliper 1-3 in breakout is near bit size. Caliper 2-4 marks the larger diameter (11 inches). Maximum ellipticity is 0.23. Azimuth of elliptical zone in upper 10 ft of log section (b) is between 300 and 320 degrees. (c) Both calipers measure larger than bit size in washout. Caliper 2-4 marks the larger diameter (11.5 inches). Maximum ellipticity is 0.19. Azimuth of elliptical zone in upper 10 ft of log section (c) is 355 degrees. Major vertical divisions on log represent 10 ft.

Initially, the criteria used by Plumb and Hickman (1985) to define breakouts (fig. 39b) were adopted and modified slightly. These included (1) axisymmetric wellbore elongations where (2) the caliper tool stops rotating in the zone of elongation as it is raised up the hole, (3) the smaller of the caliper readings is close to bit size, and (4) the height of the elliptical zone covers at least one 2-ft interval on the ellipticity log.

The first criterion could be applied to only one well, Holditch Howell No. 5, which had BHTV logs. Other wells had no means of confirming the symmetry of the elongated zone. However, later work by Plumb and Cox (1987) showed that it is not necessary to prove that the elongations are symmetrical to define regional stress directions. Plumb and Cox analyzed wellbore elongations over a wide area of the Appalachian Basin and found them aligned with the least horizontal principal stress. Consequently, the symmetry criterion was not applied to the elongation data in this study. To ensure that wellbore elongations were not the result of wellbore deviation, the inclination and direction of wellbore deviation were checked. Deviation never exceeded 2 degrees. Nevertheless, no elongations were included that were parallel or 180 degrees opposite to the direction of wellbore deviation.

The strict application of the third criterion produced only 35 breakouts. This number of breakouts may be too small for reliable statistical analysis of directional data. Therefore, the third criterion was replaced by a minimum value (0.03) of ellipticity, corresponding to differences inch caliper readings of 0.24 to 0.30 inch for the range in bit sizes used in these wells. A total of 574 elliptical zones were detected (table 2). Many of these elliptical zones are washouts in the classification of Plumb and Hickman (1985) because both calipers register borehole that is larger than bit size (fig. 39c). Nevertheless, these elliptical zones may be enlarged by stress-induced spalling or erosion of the wellbore along stress-related fractures.

Table 2. Wellbore ellipticity data from seven wells in East Texas.*

Well Name (Owner-Lease)	n	H Az.	H Mag.	Height (ft) Max.	Ellipticity Mean	Ellipticity Max.	Ellipticity Min.	Bit Size
ARCO Phillips No. 1	26	329°	85	30 8.0	0.38	0.06	0.14	8 3/4"
" "	"	64°	7	14 5.2	0.10	0.03	0.08	
Arkla Scott No. 5	137	38°	74	36 9.5	>0.50	0.07	>0.18	7 7/8"
" "	"	85°	13	22 7.8	0.41	0.07	0.16	
Ashland SFOT No. 1	151	79°	199	24 4.6	>0.50	0.04	>0.22	8 3/4"
Holditch Howell No. 5	72	69°	125	22 6.5	0.44	0.03	0.12	8 3/4"
Mobil Cargill No. 14	30	340°	146	10 3.7	>0.50	0.07	>0.21	9 7/8"
Prairie Mast No. 1A	137	347°	210	34 5.3	0.50	0.03	0.13	8 3/4"
Williams Hughes No. 1	21	78°	48	10 3.3	0.24	0.04	0.08	7 7/8"
All data	574	74°	229	24 5.6	>0.50	0.03	>0.16	-------
" "	"	344°	101	34 5.7	>0.50	0.03	>0.16	-------
Upper 370 ft of Travis Peak Fm.	159	77°	180	34 5.3	>0.50	0.03	>0.17	-------
Lowest Travis Peak Fm. in 3 wells	99	346°	177	34 8.9	>0.50	0.03	>0.15	-------
Breakouts only	35	338°	103	14 3.7	>0.50	0.07	>0.26	-------

*Number of continuous elliptical zones is shown by n. Bernshtein accuracy criterion (H) shows the azimuth and magnitude of vector sums of elliptical zones. Height of continuous elliptical zones is measured in 2-ft increments on ellipticity logs. Minimum height is 2 ft. Ellipticity is the difference between caliper readings in each 2-ft elliptical zone divided by bit size, as shown on ellipticity logs. Height and ellipticity data are for only those elliptical zones that comprise the significant vector sums of elliptical zones. For location of wells see figure 38.

Data from each well and from all wells combined were used to define directions of wellbore elongation (table 2). For each 2-ft interval on the log where the borehole is elliptical the magnitude of ellipticity and its azimuth were recorded. Azimuth was measured to the nearest 5 degrees. These measurements were grouped into 10-degree wide sectors. For example, azimuths of 0 and 5 degrees, which cover the interval 0 to 9 degrees, were grouped together as the 0-degree sector. The lengths of vertically continuous elliptical zones with the same azimuth were summed. Finally, to define a value of significant wellbore ellipticity for each well, the number, length, and azimuth of elliptical zones were treated as follows.

Orientations of the elliptical zones were first displayed as polar diagrams of length-weighted frequency (F) following the procedure outlined by Dix and Jackson (1981). As mentioned above, sector width of 10 degrees was used. Adjacent sectors larger than the mean value of F were summed and the resultant vector was plotted. Finally, a chi square test was applied to each vector to determine its level of significance (Vistelius, 1966; Dix and Jackson, 1981). The resultant value, known as the Bernshtein accuracy criterion (H), was plotted with the same azimuth as the vector sum (fig. 38). The 99-percent confidence level was used to define significant sector peaks because Dix and Jackson (1981) showed that sector peaks significant at lower confidence levels can be obtained with synthetic directional features derived from a random number table.

The small numbers of elliptical zones in individual wells may generate orientation peaks that are not statistically valid. Dix and Jackson (1981), in a study of randomly generated "lineaments," found that data sets smaller than 200 contained peaks that were significant even at the 99-percent confidence level. As a result, they recommended that directional data sets have at least 200 values to avoid including spurious peaks. If the same standard is applied to the present study, then none of

the data sets of wellbore ellipticity from individual wells would be large enough to exclude spurious peaks. However, the consistent pattern of northeast- and northwest-trending ellipticity, nearly at right angles, indicates that the significant peaks of ellipticity for individual wells are not strongly affected by random processes or by spurious peaks. Furthermore, if all data from all wells are combined the resulting set contains 574 elliptical zones with two significant peaks, which are exactly perpendicular: one at 344 degrees and the other at 74 degrees (table 2).

WELLBORE ELLIPTICITY--SIGNIFICANT ORIENTATIONS

The significant values of wellbore ellipticity were arranged in two groups: northwest-oriented (from 329 to 347 degrees) and northeast-oriented (from 38 to 85 degrees) (fig. 38) (all directions in this report are referred to using the northern half of the compass: 270 to 0 to 90 degrees). Most orientations of the significant vector sums of ellipticity from individual wells (table 2, fig. 38) are subparallel either to the north-northwest-oriented minimum horizontal principal stress in the region (Collins and others, 1980; Zoback and Zoback, 1980) or to east-northeast-trending fractures (Part One, this report). These results suggest that subsurface stress controls wellbore ellipticity either directly through spalling of the wellbore (breakouts, fig. 39b), or indirectly, through erosion of the borehole along vertical fractures (washouts, fig. 39c). To test the hypothesis that wellbore ellipticity was produced by these two mechanisms, directions of ellipticity were compared with orientations of fractures and of least horizontal principal stress.

Ellipticity and Fractures

Fracture Trends and Borehole Televiewer Results

The predominant trend of natural and coring-induced fractures in the Travis Peak Formation is east-northeast to east (figs. 3 and 5). The orientation of these fractures is approximately perpendicular to the extension direction in the northern Gulf of Mexico stress province (an extensional stress regime) and, presumably, approximately perpendicular to least horizontal stress. Preexisting or drilling-induced fractures can act as initiation points for spalls (fig. 34), resulting in elongated boreholes parallel to fractures. These elongated sections of borehole are probably washouts (fig. 39) as defined by Plumb and Hickman (1985), and the elongations that develop along them probably result indirectly from in situ stress. However, it is also possible that some of the east-northeast-trending fractures did not form as a result of the current stress regime. In that case, borehole elongations along these fractures would not be diagnostic of current stresses.

Ellipticity and Depth

Analysis of BHTV logs shows that fractures are significantly longer in the upper Travis Peak than in the lower part of the formation (fig. 5). If some wellbore elongations are caused by fractures, then they should demonstrate the same relationship with respect to depth. Wellbore ellipticity and depth were examined in seven wells. Because all wells do not penetrate to the same depth or cover the same intervals in the Travis Peak Formation (fig. 40), a ratio was defined so that measurement of elliptical zones was not weighted in favor of zones with more data:

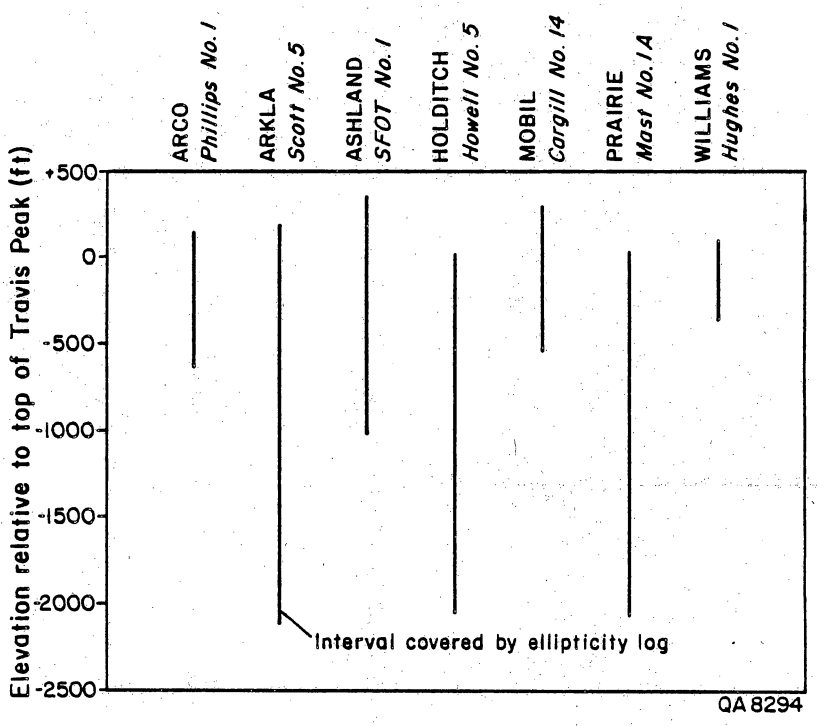

Figure 40. Plot of wells showing intervals in Travis Peak Formation covered by ellipticity logs in this study.

$$\text{ellipticity ratio} = Ne/Nw \quad (3)$$

where: Ne = number of 2-ft elliptical log intervals

Nw = number of wells with data

Values of Ne and Nw were determined for 100-ft intervals.

The ellipticity data were divided into two groups based on the previous determination of significant wellbore orientations (as described above, table 2). Six 10-degree wide sectors (320 to 10 degrees) of the significant northwest peaks comprised one group. Nine 10-degree wide sectors (20 to 100 [=280] degrees) of the northeast peaks were the other. Some of the 10-degree-wide sectors in each group fall outside the boundaries of the respective quadrant (northeast or northwest) because a significant peak in that quadrant contained them.

Ellipticity ratios were calculated for the northwest and northeast groups for each 100-ft interval of well log data. The ratio data were then smoothed using a 3-interval moving average to subdue large "peaks" and "valleys" caused by using 100-ft intervals to subdivide the data. The moving averages were plotted against two measures of depth: (1) depth below Kelly bushing (approximate ground surface), and (2) depth below top of the Travis Peak Formation (figs. 41 and 42).

To determine whether ellipticity direction has a significant correlation with depth, the 99-percent confidence level was calculated for both groups. Values of ellipticity ratio larger than the 99-percent confidence level are considered significantly larger than the mean value. For the plot of ellipticity ratio and depth below Kelly bushing, no trend is apparent (fig. 41). Northwest- and northeast-trending peaks significant at the 99 percent confidence level occur throughout the interval covered by the well logs. However, for ellipticity data plotted relative to the top of the Travis Peak, a marked

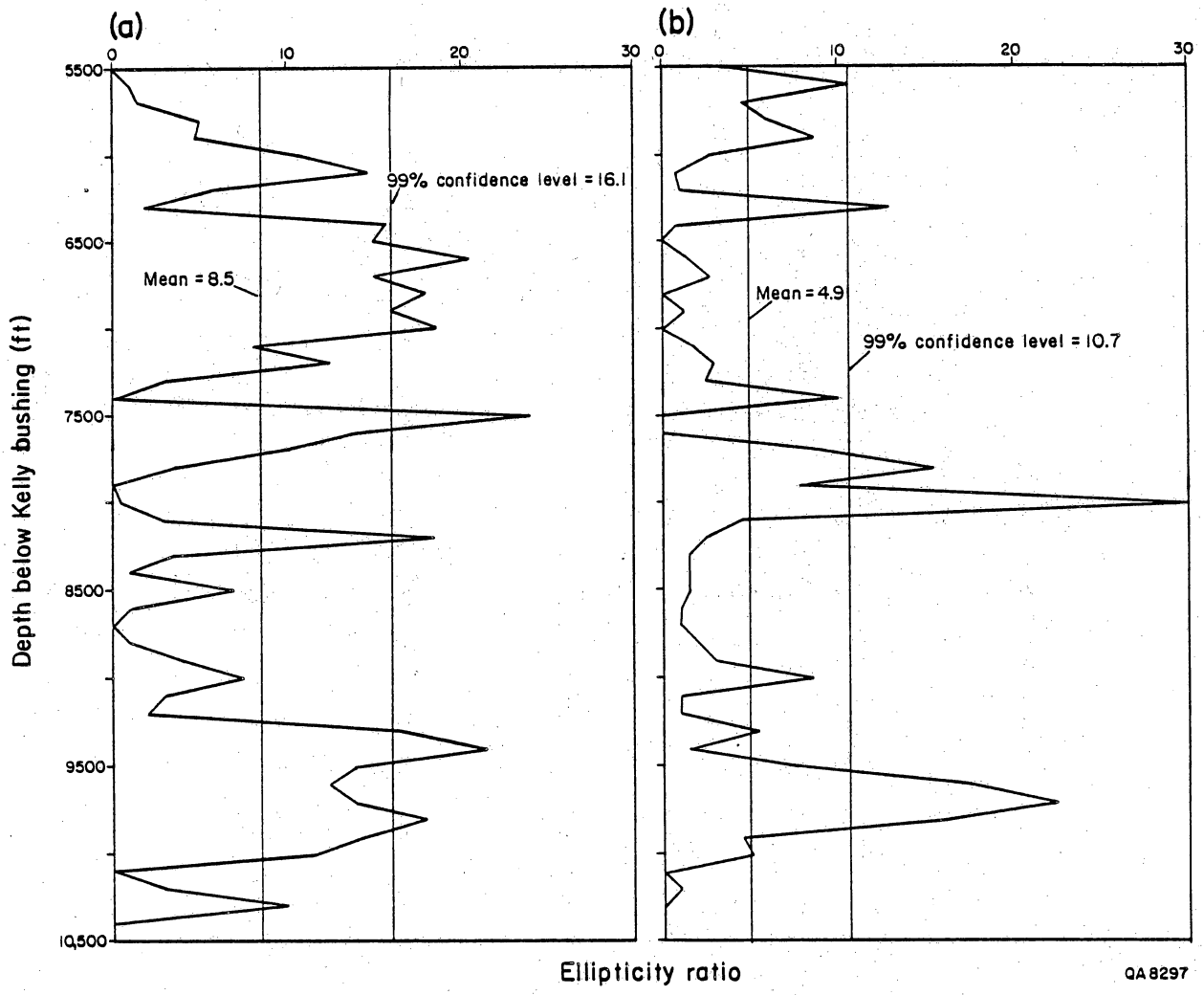

Figure 41 Plots of ellipticity ratio vs elevation relative to Kelly bushing (approximate ground surface). (a) Northeast peaks (b) Northwest peaks No clear distinction exists between the northeast and northwest peaks relative to depth below Kelly bushing.

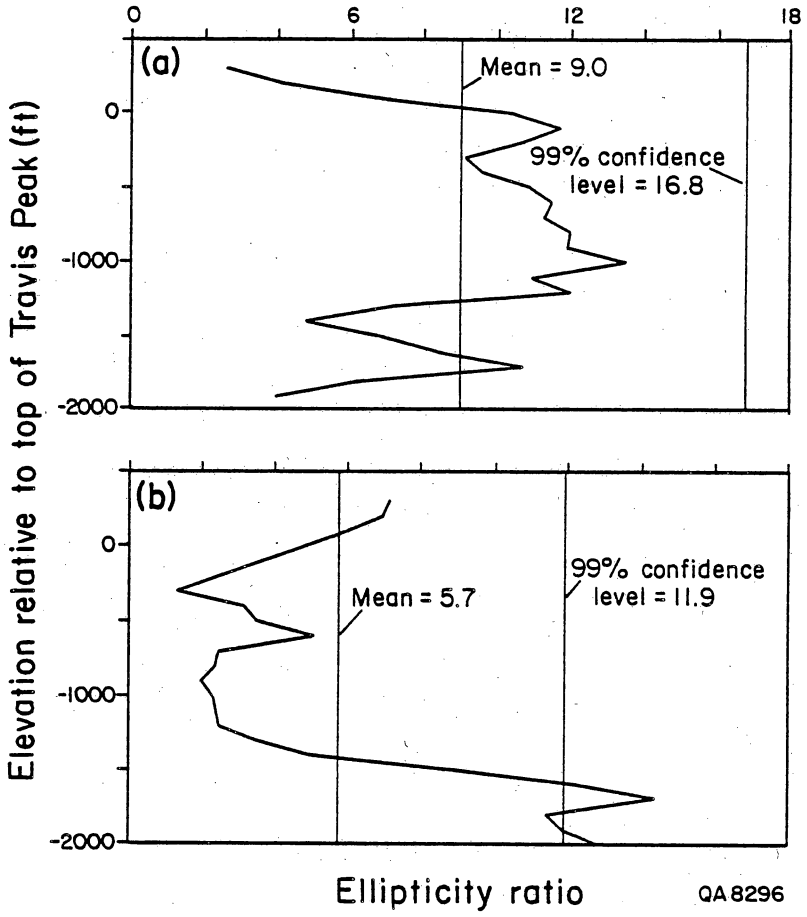

Figure 42 Plots of ellipticity ratio vs. elevation relative to top of the Travis Peak Formation. (a) Northeast peaks. (b) Northwest peaks. Ellipticities can be divided into two classes based on stratigraphic depth Northeast peaks are concentrated above -1,300 ft. Northwest peaks are located principally below -1,500 ft.

difference exists between the distribution of the northeast- and northwest-trending peaks (fig. 42). For the northeast-trending data, there are no zones significant at the 99-percent confidence level, but those larger than the mean are mostly higher than 1300 ft below the top of the Travis Peak (fig. 42a). For the northwest-trending data, ellipticity ratios significant at the 99-percent confidence level occur only lower than 1500 ft below the top of the Travis Peak (fig. 42b).

Likewise, significant azimuths of wellbore elongation for the shallow and deep parts of the Travis Peak are quite different. For the part of the Travis Peak Formation that all wells penetrate (upper 370 ft) the significant elongation azimuth is 77 degrees (table 2). Conversely, for the lowest 580 ft of the Travis Peak penetrated by three wells (Arkla Scott No. 5, Holditch Howell No. 5, and Prairie Mast No. 1-A) (fig. 40) the significant azimuth of elongations is 346 degrees. This zone is about 1,090 ft below the 370-ft zone penetrated by all seven wells. These two azimuths are perpendicular (within the accuracy of these measurements), confirming the general trend shown in figure 42.

Clearly, there is a marked difference in ellipticity orientation with respect to depth below the top of the Travis Peak but not with respect to depth below present ground surface. The orientation of natural and drilling-induced fractures (figs. 3 and 5) parallels the trend of borehole ellipticity in the upper Travis Peak; thus, it is possible that either preexisting natural fractures, or drilling-induced fractures are controlling ellipticity in this part of the formation. In deeper parts of the formation, northwest-trending ellipticity probably is caused by spalling of the borehole (breakouts) in the regional stress regime. This hypothesis is consistent with observations of fracture length in the Holditch Howell No. 5 well. Fractures in the upper 460 ft of Travis Peak are significantly longer than in the interval between 1,394 and 1,786 ft below top of the formation (figs. 5 and 12).

Similar results have been reported by Stock and others (1984) from studies in Nevada. Natural fractures observed on borehole televiewer logs had a preferred azimuth of 10 to 40 degrees. In addition, at relatively shallow depths (1,725 to 2,225 ft), near-vertical, drilling-induced fractures were observed with orientations of 25 to 30 degrees. These were interpreted to be perpendicular to the minimum horizontal principal stress. However, wellbore breakouts near the bottom of the logged well (3,455 to 4,000 ft depth) had a mean azimuth of 300 degrees, parallel to the interpreted direction of least horizontal principal stress, and perpendicular to the natural and drilling-induced fractures.

The change in orientation of borehole ellipticity with depth below top of the Travis Peak also coincides with an increase in the degree (and possibly the age) of quartz cementation (Dutton, 1987). Except for variations in the amount of quartz cement, lithologic variations between upper and lower Travis Peak are probably not mechanically significant (Dutton, 1987; Fracasso, 1987), although the upper part of the formation contains more shale.

Ellipticity and Lithology

To distinguish between the possible effects of depth and lithology on wellbore ellipticity, the orientation of elliptical zones was compared to that of lithology logs. Lithology was determined from FRACLOG, CORELOG, and lithology log records from the seven wells shown in figure 40. These were correlated with ellipticity logs by matching caliper measurements from each pair of logs from each well. The lithology for each 2-ft interval was defined as whatever rock type composed more than 50 percent of the interval.

Elliptical boreholes develop more often in shale than in sandstone. Almost half of all elliptical zones occur in shale (table 3), although shale constitutes only 19 percent of the logged lengths of the boreholes. Thus, elliptical zones occur in shale more

Table 3. Orientation and magnitude of elliptical zones in seven wells relative to lithology. Although shale is exposed in only 19 percent of the logged length of wellbores, 46 percent of all elliptical zones are in shale.

Elliptical zone:	Lithology SH	SS
Magnitude		
0.11-0.20	41	59
0.21-0.30	50	50
>0.30	56	44
Orientation		
NW (280-350°)	18	20
NE (10-80°)	19	25
N-S (350-10°)	3	2
E-W (80-90°, 270-280°)	6	6
Total (%)	46	53
Logged length (%)	19	81

SH=shale
SS=sandstone

than twice as often as they would if distribution of elliptical zones were unrelated to lithology.

Furthermore, as the magnitude of the elliptical zones increases, so does the percentage of those elliptical zones found in shale. Forty-one percent of all elliptical zones between 0.11 and 0.20 are in shale, whereas 56 percent of elliptical zones larger than 0.30 are in shale (table 3).

The orientation of elliptical zones is unaffected by lithology. Most elliptical zones in sandstone and shale are about evenly divided between northeast and northwest. Elliptical zones oriented north-south and east-west are less common, in proportion to their smaller fraction (20 degrees each) of the total range of orientation values (180 degrees).

The dependence of paleostress and modern stress indicators on stratigraphic depth, but not on depth below the surface, raises the possibility that a significant component of the horizontal stress anisotropy in the Travis Peak is a residual elastic strain (Friedman, 1972; Holzhausen and Johnson, 1979; Hoskins and Russell, 1981) locked in by the quartz cement. This possibility remains to be tested by further research.

Ellipticity and Stress

Recent work in the Holditch Howell No. 5 well provides consistent information about stress relations in Waskom field. Average azimuth of maximum horizontal stress reported by Owen and others (1987) is 77 degrees, based on "excellent" anelastic strain recovery data from six core samples. CER Corporation (1987b) reported that orientations of fractures induced by stress tests range from 72 degrees to 88 degrees, thereby confirming an east-northeast-oriented maximum horizontal stress. In addition, differential strain curve analysis (Jeffrey and others, 1987a) shows that least principal horizontal stress is oriented north-northwest.

Similar results have been reported for a large area surrounding Waskom field. Gough and Bell (1982) summarized data on the stress regime of East Texas and northwest Louisiana. Citing the presence of extensional normal faults in the East Texas Basin and growth faults to the south, they concluded that the area south of the Mexia-Talco Fault Zone is an extensional tectonic province, one in which the minimum principal stress is horizontal and approximately perpendicular to the traces of extensional faults.

Data from 50 wells scattered throughout East Texas provide important additional information about regional stress directions. Brown and others (1980) measured the azimuths of wellbore elongations in the Schuler Formation at depths below about 9,200 ft. Mean elongation azimuth for all wells was 325 degrees. Based on the orientations of vertical hydraulic fractures (east-west) (Strubhar and others, 1975) and recently active normal faults (northeast-southwest) in the area, Gough and Bell (1982) concluded that the northwest orientations of these elongation azimuths were approximately parallel to the least principal stress.

Northwest-trending wellbore elongations from wells in this study also show near-parallelism with (presumed) least principal stress (fig. 38). Azimuths for individual wells range from 329 to 347 degrees. The mean azimuth for all northwest-trending elongations is 344 degrees. Finally, the mean azimuth for only those elongations that fit Plumb and Hickman's (1985) definition of "breakout" is 338 degrees (table 2).

The parallelism between northwest-trending borehole elongations and minimum principal horizontal stress fits the model for stress-induced borehole breakouts (Gough and Bell, 1982; Plumb and Cox, 1987). It is reasonable to conclude that the northwest-oriented elliptical boreholes are a function of the regional stress regime, and they indicate that hydraulic fractures would propagate perpendicular to them.

Ellipticity and Strain Measurements

Maximum horizontal strain orientations in the upper Travis Peak Formation were calculated by Owen and others (1987) using core samples from the Holditch Howell No. 5 well. Depth of the cored interval ranged from 5,989 to 6,310.5 ft. Orientations of calculated strains were obtained from 11 samples between 5,995 and 6,305.5 ft depth (table 4). These orientations range from 28 to 127 degrees; the mean is 95 degrees. These results indicate that the maximum horizontal stress is oriented generally east-west. Consequently, tension fractures would form east-west.

Ellipticity measurements were obtained within 10 ft of nine of the strain measurements. The range of orientations of elliptical zones (40 to 80 degrees) is within the range covered by strain measurement orientations. Mean values for the overlapping zones are 93 degrees for the strain measurements and 59 degrees for the elliptical zones. These are not compellingly similar.

Owen and his coworkers (1987) identified four of their measurements as "most reliable data" (table 4). The mean orientation value for three of these with corresponding ellipticity measurements is 69 degrees. The mean direction of the three corresponding ellipticity measurements is 53 degrees. That they are subparallel suggests that ellipticity is indirectly affected by the strain, possibly by erosion along northeast-trending tension fractures. The mean direction of all four "most reliable" strain measurements is 77 degrees. The significant azimuth of wellbore elongations in the upper 370 ft of the Travis Peak (which covers most of the interval where strain measurements were made in the Holditch Howell well) for all seven wells is 77 degrees (table 2). This parallelism between strain recovery measurements in one well and widespread ellipticity measurements suggests that the stress field in the rocks is indirectly controlling ellipticity through erosion of the borehole along northeast-trending fractures.

Table 4. Strain relaxation measurements (after Owen and others, 1987, table 2) and wellbore ellipticity data from Holditch Howell No. 5 well.

Sample Number	Maximum horiz. strain Depth (ft)	Maximum horiz. strain Orientation (°)	Wellbore ellipticity Depth (ft)	Wellbore ellipticity Orientation (°)
1	5995	110	-----	---
2	6083	123	6088	80
3	6084	118	6088	80
*4	6120	68	6124	80
*5	6187.5	60	6182	40
*6	6190	80	6182	40
7	6224	124	6226	45
8	6228	110	6228	40
9	6253	127	6262	65
10	6253.5	28	6262	65
*11	6305.5	99	-----	---
Mean for all data:		95	-----	59

*"most reliable data"

CONCLUSIONS

Preliminary comparison of core with FMS and BHTV logs from the Holditch Howell No. 5 well revealed criteria for recognizing fractures on these logs. Fracture orientation and length were obtained using combined runs of the FMS and BHTV logs. Fractures 0 to 500 ft below the top of the Travis Peak Formation show preferred orientations of 60 to 90 degrees and lengths of 4 to 13 ft. Fractures 1,400 to 1,800 ft below the top of the Travis Peak have preferred orientations of 72 to 97 degrees and are 2 to 10 ft long. All fractures are subvertical to vertical.

Two directions of borehole elongation were established using the BHTV log. Results suggest different origins for the two directions of spalls. One type of elongation has the same orientation as fractures and is slightly to one side but in contact with fracture traces. These appear to be caused by drilling-related erosion of the fracture where it intersects the borehole. The second type of elongation was observed at 30 to 90 degrees to fractures and in unfractured zones. These may be related to the regional stress field.

The similarities between orientations of peaks of wellbore ellipticity (344 and 74 degrees) and (1) coring-induced fractures (60 to 90 degrees), (2) maximum strain recovery (most reliable data = 77 degrees), and (3) minimum horizontal principal stress from hydraulic fracturing data (north-northwest) (Gough and Bell, 1982) are quite strong. The significant azimuth for the 35 elongations that fit Plumb and Hickman's (1985) criteria for breakouts is 338 degrees (table 2). This orientation is subparallel (as expected, based on Plumb and Hickman's [1985] work) to the north-northwest-oriented minimum horizontal principal stress in the northern Gulf Coast region (Collins and others, 1980; Zoback and Zoback, 1980; Gough and Bell, 1982).

These results suggest that the northwest-oriented wellbore elongations fit the criteria established by Plumb and Cox (1987) for stress-related ellipticity. In addition, BHTV logs show spalls developed along fractures and fracture length and direction of wellbore elongation vary with depth. Northeast-oriented wellbore elongations appear to be functions of fracture intersection and may be indirectly caused by current or residual stress.

FUTURE WORK

The relation between wellbore elongation, fractures, lithology, and in situ stress will be the subject of further study. Further comparison between logs and core is needed to distinguish natural from drilling-induced fractures. Additional studies will quantify the direction and vertical distribution of spalls and define further the relation of wellbore elongations to fractures and regional stress. Oriented core, BHTV logs, and ellipticity logs will be used to distinguish between wellbore ellipticity controlled by fractures and that caused by spalling. These studies should assist in separating the effects of current stress and residual stress on wellbore ellipticity and fracture propagation.

ACKNOWLEDGMENTS

This work was prepared for, and funded by, the Gas Research Institute under contract No. 5082-211-0708, Robert J. Finley and Shirley P. Dutton, Co-Principal Investigators.

The cooperation of the following companies and operators is gratefully acknowledged: Amoco Production Company (USA), ARCO Oil and Gas Company,

Ashland Exploration, Inc., Prairie Producing Company, Clayton W. Williams, Jr., and Mobil Producing Texas and New Mexico, Inc.

Eric Monson, CER Corporation, analyzed fractures in the field and contributed to the development of the results presented here. Karen Herrington assisted with electron beam microscopy, and Peter Hennings assisted with petrography.

Word processing was by Kurt Johnson under the direction of Lucille C. Harrell. Illustrations were prepared by Nan Minchow-Newman, Annie Kubert-Kearns, and Margaret Evans under the direction of Richard L. Dillon. Text illustration camerawork was by James A. Morgan. Production of the contract report was by Lana Dieterich.

REFERENCES

Anderson, E. M., 1951, The dynamics of faulting: Edinburgh, Oliver & Boyd, 191 p.

Arthaud, F., 1969, Méthode de détermination graphique des directions de raccourcissement d'allongement et intermédiaire d'une population de failles: Bulletin de la Société Géologique de France, v. 11, p. 739-737.

Barton, N. R., 1986, Deformation phenomena in jointed rock: Geotechnique, v. 36, p. 147-167.

Bethke, C. M., 1985, A numerical model of compaction-driven groundwater flow and heat transfer and its application to the paleohydrology of intracratonic sedimentary basins: Journal of Geophysical Research, v. 90, p. 6817-6828.

Blanton, T. L., 1982, An experimental study of interaction between hydraulically-induced and pre-existing fractures: SPE/DOE Unconventional Gas Recovery Symposium, SPE Paper 10847, p. 559-562.

Bles, J-L., and Feuga, B., 1986, The fracture of rocks: New York, Elsevier, 131 p.

Branagan, P. T., Cipolla, C. L, Lee, S. J., and Yan, L., 1987, Case history of hydraulic fracture performance in the naturally fractured paludal zone: the transitory effect of damage: SPE/DOE Joint Symposium on Low Permeability Reservoirs, SPE Paper 16397, p. 61-73.

Brantley, S. L., Crerar, D., and Evans, B., 1986, Porosity reduction by solution transfer: experimental evidence for quartz (abs): Geological Society of America Abstracts with Programs, v. 18, p. 549.

Brown, R. O., Forgotson, J. M., and Forgotson, J. M., Jr., 1980, Predicting the orientation of hydraulically created fractures in the Cotton Valley Formation of east Texas: SPE Paper 9269, 55th Annual Fall Conference, 12 p.

Buffler, R. T., Watkins, J. S., Shaub, F. J., and Worzel, J. L., 1980, Structure and early geologic history of the deep central Gulf of Mexico, in Proceedings, Symposium on the origin of the Gulf of Mexico and the early opening of the central North Atlantic Ocean: Baton Rouge, Louisiana State University, School of Geoscience, p. 3-16.

CER Corporation, 1984, Coring and logging operations summary, Clayton Williams Sam Hughes No. 1: Report prepared for the Gas Research Institute, 34 p.

_____ 1985a, Coring and logging operations summary, Ashland Exploration S.F.O.T. No. 1: Report prepared for the Gas Research Institute, 103 p.

_____ 1985b, Summary of data acquisition and field operations, Prairie Producing Company A. T. Mast No. A-1: Report prepared for the Gas Research Institute, 157 p.

_____ 1986a, Summary of data aquisition and field operations, Marshall Exploration Werner Sawmill No. 5: Report prepared for the Gas Research Institute, 68 p.

_____ 1986b. Summary of data acquisition and field operations, Arkla Exploration T. P. Scott No. 5: Report prepared for the Gas Research Institute, 74 p.

_____ 1987a. Observations and orientations of fractures induced through open-hole stress tests: Report prepared for the Gas Research Institute, 30 p.

_____ 1987b. Summary of data acquisition and field operations, Mobil Producing Texas and New Mexico G. E. Cargill No. 14: Report prepared for the Gas Research Institute, 46 p.

Collins, E. W., Hobday, D. K., and Kreitler, C. W., 1980, Quaternary faulting in East Texas: The University of Texas at Austin, Bureau of Economic Geology Geological Circular 80-1, 20 p.

Dickenson, W. R., 1974, Subduction and oil migration: Geology, v. 2, p. 421-424.

Dix, O. R., and Jackson, M. P. A., 1981, Statistical analysis of lineaments and their relation to fracturing, faulting, and halokinesis in the East Texas Basin: The University of Texas at Austin, Bureau of Economic Geology Report of Investigations No. 110, 30 p.

Dutton, S. P., 1986, Petrography and diagenesis of the Lower Cretaceous Travis Peak (Hosston) Formation, East Texas: The University of Texas at Austin, Ph.D. dissertation, 183 p.

_____ 1987, Diagenesis and burial history of the Lower Cretaceous Travis Peak Formation, East Texas: controls on permeability in a tight gas sandstone: The University of Texas at Austin, Bureau of Economic Geology, Report of Investigations No. 164, 58 p.

Engelder, T., 1982, Is there a genetic relationship between selected regional joints and contemporary stress within the lithosphere of North America?: Tectonics, v. 1, p. 161-177.

_____ 1985, Loading paths to joint propagation during a tectonic cycle: an example from the Appalachian Plateau, U.S.A.: Journal of Structural Geology, v. 7, p. 459-476.

_____ 1987, Joints and shear fractures in rock: in Atkinson, B. K., ed., Fracture mechanics of rock: New York, Academic Press, p. 27-65.

Etheridge, M. A., Wall, V. J., and Cox, S. F., 1984, High fluid pressures during regional metamorphism and deformation: implications for mass transport and deformation mechanisms: Journal of Geophysical Research, v. 89, p. 4344-4358.

Fournier, R. O., and Potter, R. W., 1982, An equation correlating the solubility of quartz in water from 25° to 900°C at pressures up to 10,000 bars: Geochimica et Cosmochimica Acta, v. 46, p. 1969-1973.

Fracasso, M. A., 1987, Staged Field Experiment site selection and geological characterization of the upper Travis Peak Formation, Harrison and Panola

Counties, East Texas: The University of Texas at Austin, Bureau of Economic Geology, topical report prepared for Gas Research Institute under contract no. 5082-211-0708, 45 p.

Friedman, M., 1972, Residual elastic strain in rocks: Tectonophysics, v. 15, p. 297-330.

Fyfe, W. S., Price, N. J., and Thompson, A. B., 1978, Fluids in the Earth's crust: Amsterdam, Elsevier, 383 p.

Gallagher, J. J., Friedman, M., Handin, J., and Sowers, G. M., 1974, Experimental studies relating to microfracture in sandstone: Tectonophysics, v. 21, p. 203-247.

Gough, D. I., and Bell, J. S., 1982, Stress orientations from borehole wall fractures with examples from Colorado, east Texas and northern Canada: Canadian Journal of Earth Sciences, v. 19, no. 7, p. 1358-1370.

Granata, W. H., Jr., 1963, Cretaceous stratigraphy and structural development of the Sabine Uplift area, Texas and Louisiana, in Hermann, L.A., ed., Report on selected North Louisiana and South Arkansas oil and gas fields and regional geology: Shreveport Geological Society Reference Volume V, p. 50-95.

Grout, M. A., and Verbeek, E. R., 1987, Regional joint sets unrelated to major folds: example from the Piceance Basin, northeastern Colorado Plateau (abs.): Geological Society of America Abstracts with Programs, v. 19, p. 279.

Halbouty, M. T., and Halbouty, J. J., 1982, Relationships between East Texas field region and the Sabine Uplift in Texas: American Association of Petroleum Geologists Bulletin, v. 66, p. 1042-1054.

Hamil, B. M., and Sriruang, S., 1976, A study of rock failure induced by dynamic tensile stress and its application to fracture mechanics in Strens, R. G. J., ed., The physics and chemistry of minerals and rocks: New York, Interscience, p. 151-196.

Haszeldine, R. S., Samson, I. M., and Cornford, C., 1984, Dating diagenesis in a petroleum basin, a new fluid inclusion method: London, Nature, v. 307, p. 354-357.

Helgeson, H. C., and Lichtner, P. C., 1987, Fluid flow and mineral reactions at high temperatures and pressures: Journal of the Geological Society of London, v. 144, p. 313-326.

Hertzberg, R. W., 1983, Deformation and fracture mechanics of engineering materials: New York, John Wiley and Sons, 697 p.

Holditch, S. A., Robinson, B. M., and Whitehead, W. S., 1987a, The analysis of complex Travis Peak reservoirs in East Texas: SPE/DOE Joint Symposium on Low Permeability Reservoirs, SPE Paper 16427, p. 381-399.

Holditch, S. A., Robinson, B. M., Whitehead, W. S., and Ely, J. W., 1987b, The GRI Stage Field Experiment: SPE/DOE Joint Symposium on Low Permeability Reservoirs, SPE Paper 16429, p. 409-429.

Holzhausen, G. R., and Johnson, A. M., 1979, The concept of residual stress in rock: Tectonophysics, v. 58, p. 237-267.

Hoskins, E. R., and Russell, J. E., 1981, The origin of measured residual strains in crystalline rocks: in Mechanical Behavior of Crustal Rocks, Geophysical Monograph 24, American Geophysical Union, Washington, D.C., p. 187-198.

Hunt, E., 1986, Development of petrophysical techniques for evolution: tight gas sands: Quarterly Technical Report prepared for Gas Research Institute, Contract Number 5084-211-1062.

Jackson, M. L. W., 1986, Structural history of the Sabine Uplift area, East Texas and North Louisiana, in Baumgardner, R. W., and Jackson, M. L. W., Landsat-based lineament analysis, East Texas Basin, and structural history, Sabine Uplift area, East Texas and North Louisiana: The University of Texas at Austin, Bureau of Economic Geology, topical report prepared for Gas Research Institute under contract no. 5082-211-0708.

Jackson, M. L. W., and Laubach, S. E., 1987, Evidence for Sevier and Laramide deformation in the Gulf of Mexico Basin (abs.): Geological Society of America Abstracts with Programs, v. 19, p. 285.

Jackson, M. P. A., 1982, Fault tectonics of the East Texas Basin: The University of Texas at Austin, Bureau of Economic Geology Geological Circular 82-4, 31 p.

Jeffrey, R. G., Skach, E. W., Nimerick, K., and Redmond, J., 1987a, Rock mechanics testing of core samples from Staged Field Experiment Well Howell No. 5., Report prepared for the Gas Research Institute by Dowell Schlumberger, 42 p.

Jeffrey, R. G., Vandamme, L., and Roegiers, J-C., 1987b, Mechanical interactions in branched or subparallel hydraulic fractures: SPE/DOE Joint Symposium on Low Permeability Reservoirs, SPE Paper 16422, p. 333-343.

Kemeny, J., and Cook, N. G. W., 1985, Formation and stability of steeply dipping joint sets: 26th U.S. Symposium on Rock Mechanics, p. 471-478.

Krantz, R. L., 1983, Microcracks in rocks: a review: Tectonophysics, v. 100, p. 449-480.

Kulander, B. R., Barton, C. C., and Dean, S. L., 1979, The application of fractography to core and outcrop fracture investigations: Morgantown Energy Technology Center, report prepared for U.S. Department of Energy, METC/SP 79/3, 174 p.

Ladeira, F. L., and Price, N. J., 1981, Relationship between fracture spacing and bed thickness: Journal of Structural Geology, v. 3, p. 179-183.

Lamont, N., and Jessen, F. W., 1963, The effects of existing fractures in rocks on the extension of hydraulic fractures: Journal of Petroleum Technology, v. 15, p. 203-209.

Land, L. S., and Dutton, S. P., 1979. Cementation of sandstones - reply: Journal of Sedimentary Petrology, v. 49, p. 1359-1362.

Laubach, S. E., and Griffiths, W., 1986. True "fracture cleavage" in the Palmerton Sandstone, Eastern PA (abs.): Geological Society of America, Abstracts with Programs, v. 18, p. 667.

Lemmlein, G. C., and Kliya, M. O., 1960. Distinctive features of the healing of a crack in a crystal under conditions of declining temperature: International Geology Review, v. 2, p. 125-128.

Lerche, I., and Narr, W., 1986. Estimating subsurface fracture density in core: effects resulting from variable fracture spacing: SPE Formation Evaluation, p. 249-258.

Lespinasse, M., and Pecher, A., 1986. Microfracturing and regional stress field: a study of the preferred orientation of fluid-inclusion planes in a granite from the Massif Central, France: Journal of Structural Geology, v. 8, p. 169-180.

Magara, K., 1975. Importance of aquathermal pressuring effect in Gulf Coast: American Association of Petroleum Geologists Bulletin, v. 59, p. 2017-2045.

_____ 1981. Mechanisms of natural fracturing in a sedimentary basin: American Association of Petroleum Geologists Bulletin, v. 65, p. 123-132.

McKenzie, D., 1978, Some remarks on the development of sedimentary basins: Earth and Planetary Science Letters, v. 40, p. 25-32.

Means, W. D., in press, A newly-recognized type of slickenside striation: Journal of Structural Geology.

Murray, G. E., 1961, Geology of the Atlantic and Gulf Coastal Province of North America: New York, Harper, 692 p.

Narr, W., and Currie, J. B., 1982, Origin of fracture porosity - example from Altamont field, Utah: American Association of Petroleum Geologists Bulletin, v. 66, p. 1231-1247.

Narr, W., and Lerche, I., 1984, A method for estimating subsurface fracture density in core: American Association of Petroleum Geologists Bulletin, v. 68, p. 1637-1648.

Nelson, R. A., 1985, Geologic analysis of naturally fractured reservoirs: Contributions in petroleum geology and engineering, v. 1: Houston, Gulf Publishing Company, 320 p.

Nolte, K. G., and Smith, M. B., 1981, Interpretation of fracturing pressures: Journal of Petroleum Technology, v. 33, p. 1767-1775.

Nunn, J. A., Scardina, A. D., and Pilger, R. H., Jr., 1984, Thermal evolution of the north-central Gulf Coast: Tectonics, v. 3, p. 723-740.

Nur, A., 1982, The origin of tensile fracture lineaments: Journal of Structural Geology, v. 4, p. 31-40.

Oliver, J., 1986, Fluids expelled tectonically from orogenic belts: their role in hydrocarbon migration and other geologic phenomena: Geology, v. 14, p. 99-103.

Owen, L. B., Toronto, T. W., and Sinha, K. P., 1987, Strain recovery measurements, Howell #5 well: Terra Tek Research, final report submitted to CER Corporation, 34 p.

Pindell, J. L., 1984, Alleghenian reconstruction and subsequent evolution of the Gulf of Mexico, Bahamas and Proto-Caribbean: Tectonics, v. 4, p. 1-39.

Plumb, R. A., Brie, A., and Hsu, K., 1985, Fracture detection and evaluation using new wireline methods, in Ashworth, Eileen, ed., Research and engineering applications in rock masses: Proceedings, 26th Symposium on rock mechanics, v. 1, p. 227-228.

Plumb, R. A., and Cox, J. W., 1987, Stress directions in eastern North America determined to 4.5 km from borehole elongation measurements: Journal of Geophysical Research, v. 92, no. B6, p. 4805-4816.

Plumb, R. A., and Hickman, S. H., 1985, Stress-induced borehole elongation: a comparison between the four-arm dipmeter and the borehole televiewer in the Auburn geothermal well: Journal of Geophysical Research, v. 90, no. B7, p. 5513-5521.

Prats, M., 1981, Effect of burial history on the subsurface horizontal stresses of formations having different material properties: Journal of the Society of Petroleum Engineering, v. 40, p. 658-662.

Price, N. J., 1966, Fault and joint development in brittle and semi-brittle rock: New York, Pergamon, 176 p.

Price, N. J., 1974, The development of stress systems and fracture patterns in undeformed sediments: Proceedings, Third International Congress of Society for Rock Mechanics, p. 487-495.

Ramsay, J. G., 1980a, The crack-seal mechanism of rock deformation: London, Nature, v. 284, p. 137-139.

Ramsay, J. G., 1980b, Shear zone geometry: a review: Journal of Structural Geology, v. 2, p. 83-99.

Sand, L. B., and Mumpton, F. A., 1978, Natural zeolites, New York, Pergamon Press, 546 p.

Saucier, A. E., and Finley, R. J., 1984, The Travis Peak/Hosston Formation of East Texas and North Louisiana: a laboratory of tight gas technology development: Gas Research Institute, In Focus -- Tight Gas Sands, v. 1, no. 1, p. 15-25.

Saucier, A. E., Finley, R. J., and Dutton, S. P., 1985, The Travis Peak (Hosston) Formation of East Texas and North Louisiana: Proceedings of the 1985 SPE/DOE Joint Symposium on Low Permeability Reservoirs, p. 15-22.

Schlumberger, Ltd., 1987, Log interpretation principles/applications: Houston, Schlumberger Educational Services, 198 p.

Secor, D. T., 1965, The role of fluid pressure in jointing: American Journal of Science, v. 263, p. 633-646.

Segall, P., 1984, Formation and growth of extensional fracture sets: Geological Society of America Bulletin, v. 95, p. 454-462.

Segall, P., and Pollard, D. D., 1982, Joint formation in granitic rock of the Sierra Nevada: Geological Society of America Bulletin, v. 94, p. 563-575.

Simmons, G., and Richter, D., 1976, Microcracks in rocks, in Strens, R.G.J., ed., The Physics and Chemistry of Minerals and Rocks: New York, Interscience, p. 105-137.

Smith, D. L., and Evans, B., 1984, Diffusional crack healing in quartz: Journal of Geophysical Research, v. 89, p. 4125-4135.

Smith, J. E., 1971, The dynamics of shale compaction and evolution of pore-fluid pressures: Mathematical Geology, v. 3, p. 239-263.

Sprunt, E. S., and Nur, A., 1979, Microcracking and healing in granites: new evidence from cathodoluminescence: Washington, D.C., Science, v. 205, p. 495-497.

Stock, J. M., Healy, J. H., and Hickman, S. H., 1984, Report on televiewer log and stress measurements in core hole USW G-2, Nevada Test Site, October-November, 1982: U. S. Geological Survey Open-File Report 84-172, 31 p.

Strubhar, M. K., Fitch, J. L., and Glenn, E. E. Jr., 1975, Multiple, vertical fractures from an inclined wellbore--a field experiment: Journal of Petroleum Technology, v. 27, p. 641-647.

Teufel, L. W., 1982, Prediction of hydraulic fracture azimuth from anelastic strain recovery measurements of oriented core, in Goodman, R. E., and Hughs, F. F., eds., Proceedings, 23rd Symposium on Rock Mechanics: Issues in Rock Mechanics, New York, SME/AIME, p. 29-33.

Tuttle, O. F., 1949, Structural petrology of planes of liquid inclusions: Journal of Geology, v. 57, p. 331-356.

Van Alstine, D. R., 1986, Paleomagnetic core orientation results from Holditch Howell No. 5 core: report submitted to CER Corporation, 19 p.

Verbeek, E. R., and Grout, M. A., 1982, Dependence of joint spacing on layer thickness in sedimentary rocks (abs.): Geological Society of America, Abstracts with Programs, v. 14, p. 637-638.

Vistelius, A. B., 1966, Structural diagrams: New York, Pergamon, 178 p.

Voight, B., and St. Pierre, B. H. P., 1974, Stress history and rock stress: Proceedings, 3rd Rock Mechanics Congress, ISRM v. 2, p. 580-582.

Walcott, R. I., 1972, Gravity, flexure, and the growth of sedimentary basins at a continental edge: Geological Society of America Bulletin, v. 83, p. 1845-1848.

Ward, B. J., Nelson, R. A., and Lenox, L. C., 1987, Oriented core: its use, error, and uncertainty: American Association of Petroleum Geologists Bulletin, v. 71, p. 357-368.

Warpinski, N. R., 1986, Elastic and viscoelastic calculations of stresses in sedimentary basins: SPE/DOE Unconventional Gas Technology Symposium, SPE Paper 15243, p. 409-417.

Warpinski, N. R., and Teufel, L. W., 1987, Influence of geologic discontinuities on hydraulic fracture propagation: Journal of Petroleum Technology, v. 39, p. 209-220.

Watts, A. B., and Ryan, W. B. F., 1976, Flexure of the lithosphere and continental margin basins: Tectonophysics, v. 36, p. 25-44.

Whitehead, W. S., Hunt, E. R., Finley, R. J., and Holditch, S. A., 1986, In-situ stresses: a comparison between log derived values and actual field-measured values in the Travis Peak Formation of East Texas: SPE Unconventional Gas Technology Symposium, SPE Paper 15209, p. 201-212.

Zemanek, J., Glenn, E., Norton, L. J., and Caldwell, R. L., 1970, Formation evaluation by inspection with the borehole televiewer: Geophysics, v. 35, p. 254-269.

Zoback, M. D., Moos, D., Mastin, L., and Anderson, R. N., 1985, Well bore breakouts and in situ stress: Journal of Geophysical Research, v. 90, no. B7, p. 5523-5530.

Zoback, M. L., and Zoback, M., 1980, State of stress in the conterminous United States: Journal of Geophysical Research, v. 85, no. B11, p. 6113-6156.